HYDRODYNAMICALLY INDUCED FORMATION
OF
CELLULOSE FIBRES

A Thesis

by

Bernhard Kalb, Dipl. Ing., Technische Hochschule Graz, Austria

Submitted to the Faculty of Graduate Studies
and Research of McGill University in partial
fulfilment of the requirements for the
degree of Doctor of Philosophy

Department of Chemistry
McGill University
Montreal, Quebec, Canada

August, 1978

Meinen Eltern und Evelyn gewidmet

ABSTRACT

A study has been made of the process of fibre formation which occurs when a cellulose solution is introduced into a stirred coagulant. The mechanism of fibre formation involves the dispersion of the viscous cellulose solution as droplets in the stirred coagulant and the deformation of these droplets by the action of local extensional flow. Coagulation occurs when sufficient coagulant has diffused into the deforming drop yielding a cellulose fibre.

In order to predict the fibre dimensions as a function of various experimental parameters, theoretical droplet deformation and coagulation studies were carried out. Theories for large deformations at low and high strain rates in a defined extensional flow field (hyperbolic flow) were developed for systems with negligible interfacial tension. The theories predict that the strain rate inside the drop increases with time and becomes equal to that outside the drop when large deformations are reached. This increase in the strain rate may favour the achievement of good molecular orientation in the fibres. Experimental studies at low strain rates in plane hyperbolic flow were performed using a four-roller-mill. Based on the results of these experiments, semi-empirical equations have been obtained describing the whole range of small to very large deformations. These expressions for the droplet deformation have been used in an idealized coagulation process that is treated theoretically. The theoretical predictions are shown to be in good qualitative agreement with the experimental results.

Finally, on the basis of the present work, a new fibre spinning process is proposed in which, during solidification of the fibre, extensional flow is applied.

RESUME

Cette étude décrit le processus de formation de fibres, quand une solution de cellulose est mise en contact avec un coagulant en agitation. Le mécanisme de formation des fibres implique la dispersion de la solution visqueuse de cellulose sous forme de gouttelettes dans le coagulant en agitation, et l'action d'un écoulement local d'extension qui déforme ces gouttelettes. La coagulation se produit quand une quantité suffisante de coagulant a diffusé à l'intérieur de la gouttelette en déformation.

Afin de prédire les dimensions des fibres en fonction de certains paramètres expérimentaux, des études de coagulation, ainsi que des travaux théoriques sur la déformation des gouttelettes, ont été entrepris. En effet, des théories couvrant les déformations importantes à des gradients de vélocité faibles et élevés dans un champ d'extension (écoulement hyperbolique), furent développées pour des systèmes dont la tension interfaciale est négligeable. Ces théories prédisent que le gradient de vélocité à l'intérieur de la gouttelette augmente avec le temps et devient égal à celui de l'extérieur de la gouttelette pour les déformations importantes. Cette augmentation du gradient de vélocité favorise alors l'orientation moléculaire des fibres. Des études expérimentales à faibles gradients de vélocité furent menées, et ce dans un écoulement hyperbolique bidimensionnel, obtenu grâce à "l'appareil à quatre rouleaux". A partir de ces résultats expérimentaux, furent dérivées des équations semi-empiriques, décrivant l'échelle complète des déformations, soit des faibles aux très grandes. Ces expressions décrivant la déformation d'une gouttelette furent utilisées pour le traitement théorique d'un processus de coagulation idéalisé. Il est d'ailleurs montré que ces prédictions théoriques sont qualitativement

en bon accord avec les résultats expérimentaux.

Enfin, à partir de ce travail, un nouveau procédé de filature de fibres est suggéré, dans lequel un écoulement d'extension est appliqué pendant la solidification de la fibre.

ACKNOWLEDGEMENTS

The author wishes to express his sincere thanks and appreciation to

Dr. R. St. John Manley

for his valuable guidance, encouragement and assistance as director of this research.

Grateful acknowledgement is also made to:

Dr. R. G. Cox for advice and discussions on the theoretical parts of this thesis;

Drs. S. G. Mason, H. I. Bolker, A. J. Pennings, H. D. Chanzy, P. Smith, J.-C. Wittmann, and J. Cornibert for their interest in this work and their stimulating discussions; and H. D. Chanzy also for the electron micrograph on page 45;

Miss L. Larrondo, and many other fellow graduate students for their friendship, helpful discussions and moral support;

The D. S. and R. H. Gottesman Foundation for a Fellowship during the session 1975-76;

Kimberley-Clark of Canada Limited for a Scholarship from 1976-77;

The Pulp and Paper Research Institute of Canada for a Studentship in 1977-78, laboratory accomodation, and the use of facilities and services;

Messrs. H. Kirchenberger and S. Rychel for their assistance in the photographic work; and

Messrs. A. Sulany and W. See for their skillful shop work on the four-roller-mill.

Last, but not least, I thank my wife for her persistent patience and for typing this thesis.

FOREWORD

The work described in this thesis forms part of a research programme, directed by Dr. R. St. John Manley in the physical chemistry division of the Pulp and Paper Research Institute of Canada at McGill University, designed to contribute to a better understanding of the crystallization process of natural and synthetic polymers in flow fields. The general aim of the research is to make a detailed study of the process of cellulose fibre formation in flowing solutions.

The chapters in the thesis have been written in the form of self-contained scientific papers which may be submitted for publication with minor changes. The thesis is presented in the following format:

Chapter I - a general introduction containing discussions of: the morphology of cellulose fibres and synthetic polymer crystals, the crystallization process in flow fields, the flow field, molecular deformation by flow fields, some aspects of conventional fibre spinning processes, and a brief survey of previous work related to the present fibre formation process.

Chapter II - a study of cellulose fibre formation from stirred solutions and the properties of the fibres obtained.

Chapter III - an investigation of fibre formation by deformation of droplets in defined extensional flow at low strain rates.

Chapter IV - a theoretical study of fibre formation by deformation of droplets in defined extensional flow at high strain rates.

Chapter V - a theoretical and experimental investigation of the coagulation process.

Chapter VI - a proposal of a new fibre spinning process; this chapter is intended to be submitted for publication as a note.

Appendices - supplementary material such as experimental data and derivations of formulas.

The thesis is concluded with claims to original research and suggestions for further work.

TABLE OF CONTENTS

LIST OF FIGURES

Figure No. Page

CHAPTER I

CHAPTER II

CHAPTER III

CHAPTER IV

CHAPTER V

CHAPTER VI

APPENDIX III

LIST OF TABLES

Table No. Page

CHAPTER II

CHAPTER III

CHAPTER V

CHAPTER I

GENERAL INTRODUCTION

The last twenty years have witnessed a great increase in our understanding of crystallization phenomena in polymers. It is now known that crystallization may take place in two fundamentally different ways, namely, lamellar growth and fibrous growth. Lamellar growth occurs in dilute quiescent systems and gives thin folded-chain crystals. Fibrous growth, on the other hand, may occur in flowing solutions and generally yields fibrous crystals that are composed of more or less extended chains.

This thesis deals with the crystallization of cellulose under flow conditions, a subject which is part of the general topic of crystallization phenomena in polymers. Therefore, it seems appropriate to begin this introduction with a discussion of the ultrastructure of cellulose fibres, and the morphology of synthetic polymer crystals especially those that are fibrous. Subsequently, the nucleation and growth of fibrous crystals will be discussed; the discussion being mainly based on our knowledge of the behaviour of synthetic polymers.

Flow fields are a major factor in inducing molecular deformation and fibrous crystallization. Accordingly, some aspects of the work that led to the recognition of the influence of flow and some theories of molecular deformation will be presented. One particular type of flow, namely extensional flow, appears to be most effective for inducing fibrous crystallization. This type of flow has been used for theoretical and experimental studies throughout the major part of the thesis. Therefore, it seemed appropriate to present a brief discussion of its characteristics and its effects on molecular deformation in comparison with shear flow.

In the penultimate section the topics covered are: cellulose solvent systems, the problems of conventional fibre spinning, and previous work on the formation of fibrous precipitates of polymers from solution.

Finally, the introduction closes with a presentation of the scope and aims of the present research.

Fine Structure and Morphology of Cellulose Fibres

Cellulose is a linear polymer consisting of D-glucose monomeric units which are linked by (1-4')-β-glucosidic bonds, as illustrated in Figure 1. The degree of polymerization is suggested to be higher than 15,000 for natural cellulose[1] (generally referred to as cellulose I), while it is of the order of 500 for regenerated and mercerized cellulose (cellulose II)[2]. Both the natural and regenerated form have a fibrillar structure, with microfibrils 7 to 70 nm in diameter which are composed of smaller morphological units, the so-called elementary fibrils, that are approximately 3.5 x 2 nm in cross-section[3].

The exact crystal structure of cellulose is still a matter of controversy, though the unit cell dimensions seem to be well established. From X-ray diffraction studies it was concluded that the crystal structure of cellulose I can be adequately approximated by the monoclinic unit cell that was first proposed by Meyer and Misch[4] (Figure 2). It has dimensions of $a = 0.835$ nm, $b = 1.03$ nm (fibre axis), $c = 0.79$ nm and $\beta = 84^\circ$, and contains two cellobiose residues per unit cell. The unit cell of bacterial and Valonia cellulose is larger[5,6], but can still be approximated by four Meyer and Misch subcells. The crystal unit cell of cellulose II is also monoclinic and has dimensions of $a = 0.793$ nm, $b = 1.034$ nm (fibre axis), $c = 0.918$ nm and $\beta = 62.7^\circ$ [5,7,8]. In all these unit cells cellulose assumes a 2_1 helical conformation.

The polarity of the chains of cellulose II with respect to each other

Figure 1

The structural formula of cellulose with a degree of polymerization n.

Figure 2

The monoclinic unit cell of cellulose I proposed by Meyer and Misch[4]. The fibre axis lies parallel to b and the molecules are in the anti-parallel chain arrangement.

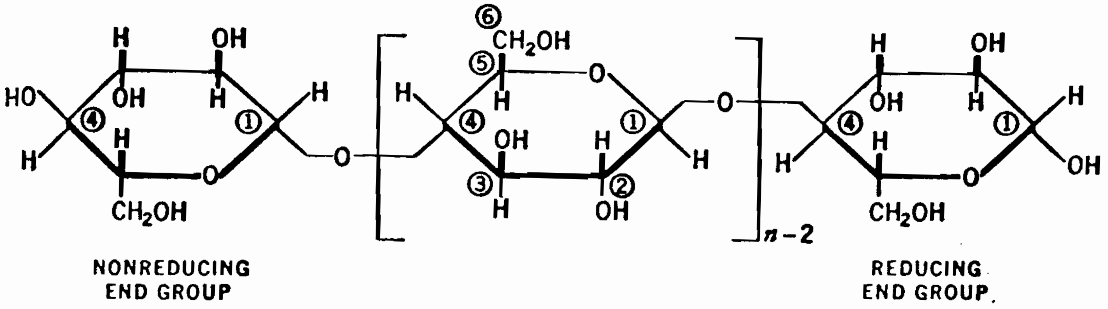

FIGURE 1

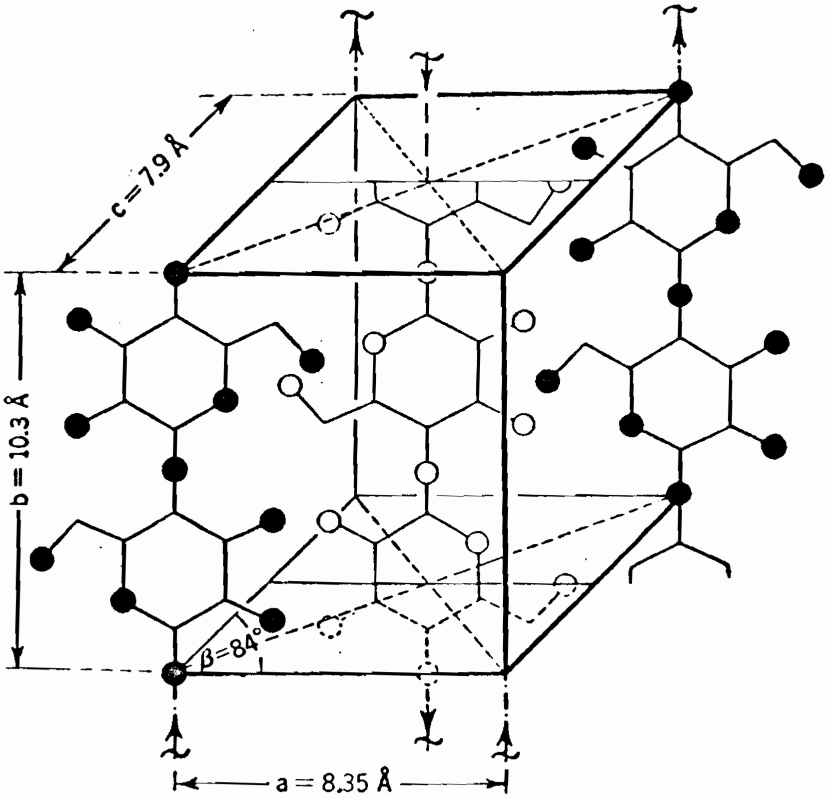

FIGURE 2

in the crystal lattice seems to be accepted as being anti-parallel[5,7,9]. Unresolved, however, is the question of the chain packing in cellulose I. The schools of Blackwell[5] and Sarko[7,9] conclude from their studies that cellulose I is packed parallel, contradicting previous suggestions[4]. It is known, however, that cellulose I can be transformed, for example by mercerization, into cellulose II without disruption of the elementary fibrils. It is clearly difficult to conceive how a rearrangement of the long chain molecules from parallel to anti-parallel packing can occur under these conditions. To date, the problem has not been resolved.

The parallel or anti-parallel arrangement of the cellulose chains is also directly related to the question of the detailed molecular structure of the elementary fibril. A parallel chain structure would rule out any model that contains chain-folded molecules. Some[10-14] of the many models suggested both for cellulose I and II are given in Figure 3. In all cases the chains are oriented in the fibre axis direction within the 3.5 nm elementary fibrils, as required by X-ray diffraction evidence. Basically, the models are of two types, namely, folded and extended-chain models. At the present time, however, there is no conclusive evidence in favour of either kind of model and the question of the molecular architecture of the cellulose elementary fibril remains open.

The elementary fibril is the fundamental morphological constituent of all cellulose fibres. In wood the cellulose in the form of elementary fibrils is laid down in a matrix of lignin and hemicelluloses in the primary and the secondary wall of the hollow plant cells. Length dimensions of cellulose fibres obtained from wood by delignification vary between about 1 and 3 mm, depending on the source of the cells (see e.g. reference 15). In regenerated celluloses the elementary fibrils constitute larger microfibrils with diameters that depend on the production conditions, but are generally of the order of

Figure 3

Structure models of the elementary fibril:

(a) Pleated ribbon of folded chains (Manley[3])

(b) Extended-chain model with chain dislocations due to chain-ends (Mühlethaler[10])

(c) Fringed micellar concept (Frey-Wyssling[11])

(d) Extended-chain model with a regular sequence of crystalline and para-crystalline areas (Hess et al[12])

(e) Folded-chain arrangement (Dolmetsch and Dolmetsch[13])

(f) Interlinked folded-chain conformation (Marx-Figini and Schulz[14])

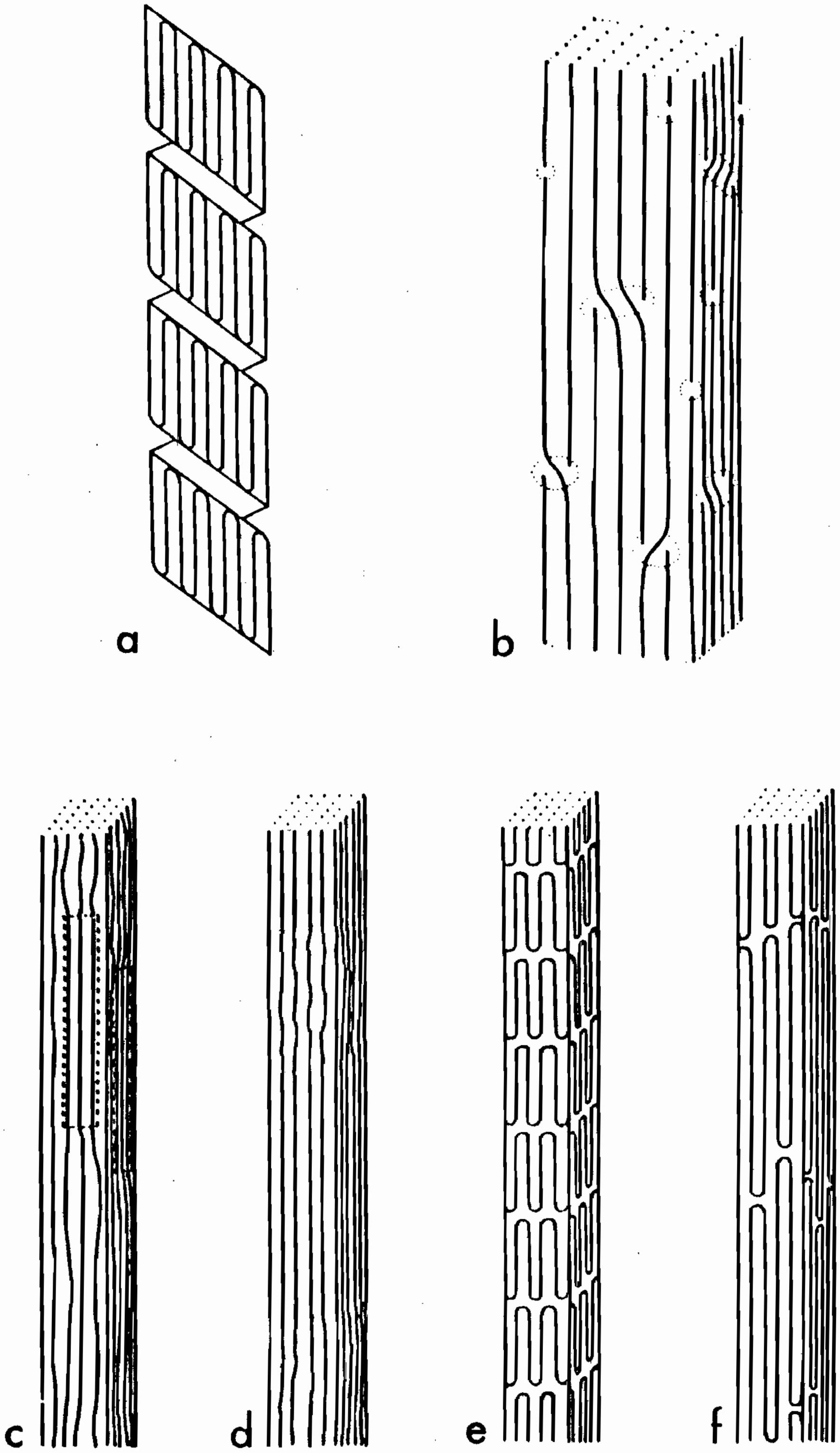

FIGURE 3

7 to 30 nm [2,3]. These regenerated celluloses are mainly produced in the form of viscose rayons that often exhibit a skin-core structure[16].

The Morphology of Synthetic Polymer Crystals

Polymer crystals may be of two types, viz. lamellar and fibrous. Lamellar crystals may grow from supercooled solutions or melts and, are composed of folded chain-molecules[17-20], as shown in Figure 4. The fold length varies with the crystallization conditions (especially the crystallization temperature) but is generally of the order of 10 nm. By crystallization from dilute solution, the lamellae grow in the form of single crystals, while by crystallization from concentrated solutions or melts, they appear as the substructure of spherulites. Various other types of lamellar structures have been obtained under different conditions of crystallization[20]. When crystallized under high pressure, the lamellae can be composed of chain-extended molecules[21,22]; the thickness of the lamellae is then greater and may correspond to the lengths of the fully extended molecules.

Fibrillar crystals have been obtained for a number of polymer systems and by various mechanisms[20,23]. Fibres are formed by flow induced crystallization[23-30], by crystallization during polymerization[31-33] (which probably also includes the synthesis of cellulose[2,34]), and thirdly by aggregation of stiff molecules in solution[35-37].

The fibrillar crystals produced by flow induced crystallization from e.g. supercooled solutions of polyethylene are referred to as "shish-kebabs". The generally accepted model that represents the morphology of these composite crystals is shown in Figure 5. Shish-kebabs consist of a central core

Figure 4

Lamellar crystal with chain-folded molecules.

Figure 5

The Pennings model of shish-kebabs[23]; the shish-kebabs consist of a central core with extended chains and a chain-folded overgrowth.

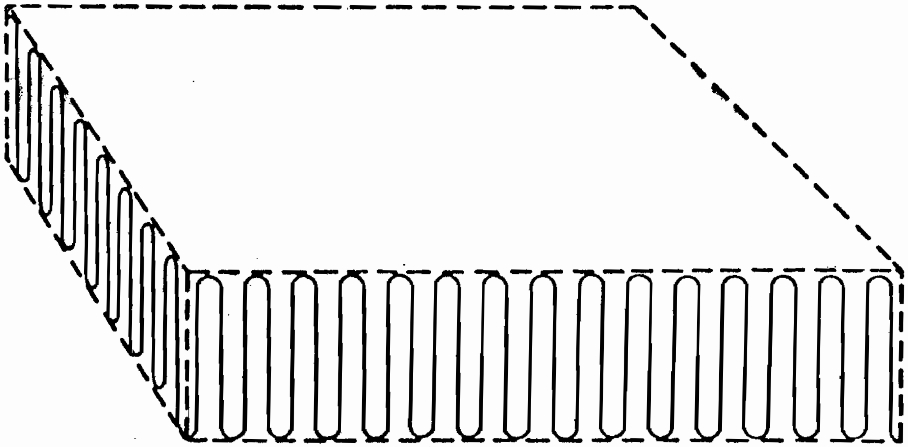

FIGURE 4

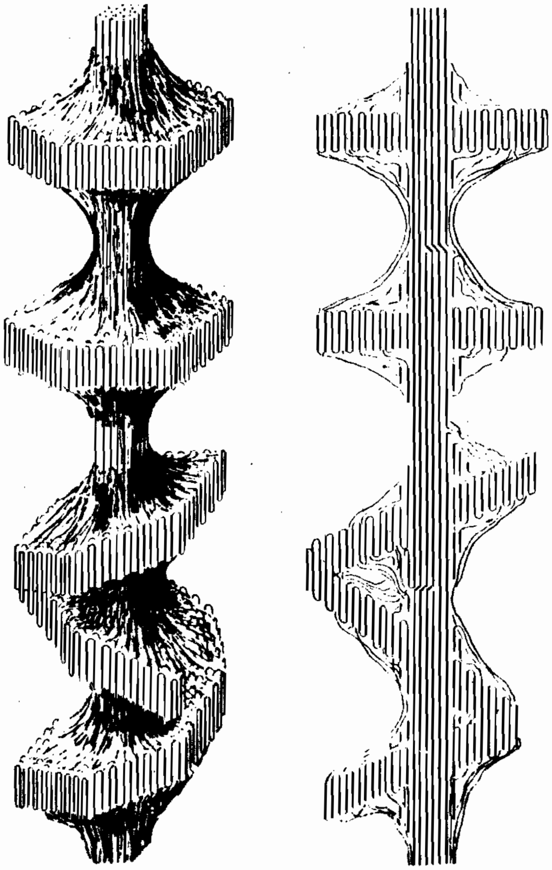

FIGURE 5

with extended and aligned molecules and a transverse chain-folded lamellar overgrowth[38,39]. The chain-extended core is suggested to result from the nucleation and growth of molecules in the extensional flow that is produced, for example, in some regions of the turbulent flow field in a stirred system[23,25,38]. On this core, epitaxial crystallization of the chain-ends (cilia) emanating from the core[39] occurs together with the molecules that still remained in solution after the agitation has ceased and the system is cooled down.

There still exists some uncertainty on the microstructure of the shish-kebabs. The school of Keller[40,41] distinguishes between two types of shish-kebab structures. At high temperatures, exceeding the highest temperature at which lamellar crystals may grow from dilute solution (i.e. 96°C for the system polyethylene/para-xylene), only micro-shish-kebabs having small striations along the backbone are produced. At lower temperatures, on the other hand, these micro-shish-kebabs align and act as nuclei for the growth of lamellar crystals to form the usual shish-kebabs. The micro-shish-kebabs are suggested by these authors to be the "representative product of flow induced crystallization"[40]. The question of the exact morphology of the micro-shish-kebabs, particularly the origin of the striations, has not been answered.
Pennings[23,39,42], on the other hand, does not make a distinction between high and low-temperature fibres. According to his view, the representative product of flow induced crystallization is the fibrous backbone consisting of highly extended chain molecules. The striations as well as the lamellar overgrowths are only formed by the crystallization of cilia and molecules in solution when the flow has ceased and the system is cooled down.

Crystallization in Flow Fields

The formation of cellulose fibrous crystals from solution, as described in this thesis, is believed to be based on a crystallization process which is similar to that of synthetic polymers. In the following, some of the recent knowledge of the influence of flow on the crystallization process for synthetic polymers will be recapitulated.

Generally, crystallization is a two-step process that comprises nucleation and growth of the crystallizable polymer[20,43]. The nucleation process involves the formation of a nucleus of critical size that must be achieved in order that the nucleus can be thermodynamically stable. Subsequently, molecules are added to this primary nucleus by a secondary nucleation process which results in the growth of the crystal. Nucleation and growth are very similar processes, since in both cases the rate is determined mainly by the transport of molecules to the site of crystallization and the free enthalpy of formation of a nucleus of critical size. An expression for the nucleation rate, I, the number of nuclei formed per unit volume and per second, was first derived by Turnbull and Fisher[44] and can be written as eq. 1,

$$I = I_o \exp\{-(\Delta G_a + \Delta G^*)/kT\} \qquad 1$$

where I_o is a pre-exponential factor and ΔG_a and ΔG^* are the activation free energy of transport of a molecule and the free energy of formation of a nucleus of critical size respectively; k denotes the Boltzmann constant and T the absolute temperature. The expression for secondary nucleation (i.e. growth) has the same essential features as eq. 1. Further theories for the nucleation and growth of lamellar polymer crystals under quiescent conditions may be found in the literature[43,45-48].

A theory for fibrous nucleation (called bundle-like[23] or row[50] nucleation) has been given earlier[49,23]. Pennings[23] derived an expression for the steady state nucleation frequency, given by eq. 2.

$$I = I'\sinh\left(\frac{AP_{12}}{kT}\right)\exp\left[-\frac{\Delta G_a}{kT} - \frac{32\sigma_1\sigma_2^2 - (16/A_c)\sigma_2^2 kT\ln(\wp/\chi^{2\delta})}{kT(\Delta\mu + \Delta\mu_{elast})^2}\right] \qquad 2$$

Here I' contains a non-equilibrium term and the pre-exponential factor. σ_1 and σ_2 are the surface free energies of the crystal at the surfaces of the nucleus which are orthogonal and parallel to the fibre axis direction respectively. A_c, $\wp$, χ and δ denote the cross-sectional area of a single chain, the polymer volume fraction in the system, the number of segments per chain, and a term accounting for the number of possible chain conformations respectively. $\Delta\mu$ represents the driving force for crystallization in the absence of flow and is defined by the difference in the free enthalpy of a molecule in the crystalline and liquid state. It is given by $\Delta H\Delta T/T_m$, where ΔH is the molar enthalpy of fusion, T_m the equilibrium melting point and ΔT the degree of supercooling ($\Delta T = T_m - T$). T_m is defined as the melting point of an infinitely large extended chain crystal of molecules with infinitely high molecular weight. Special attention must be drawn to the terms AP_{12}, reflecting the influence of the shear force at the crystal surface, and $\Delta\mu_{elast}$ which represents the elastically stored free energy resulting from the deformation of a random coil in the flowing solution. Since $\Delta\mu_{elast}$ and AP_{12} increase with the hydrodynamic forces that are applied, the rate of nucleation will also increase according to eq. 2. Therefore the kind of flow that causes large molecular elongations will have the greatest effect on the rate of crystallization.

As discussed earlier, the growth of polymer crystals is a secondary nucleation process. Therefore, the equation for the growth rate is similar to that for the nucleation rate. An equation for the longitudinal growth rate of fibrous crystals (R_ℓ) was derived on the basis of theories of crystal growth[43,45,51] by Pennings[23] and has the form of eq. 3,

$$R_\ell = R'\sinh\left(\frac{AP_{12}}{kT}\right)\exp\left(-\frac{G_a}{kT} - \frac{4L\sigma_2^2}{kT(\Delta\mu + \Delta\mu_{elast})}\right) \qquad 3$$

where L is the repeat unit of the molecule and R' a term that contains the pre-exponential factor. The conclusions to be drawn as to the effect of the flow on the growth rate are similar to those for the nucleation rate. Hence the growth rate increases with the molecular deformation due to flow.

Comparisons between the theoretical expressions above and experiments cannot be made, since the exact correlation between $\Delta\mu_{elast}$ and flow parameters is not known. However, the equations describe at least qualitatively the effect of flow on the crystallization rates and explain the experimental observations that have been made.

The longitudinal growth of fibrous crystals is envisaged as occurring by an "unrolling" mechanism[23] of the chain molecules. In this mechanism, a macromolecule, that is partially attached to the fibrous seed, unrolls due to the hydrodynamic forces and becomes incorporated in the crystal. This growth mechanism is thought to proceed very fast, since the entropy of a polymer chain that is partially attached to a crystal is relatively low in comparison with that of a molecule in solution; this results in an increased driving force for crystallization.

In experimental studies with flowing polymer solutions, it was shown that above the maximum crystallization temperature for folded-chain crystals considerable rates of nucleation and growth of fibrous crystals can be achieved[23,42]. In this respect a very interesting discovery[23] should be mentioned, namely, that bundle-like nucleation can occur even above the equilibrium dissolution temperature of polyethylene in p-xylene (118.9°C). The equilibrium dissolution temperature is defined as the temperature at which an infinitely large extended-chain crystal, consisting of a polymer with infinite molecular weight, dissolves; practical samples having finite molecular weights dissolve at lower temperatures. The stress on the entangled and nucleated molecules due to the flow seems to have increased the dissolution temperature considerably.

The Flow Field

From experimental studies, it has been concluded that there exists a certain type of flow which is most effective for fibrous crystallization[52-60]. The work of Pennings[52,23] yielded the first clear picture for the involvement of flow in the crystallization of agitated dilute polymer solutions. He and his co-workers demonstrated that in a Couette system with a rotating inner cylinder, the critical speed of rotation for the onset of Taylor[61] and Pai[23] vortex motion corresponds to a sudden change in the rate of crystallization and the formation of fibrous crystals. Below the critical speed where the flow corresponds to simple shear, only folded-chain lamellar crystals are formed. The critical speed, n_{crit}, is given by eq. 4 (with n_{crit} in rpm, other variables in c.g.s. units):

$$n_{crit} = 395(\mu/\rho)\left(R(\Delta R)^3\right)^{-1/2} , \qquad 4$$

where μ and ρ are the viscosity and density of the polymer solution and R and ΔR represent the radius of the rotating inner cylinder, and the annular gap width respectively. Figure 6 shows a schematic diagram of the flow field in the Couette apparatus when Taylor vortices have developed. In Figure 7, the

<u>Figure 6</u>

Illustration for the formation of Taylor vortex flow in a Couette system above a critical speed (after Pennings[25]). The rings around the inner cylinder are aggregates of crystallized fibres that deposit at certain distances from each other.

<u>Figure 7</u>

A sudden change in the rate of crystallization of polyethylene is observed at a critical speed of the rotating inner cylinder in the Couette system (after Pennings[52]). The crystallization temperature in this case was 91°C.

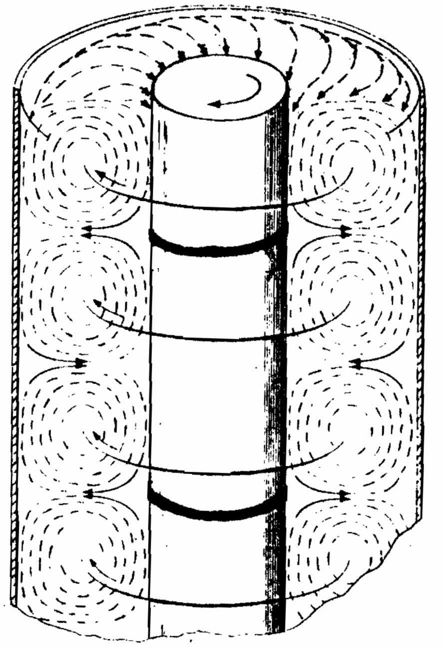

FIGURE 6

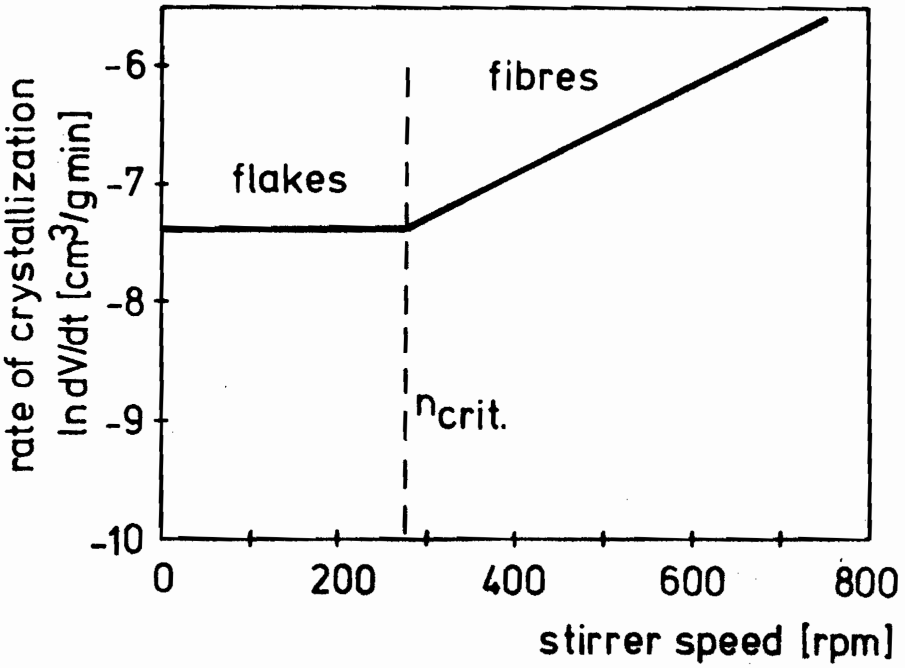

FIGURE 7

rate of crystallization is plotted against the speed of rotation (n). It can be seen that the rate of crystallization increases suddenly at the critical speed (n_{crit}). A still steeper increase has been observed after the formation of Pai vortices[23]. This phenomenon suggests that the increase in the rate of crystallization is related to the occurence of extensional flow that develops especially in regions where the vortex flow approaches the wall of the inner cylinder. It is now generally accepted[52-60] that extensional flow is the most efficient type of flow for fibrous crystallization. An illustration of an extensional flow field is given in Figure 8. The velocity increases in the flow direction (longitudinal velocity gradient) while in simple shear flow, as shown in Figure 9, the velocity increases orthogonally to the flow direction (transversal velocity gradient). The reason why simple shear does not promote fibrous crystallization can be found if the two components of shear flow are considered (Figure 10). These are an extensional flow component that causes the elongation of the molecules, and a rotational component that rotates the molecules. Since there also exists compressional flow orthogonal to the extensional flow direction, the molecules will become extended and compressed periodically, thus making only small elongations possible.

Various devices that are capable of producing extensional flow are illustrated in Figure 11. The rotating paddle stirrer produces a turbulent flow field which contains local regions with extensional flow components; the Couette apparatus develops extensional flow where the Taylor vortex motion approaches the walls of the cylinders. The other devices are: converging channels, impinging jets, and the four-roller-mill. Only the last two devices can produce pure extensional flow fields. The four-roller-mill was first introduced by Taylor[62]. It generates a two-dimensional hyperbolic flow field (the streamlines are hyperbolae) that can be described by simple mathematical

Figure 8

Illustration of an extensional flow field. x and y are the coordinates, where x corresponds to the flow direction. As can be seen, the velocity (arrows) increases in the x-direction, which results in a longitudinal velocity gradient.

Figure 9

The velocity (arrows) is parallel to the flow direction, x, and increases in the direction orthogonal to x. Thus the flow field has a transversal velocity gradient.

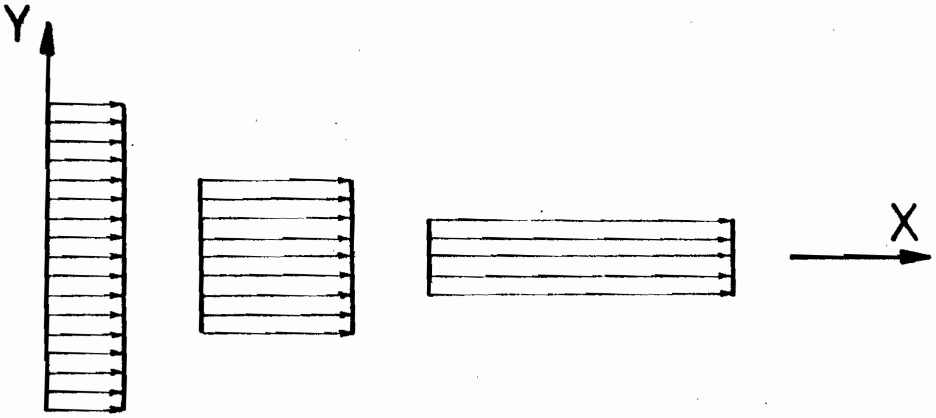

FIGURE 8

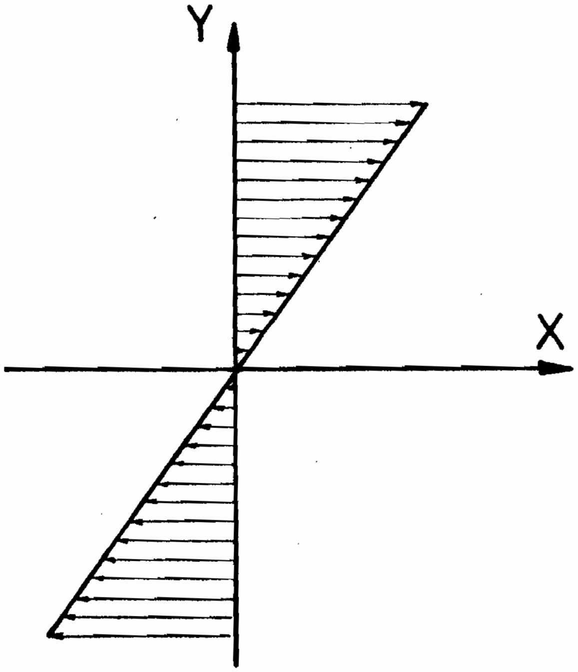

FIGURE 9

Figure 10

Schematic drawing illustrating the two components of simple shear. The extensional component (pure shear) causes the elongation of the molecules, while the rotational component rotates the molecules. Since there exists compressional flow orthogonal to the extensional flow direction, the molecules will become extended and compressed periodically, thus making only small elongations possible.

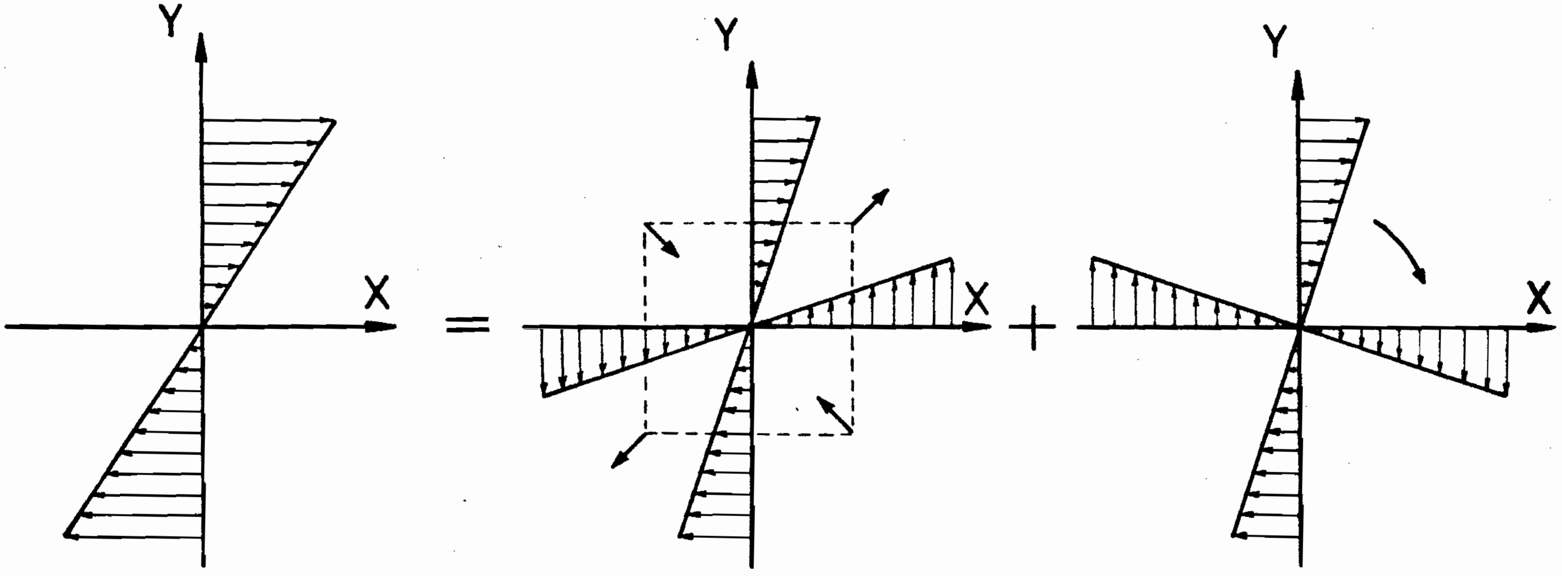

simple shear　　pure shear　　rotation

FIGURE 10

<u>Figure 11</u>

Various devices that are capable of producing extensional flow. From left to right: paddle stirrer, Couette apparatus, converging channel, impinging jet, and four-roller-mill. The thin lines represent the streamlines, while the heavy arrows indicate the flow direction.

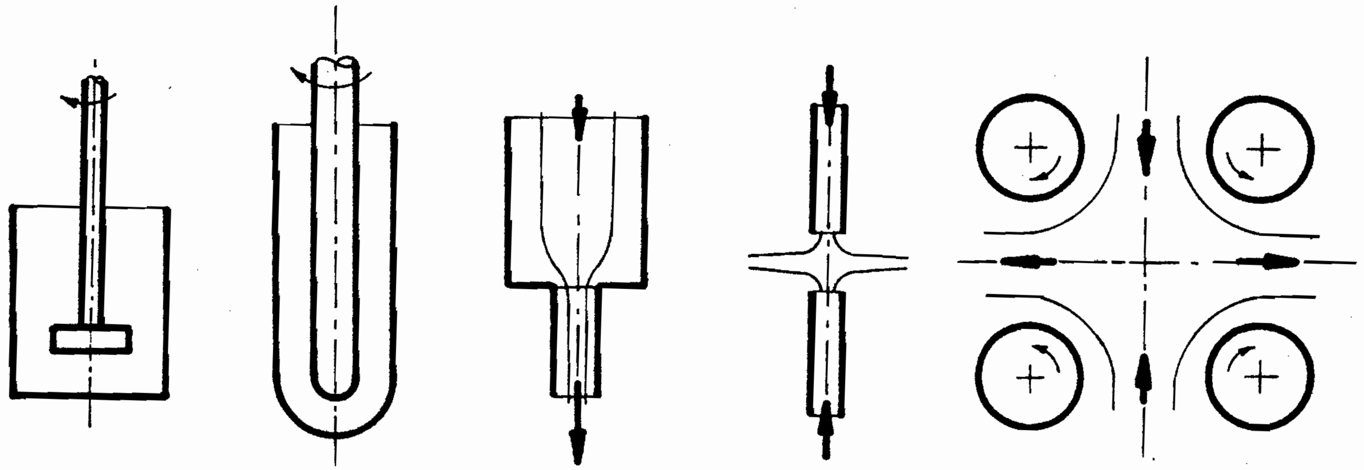

FIGURE 11

formulas, as will be seen subsequently.

Molecular Elongation by Extensional Flow

It was mentioned above that the rate of fibrous crystallization is very much dependent on the degree of elongation of the molecular coils. The deformation of molecules is influenced by the magnitude of the longitudinal velocity gradient, the molecular weight and the viscosity of the solvent[63-68]. A theory for the deformation behaviour of macromolecules in longitudinal and transversal velocity gradients has been derived by Peterlin[69,70]. In this theory a dumbbell model is assumed and the deformation, ε, is defined by

$$\varepsilon = \frac{h - h_o}{h_o}$$

where h_o and h are the lengths of the dumbbell, undeformed and deformed respectively. It was shown[71] that for the transversal (ε_t) and longitudinal (ε_ℓ) velocity gradients the deformation can be described by eqs. 5 and 6,

$$\varepsilon_t = \left(1 + \frac{\beta^2}{6}\right)^{1/2} - 1 \qquad 5$$

$$\varepsilon_\ell = \left[\frac{(2 - \beta)}{(1 - \beta)\ (2 + \beta)}\right]^{1/2} - 1 \qquad 6$$

where $\beta = \dot{\gamma}\tau$. $\dot{\gamma}$ is the velocity gradient and τ the molecular relaxation time for the rubbery retraction of the molecule to a random coil. The deformation behaviour according to these formulae is shown in Figure 12, where it is seen that the deformation in longitudinal velocity gradients increases sharply above a certain critical value of β, while ε_t increases only slowly and steadily. This difference in behaviour is explained by the effect of the rotational

Figure 12

The logarithm of the deformation, logε, is plotted against logβ, where β is the product of molecular relaxation time and velocity gradient. It can be seen that the deformation in extensional flow (ε_{ℓ}) increases rapidly when a certain β is reached.

Figure 13

The logarithm of the deformation, logε, is plotted as a function of the logarithm of the molecular weight, logM, for different velocity gradients. Evidently, for a given strain rate, $\dot{\gamma}$, there is a minimum molecular weight below which the molecules cannot be fully extended.

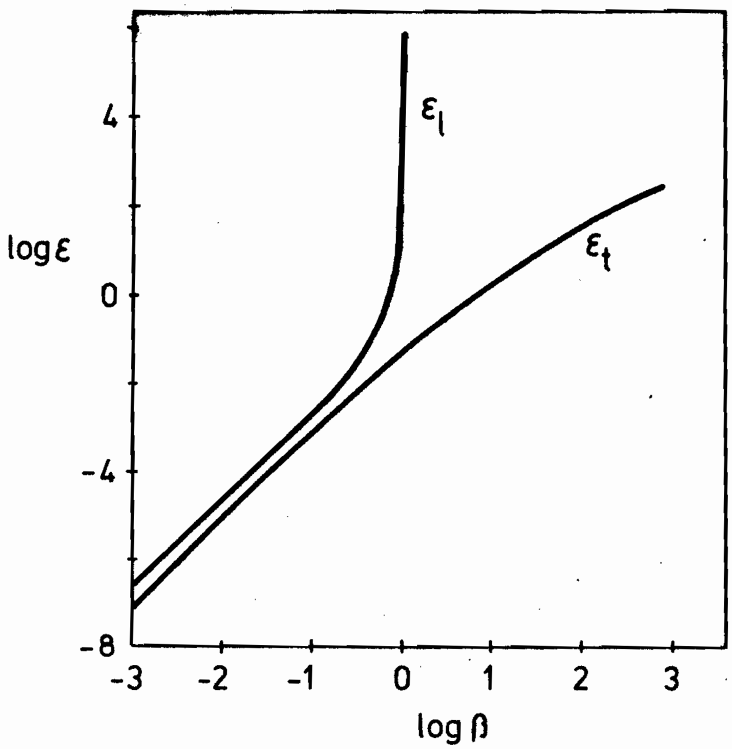

FIGURE 12

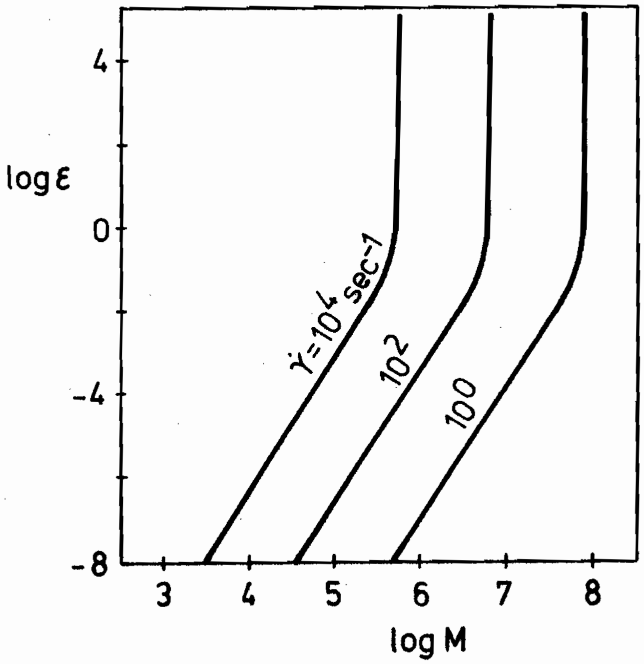

FIGURE 13

velocity component in fields with transversal velocity gradients, as discussed earlier. Similar results for a deformable sphere were obtained by Hlaváček and Seyer[72].

The molecular weight dependence of the deformation has been discussed by Mackley[71] using a molecular model that is intermediate between a free draining and a non free draining coil. For such an intermediate model the molecular relaxation time may be expressed by

$$\tau = cM^{7/4} , \qquad 7$$

where c is a constant that depends on the system; M is the molecular weight. If eq. 7 is substituted in eq. 6 the following expression can be obtained:

$$\varepsilon_{\ell} = \left[\frac{(2 - \dot{\gamma}cM^{7/4})}{(1 - \dot{\gamma}cM^{7/4})\ (2 + \dot{\gamma}cM^{7/4})}\right]^{1/2} - 1 \ . \qquad 8$$

The molecular weight dependence of the deformation according to eq. 8 and for $c = 1.1 \times 10^{-14}$ (polyethylene in xylene at 127°C) is shown in Figure 13 for various longitudinal velocity gradients. Figure 13 shows that for a given molecular weight, the velocity gradient has to assume certain magnitudes in order that high molecular extensions can be achieved. It also shows that for a given gradient only molecules above a certain critical size can be fully extended.

Based on the above theory and on other theories describing the rheology of polymer solutions[76,77], it is possible to establish criteria for the conditions under which long chain molecules may become fully extended. For polymer solutions at very low polymer concentrations, full elongation and alignment of the molecules is achieved when the following conditions are satisfied[64]:

$$\dot{\gamma}\tau > 1 \qquad 9$$

$$\dot{\gamma}\tau > \alpha \ . \qquad 10$$

τ denotes the time needed for stretching and alignment to be completed and α is a number depending on the physical properties of the molecule. The magnitude of α is of the order of 4 for intermediate, and >4 for high molecular weights. The second inequality defines the time over which $\dot{\gamma}$ has to be applied in order to achieve full molecular extension. As can be seen from eqs. 9 and 10, for τ values of the order of 10^{-4} to 10^{-5} sec, corresponding to normal high molecular weight polyethylenes, the strain rate has to assume values of the order of 10^4 to 10^5 sec^{-1} for full molecular extension to be achieved. This might cause difficulties in practice and high extension will therefore only be accomplished for extremely high molecular weights. For solutions with higher polymer concentrations, the theories are not exactly valid. However, it is expected that τ increases due to molecular entanglement thus making it possible to satisfy the conditions of eqs. 9 and 10 on a qualitative basis. For concentrated polymer solutions and melts, where the molecules are closely entangled and penetrate each other, criteria for full extension have yet to be established.

The extension and alignment of molecules is accompanied by large changes in the elongational viscosity. The elongational viscosity (μ_{el}) is defined by eq. 11,

$$\mu_{el} = \frac{P_{11} - P_{22}}{\dot{\gamma}} \qquad 11$$

in contrast to the better known shear viscosity (μ) defined by eq. 12.

$$\mu = \frac{P_{12}}{\dot{\gamma}} \qquad 12$$

Here $P_{11} - P_{22}$ is the first normal stress difference, P_{12} the shear stress, and $\dot{\gamma}$ the velocity gradient being the shear rate in eq. 11 and the strain rate in eq. 12. Elongational viscosity, according to eq. 11, is related to the resistance of a medium to strain. It has been shown by experimental and theoretical studies[73-75,78] (reviewed in references 76 and 77) that the elongational viscosity can increase greatly with increasing strain rates and can reach values that are orders of magnitude higher than the shear viscosity. This behaviour can be explained as being directly related to the high extension of the polymer molecules which are now subjected to large frictional forces, due to intermolecular interaction. The appearance of high μ_{el} is therefore an indication that high molecular extension has been achieved.

It is interesting and important to note that the deformation of molecular coils is closely related to the deformation of liquid droplets, when the macromolecule is imagined to be an extremely small homogeneous drop. In studies on droplet deformation[79-84], it has been demonstrated that drops with viscosity ratios (shear viscosity of drop divided by that of the suspending medium) of about 20 were easily deformed into threads already at low longitudinal velocity gradients. No gradient, however, could extend and break drops with viscosity ratios greater than 3.5 in flow fields with transversal velocity gradients (shear flow). This interesting result is again an indication that extensional flow is much more effective than shear flow for the deformation of particles.

Cellulose Dissolution and Fibre Formation

Cellulose can be dissolved in a number of different solvents. Of greatest industrial importance at present are the processes that transform cellulose into a derivative followed by dissolution in one of the many available solvents[85,86]. Generally, cellulose solvents can be acids, bases and salt solutions, as well as metal complexes[85,87] and non-aqueous solvents[85,88-91]. The dissolution of cellulose is often accompanied by a severe degradation of the molecules. As seen in eq. 9, the strain rate employed to achieve good orientation can be smaller when higher relaxation times are present. Since the relaxation time increases with the molecular weight of the polymer, it is extremely important to preserve the polymer in a high molecular weight range. It is therefore necessary to use cellulose solvents that are less degradative. Only some of the metal complexes and the recently discovered non-aqueous solvents are believed to be non-degradative. In particular, the non-aqueous dimethyl sulfoxide/paraformaldehyde is of great interest for fibre spinning methods[92].

Fibres of cellulose and its derivatives are at the present mostly formed by extruding solutions or melts through small orifices. The fibres are solidified by coagulation in a coagulant bath, by evaporation of the solvent or by cooling the hot melt. The viscose process is utilized for the greatest part of cellulose fibres produced today. Viscose is a cellulose xanthate in an aqueous solution of sodium hydroxide. The process[93-95] consists of a large number of steps that include steeping (alkaline treatment), shredding, aging (depolymerization), xanthation with carbon disulfide, dissolution in sodium hydroxide solution, blending, ripening (to increase the spinnability), filtration (to screen big particles), spinning, neutralization, purification and finally drying.

Some of the numerous steps mentioned above are absolutely essential to render the fibre spinning possible. Their application, however, has certain consequences in the quality and cost of the product. Especially the aging step, which produces smaller molecular weights of the cellulose and is used in order to keep the viscosity of viscose low for effective spinnability, can have negative effects on the molecular orientation and the strength of the fibres. Great problems are encountered in the filtration of viscose, because of its high viscosity and the frequent clogging of the filters. The spinning of the fibres is itself the most critical part of the process since it is often interrupted by the clogging of the orifices[97]. Furthermore, the spinning through the spinnerets involves large transverse velocity gradients which are ineffective for the achievement of good molecular orientation, as has been shown earlier in this introduction.

From the discussion above, it is evident that the study of fibre formation methods that eliminate some of the problematic steps seems to be of great importance. With this intention, such a process has been studied by Allen et al[96]; essentially it involves the precipitation of viscose introduced in small portions into a stirred coagulant. Fibres with dimensions of the order of normal wood fibres were produced. Hence, the need for small orifices as well as the need for cutting procedures to obtain short fibres from continuous rayons were eliminated. The fibres thus obtained were thought to be of interest for use in the non-wovens industry.

The patent literature contains patents where the formation of fibrous cellulose structures[98-100] and fibrids[101-111] (fibrous structures of synthetic polymers) by precipitation under flow has been described. The fibrous structures were mainly produced by introducing polymer solutions into coagulants, to which high shear was applied. The coagulation has been approached by qualitative mathematical expressions[102] which mainly attempt to define the conditions under which fibrous precipitation may occur. No control over fibre dimensions could be gained.

Scope and Aims of the Thesis

This thesis describes a study of the formation of cellulose fibres by precipitation from flowing solutions. The work falls within the ambit of the wider problem of the crystallization of polymers from flowing solutions. This is an area in which there is considerable current interest, since it points the way to obtaining polymeric fibres with greatly enhanced tensile properties[63]. Although work of a similar nature has been carried out on cellulose in the past, no detailed understanding of the mechanism has been achieved so far. In the present study, the aim is to identify the fundamental aspects of the problem and to subject them to rigorous theoretical analysis. In this way, it has been possible to make a number of important predictions and to test them experimentally.

In the experimental work it would have been possible to use a variety of solvent systems as mentioned earlier. However, since the basic mechanism of fibre formation was expected to be the same in all cases, the decision was made to restrict the investigation to the system cellulose/dimethyl sulfoxide/paraformaldehyde. This solvent was specifically chosen because it is known to be non-degradative and stable at room temperature.

According to our present knowledge of crystallization and orientation of polymers in flow fields, as outlined in this introduction, fibrous crystallization of cellulose must occur in extensional flow fields if good molecular orientation and high tensile strengths are to be achieved. Therefore, the bulk of the investigation has been carried out in a hyperbolic flow system in which well defined extensional flow is generated.

The work is presented in five sections as follows.

In chapter II, two methods of cellulose fibre formation from stirred dimethyl sulfoxide/paraformaldehyde solutions are described. These are: i) fibre formation by adding precipitant to a stirred cellulose solution, and ii) addition of a viscous cellulose solution to a stirred coagulant. The two methods involve different mechanisms of fibre formation. In the first case the cellulose is initially precipitated as elementary fibrils which subsequently aggregate laterally under the influence of the flow field to form macroscopic fibres. Since this method was not accessible to detailed theoretical analysis, it was not investigated further. The second method involves dispersion of the cellulose solution as droplets in the stirred coagulant; subsequently the droplets are deformed into thin liquid threads which coagulate forming fibres. This method was selected for further detailed investigations for two reasons. First, because it allows the production of highly oriented fibres and secondly, because it is amenable to rigorous theoretical analysis.

Chapter III contains a theoretical and experimental study of droplet deformation in a model system in which the coagulation step has been eliminated. Particular interest lies in the variation of the length of the droplets with the duration of deformation and the strain rate inside the drop. The latter is important because it influences the orientation that can be achieved in the fibres.

In chapter IV, the droplet deformation process is studied theoretically at high strain rates of the extensional flow outside the drop, since high strain rates are necessary to achieve good molecular orientation in the practical application of this fibre formation process.

In chapter V, the droplet deformation has been combined with the coagulation process; both processes proceed simultaneously. A slow coagulant has been used for the precipitation of the cellulose from solution in DMSO/PF, in order to be able to follow the formation of the fibres photographically. The predictions for the variation of the fibre length with different parameters are compared with the experimental results. It is shown that reasonably good control over the fibre dimensions was obtained.

Finally, on the basis of the work in previous chapters, a new fibre spinning process is proposed in chapter VI.

References

1. Goring, D.A.I., and Timell, T.E., Tappi 45, 454 (1962).
2. Preston, R.D., "The Physical Biology of Plant Cell Walls", Chapman and Hall London, 1974.
3. Manley, R.St.John, J. Polym. Sci. A-2, 9, 1025 (1971).
4. Meyer, K.H., and Misch, L., Helv. Chim. Acta 20, 232 (1937).
5. Blackwell, J., Kolpak, F.J., and Gardner, K.H., ACS Symp. Series 48 42 (1977).
6. Herbert, J.J., and Muller, L.L., J. Appl. Polym. Sci. 18, 3373 (1974).
7. Sarko, A., and Muggli, R., Macromolecules 7, 486 (1974).
8. Andress, K.R., Z. Physik. Chem. B4, 190 (1929).
9. Stipanovic, A.J., and Sarko, A., Macromolecules 9, 851 (1976).
10. Mühlethaler, K., J. Polym. Sci. C, 28, 305 (1969).
11. Frey-Wyssling, A., Science, 119, 80 (1954).
12. Hess, K., Mahl, H., and Gütter, E., Kolloid Z. 155, 1 (1957).
13. Dolmetsch, H., and Dolmetsch, H., Kolloid Z. 185, 106 (1962).
14. Marx-Figini, M., and Schulz, G.V., Naturwiss. 53, 466 (1966).
15. Raab, D., et al, "Zellstoff-Papier", VEB Fachbuchverlag, Leipzig, 1970.
16. Szabolcs, V., and Szabolcs, I., in "Man-Made Fibers", Mark, H.F., Atlas, S.M., and Cernia, E., Eds., Interscience, N.Y., 1967, Vol. I, Page 341.
17. Keller, A., Phil. Mag. 2, 1171 (1957).
18. Fischer, E.W., Z. Naturf. 12a, 753 (1957).
19. Geil, P.H., "Polymer Single Crystals", Interscience, N.Y., 1963.
20. Wunderlich, B., "Macromolecular Physics", Academic Press, N.Y., Vol. I, 1973 and Vol. II, 1976.
21. Basset, D.C., Polymer 17, 460 (1976).
22. Stamhuis, J.E., and Pennings, A.J., Polymer 18, 667 (1977).

23. Pennings, A.J., J. Polym. Sci.: Polym. Symp. 59, 55 (1977).

24. Pennings, A.J., and Kiel, A.M., Kolloid Z. u. Z. Polymere 205, 160 (1965).

25. Pennings, A.J., van der Mark, J.M.A.A., and Booij, H.C., Kolloid Z. u. Z. Polymere 236, 99 (1970).

26. Wikjord, A.G., and Manley, R.St.John, J. Macromol. Sci. (Phys.) B4, 397 (1970).

27. Pelzbauer, Z., and Manley, R.St.John, J. Macromol. Sci. (Phys.) B4, 761 (1970).

28. Keller, A., and Willmouth, F.M., J. Macromol. Sci. (Phys.) B6, 493 (1972).

29. Mackley, M.R., and Keller, A., Polymer 14, 16 (1973).

30. Peterlin, A., Polymer Preprints - ACS 16, 315 (1975).

31. Blais, P., and Manley, R.St.John, Science 153, 539 (1966).

32. Wunderlich, B., Fortschr. Hochpolym. Forsch. 5, 568 (1968).

33. Chanzy, H.D., Bonjour, E., and Marchessault, R.H., Colloid Polym Sci. 252, 8 (1974).

34. Cooper, D., Ph.D. Thesis, McGill University, Montreal, 1973.

35. Flory, P., Proc. Roy. Soc. (London) A, 234, 73 (1956).

36. Ciferri, A., Polym. Eng. Sci. 15, 191 (1975).

37. Preston, J., Polym. Eng. Sci. 16, 298 (1976).

38. Wikjord, A.G., and Manley, R.St.John, J. Macromol. Sci. (Phys.) B2, 501 (1968).

39. Pennings, A.J., van der Mark, J.M.A.A., and Kiel, A.M., Kolloid Z. u. Z. Polymere 237, 336 (1970).

40. Keller, A., and Willmouth, F.M., J. Macromol. Sci. (Phys.) B6, 493 (1972).

41. Keller, A., and Mackley, M.R., Pure Appl. Chem. 39, 195 (1974).

42. Pennings, A.J., Lageveen, R., and de Vries, R.S., Colloid Polym. Sci. 255, 532 (1977).

43. Mandelkern, L., "Crystallization of Polymers", McGraw-Hill, N.Y., 1964.

44. Turnbull, D., and Fisher, J.C., J. Chem. Phys. 34, 820 (1949).

45. Lauritzen, Jr., J.I., and Hoffman, J.D., J. Chem. Phys. 31, 1680 (1959).

46. Price, F.P., in "Nucleation", Zettlemoyer, A.C., Ed., Marcel Dekker, N.Y., 1969.

47. Frank, F.C., and Tosi, M., Proc. Roy. Soc. (London) A, 263, 323 (1960).

48. Sanchez, I.C., and Di Marzio, E.A., J. Chem. Phys. 55, 893 (1971).

49. McHugh, A.J., J. Appl. Polym. Sci. 19, 125 (1975).

50. Keller, A., J. Polym. Sci. 15, 31 (1955).

51. Lauritzen, Jr., J.I., J. Res. Nat. Bur. Stand. 79A, 617 (1975).

52. Pennings, A.J., and Pijpers, M.F.J., Macromolecules 3, 261 (1970).

53. Zwijnenburg, A., and Pennings, A.J., Colloid Polym. Sci. 254, 868 (1976).

54. Peterlin, A., Polym. Eng. Sci. 16, 126 (1976).

55. Mackley, M.R., and Keller, A., Polymer 14, 16 (1973).

56. Torza, S., J. Polym. Sci. (Phys.) 13, 43 (1975).

57. Crowley, D.G., Frank, F.C., Mackley, M.R., and Stephenson, R.G., J. Polym. Sci. (Phys.) 14, 1111 (1976).

58. Frank, F.C., and Mackley, M.R., J. Polym. Sci. (Phys.) 14, 1121 (1976).

59. Pope, D.P., and Keller, A., Colloid Polym. Sci. 255, 633 (1977).

60. McHugh, A.J., and Schultz, J.M., Kolloid Z. u. Z. Polymere 251, 13 (1973).

61. Taylor, G.I., Phil. Trans. A, 223, 289 (1923).

62. Taylor, G.I., Proc. Roy. Soc. (London) A, 146, 501 (1934).

63. Frank, F.C., Proc. Roy. Soc. (London) A, 319, 127 (1970).

64. Marrucci, G., Polym. Eng. Sci. 15, 229 (1975).

65. Takserman-Krozer, R., J. Polym. Sci. A1, 2477 (1963).

66. Takserman-Krozer, R., J. Polym. Sci. A1, 2487 (1963).

67. Ziabicki, A., J. Polym. Sci. 2, 24 (1959).

68. Peterlin, A., Polym. Eng. Sci. 16, 126 (1976).

69. Peterlin, A., Polymer 2, 257 (1961).

70. Peterlin, A., J. Polym. Sci. B4, 287 (1966).

71. Mackley, M.R., and Keller, A., Phil. Trans. A, 278, 29 (1974).

72. Hlaváček, B., and Seyer, F.A., Kolloid Z. u. Z. Polymere 243, 32 (1971).

73. Meissner, J., Rheol. Acta 10, 230 (1971).

74. Wagner, M.H., Rheol. Acta 15, 133 (1976).

75. Lodge, A.S., "Elastic Liquids", Academic Press, N.Y., 1964.

76. Williams, M.C., A.I.Ch.E.J. 21, 1 (1975).

77. Bird, R.B., Hassager, O., and Abdel-Khalik, S.I., A.I.Ch.E.J. 20, 1041 (1974).

78. Acierno, D., Titomanlio, G., and Nicodemo, L., Rheol. Acta 13, 1040 (1974).

79. Taylor, G.I., Proc. Roy. Soc. (London) A, 146, 501 (1934).

80. Rumscheidt, F.D., and Mason, S.G., J. Colloid Sci. 16, 238 (1961).

81. Cox, R.G., J. Fluid Mech. 37, 601 (1969).

82. Torza, S., Cox, R.G., and Mason, S.G., J. Colloid and Interface Sci. 38, 395 (1972).

83. Grace, H.P., Eng. Foundation, 3rd Res. Conf. on Mixing, Andover, N.H. (1971).

84. Acrivos, A., Proc. Int. Colloquium Drops and Bubbles, Pasadena, Ca., Vol. II, 390 (1974).

85. Treiber, E., in "Polymer Handbook", Bandrup, J., and Immergut, E.H., Eds., Interscience, N.Y., 1975.

86. Spurlin, H.M., in "High Polymers", Ott, E., and Spurlin, H.M., Eds., Interscience, N.Y., 1954, Vol. V, Part II, Page 673.

87. Jayme, G., in "High Polymers", Bikales, N.M., and Segal, L., Eds., Interscience, N.Y., 1971, Vol. V, Part IV, Page 381.

88. Philipp, B., Schleicher, H., and Wagenknecht, W., in "ACS - Symposium Series 48", Arthur, Jr., J.C., Ed., Washington, D.C., 1977.

89. Johnson, D.C., Nicholson, M.D., and Haigh, F.C., Appl. Polym. Symp. 28, 941 (1976).

90. Swenson, H.A., Appl. Polym. Symp. 28, 945 (1976).

91. Johnson, D.L. (to Eastman Kodak), Brit. 1,144,759, Sept. 1, 1967.

92. Guthrie, J.T., and Hardcastle, S.V., Polymer 18, 203 (1977).

93. von Buchner, H.P., in "Man-Made Fibers", Mark, H.F., Atlas, S.M., and Cernia, E., Eds., Interscience, N.Y., 1968, Vol. II, Page 7.

94. McGarry, W.J., and Priest, M.H., in "Man-Made Fibers", Mark, H.F., Atlas, S.M., and Cernia, E., Eds., Interscience, N.Y., 1968, Vol. II, Page 43.

95. Kline, E., In "High Polymers", Ott, E., and Spurlin, H.M., Eds., Interscience, N.Y., 1971, Vol. V, Part II, Page 959.

96. Allen, S.L., Turvey, R.W., and Bolker, H.I., Appl. Polym. Symp. 28, 903 (1976).

97. Blades, H., and White, J.R. (to du Pont), U.S. 3,081,519, March 19, 1963.

98. Parrish, E. (to du Pont), U.S. 3,114,747, December 17, 1963.

99. Miller, I.K. (to du Pont), U.S. 3,338,884, August 29, 1967.

100. Parrish, E. (to du Pont), U.S. 3,419,345, December 31, 1968.

101. Parrish, E. (to du Pont), U.S. 2,988,782, June 20, 1961.

102. Morgan, P.W. (to du Pont), U.S. 2,999,788, September 12, 1961.

103. Duggins, R.B. (to du Pont), U.S. 3,018,091, January 23, 1962.

104. Parrish, E. (to du Pont), U.S. 3,062,702, November 6, 1962.

105. Blades, H. and While, J.R. (to du Pont), U.S. 3,081,519, March 19, 1963.

106. Schott, H. (to du Pont), U.S. 3,114,672, December 17, 1963.

107. Brundage, M.M., Hunger, G.K., Kohne, Jr., H.F., and Kurrle, F.L. (to West Virginia Pulp and Paper), U.S. 3,342,921, September 19, 1967.

108. Parrish, E. (to du Pont), U.S. 3,385,916, May 28, 1968.

109. Voith, J.M., GmbH, Brit. 1,205,509, September 16, 1970.

110. Kohne, Jr., H.F., Kurrle, F.L., and Li, F.S. (to Westvaco), U.S. 3,597,312, August 3, 1971.

111. Fowells, R.W. (to Crown Zellerbach), Can. 903,974, July 4, 1972.

CHAPTER II

OBSERVATIONS ON THE FORMATION OF CELLULOSE FIBRES FROM STIRRED SOLUTIONS

ABSTRACT

Like synthetic polymers a natural polymer such as cellulose may crystallize in fibrous form from stirred solutions. In the present work, it is demonstrated that cellulose fibres can be formed by precipitation from dimethyl sulfoxide/paraformaldehyde solutions by two different methods that involve different mechanisms of fibre formation, viz.:

A) Precipitation of cellulose by addition of non-solvent to the stirred cellulose solution;

B) Precipitation of cellulose by coagulation of droplets of cellulose solution in a stirred precipitant.

Both processes yield fibres with properties depending on the stirring speed and the coagulant strength. The molecular orientation and tensile strength of the fibres produced by method A was low, but increased with the stirring speed, while some fibres formed by method B reached extremely high orientation, depending on the thickness of the fibres. The two different mechanisms of fibre formation are discussed on the basis of the experimental observations.

INTRODUCTION

It is well known that fibrous structures are obtained when synthetic polymers are crystallized from solution in the presence of shear fields[1-6]. The fibrillar elements have a shish-kebab structure with a long central thread of extended molecules (the shish) and closely packed transversely arranged lamellae (the kebabs) composed of folded chains. The central filament is thought to be the true primary nucleus while the folded chain component arises from subsequent epitaxial overgrowth. The formation of fibrous crystals is closely connected with the existence, during crystallization, of a flow component with a longitudinal velocity gradient which is very effective in extending and aligning the chain molecules[6].

These observations have generated considerable interest and invite the question whether cellulose and cellulose derivatives would behave in a similar manner under equivalent conditions. Quite recently, Buléon, Chanzy and Roche[7] demonstrated that cellulose shish-kebabs are formed when low molecular weight cellulose triacetate in solution was deacetylated in the presence of Valonia microfibrils. In this case, however, the formation of the shish-kebab structures did not involve crystallization in a flow field. On the other hand, Bolhuis and Pennings[8] found that amylose stirrer crystallized from aqueous chloral hydrate solutions exhibited a fibrous texture showing a close resemblance to the shish-kebabs formed by synthetic polymers. Another system of special interest for the present investigation is that of cellulose xanthate (viscose) in sodium hydroxide solution, studied by Allen et al[9]. A cellulose xanthate solution was injected into a rapidly stirred coagulant and formed fibres with dimensions in the range of normal wood fibres. Subsequent regeneration of the xanthate fibres gave cellulose fibres. It is thought that in this process the xanthate is dispersed as droplets which are deformed by the acting hydrodynamic forces into liquid filaments in microdomains of extensional flow in the stirred coagulant. Similarly several patents[10-14] describe the preparation of fibrous precipitates of cellulose and other polymers by adding the polymer solution to a sheared coagulant.

Further experimental and theoretical studies of this process are of interest. The aim of the present work is to further explore the mechanism of formation, and the structure and properties of cellulose fibres obtained from stirred solutions especially in the case where cellulose of high molecular weight is used. The present chapter is chiefly concerned with a phenomenological description of the fibrous crystallization of cellulose from the new cellulose solvent dimethyl sulfoxide/paraformaldehyde (DMSO/PF)[15]. In subsequent chapters theoretical aspects of the problem will be discussed.

EXPERIMENTAL

a) Preparation of the Cellulose Solutions and Stirrer Crystallization Experiments

The cellulose used throughout the stirrer crystallization experiments was cotton linters; it had an intrinsic viscosity in DMSO/PF of 20 dl/g, and a weight average degree of polymerization of about 2200 according to Swenson's relation[16].

Most of the work was done on solutions of cellulose in DMSO/PF but some experiments were also made with cellulose xanthate dissolved in sodium hydroxide. The solutions were made as follows.

Viscose was prepared from cotton linters using a small scale laboratory method described by Kline[17] with some modifications, such as smaller steeping and aging times of the cellulose in order to achieve higher molecular weights. The solution contained 2 to 5% cellulose with a degree of polymerization of about 400. Degree of ripening and degree of substitution were estimated to be respectively between 15 to 20, and about 0.3.

For the dissolution of cellulose in DMSO/PF, the cellulose was first dried for several hours at 105°C and then soaked in DMSO for about 30 minutes under vacuum. The DMSO was previously dried over molecular sieves. Subsequently PF (about 2 parts per 100 parts of DMSO) was added, and the suspension was heated to about 120°C under constant stirring. The cellulose dissolved within a short time (≈ 10 min) forming a transparent solution. After cooling, the solution was stored in a sealed container in order to exclude moisture. Under these conditions, the cellulose solution is stable and the polymer does not degrade[15]. In general the solutions prepared had concentrations in the range of 1 to 1.5% cellulose. More dilute solutions were obtained by addition of pure DMSO.

The fibre formation experiments were carried out with a simple stainless steel paddle stirrer driven by a variable speed motor.

Two methods of fibre formation were used, namely (i) precipitation of cellulose by addition of a non-solvent to the stirred cellulose solution, and (ii) coagulation of droplets of cellulose solution in a stirred coagulant.

In the case of cellulose xanthate the coagulation was carried out with a mixture of 0.25M sodium sulfate, 0.125M zinc sulfate and 9.5% glucose and the coagulated xanthate was regenerated with 1M sulfuric acid.

For the system cellulose/DMSO/PF the precipitants were methanol or water.

b) Characterization of the Stirrer Crystallized Fibres

The samples were characterized by wide angle X-ray diffraction and by optical as well as scanning (Cambridge Stereo-Scan Mark II A) and transmission (JEM 6A) electron microscopy. All light optical observations and birefringence measurements were performed on a Zeiss Ultraphot II microscope which was also equipped with interference optics.

For a given preparation, average fibre length measurements were made by a statistical method which involved projecting the fibre image on a square grid and counting the intersections[18]. Measurements of fibre width were carried out on the optical microscope equipped with a stage micrometer, after the wet fibres had been solvent exchanged and dried in benzene in order to allow unrestricted shrinkage.

Examination of certain samples by high resolution electron microscopy was carried out with the aid of the negative staining technique. The samples were first dispersed by ultrasonication in water. Drops of the suspension were then dried on carbon coated grids and negatively stained with a dilute solution of uranyl acetate.

For the determination of the birefringence of the fibres, it was necessary to measure the thickness of the fibres and the difference in phase retardation for light with vibration direction along the fibre axis and orthogonal to it. The thickness was determined on the interference microscope, while the difference in phase retardation was measured on the polarizing microscope with the aid of a de Sénarmont compensator.

For the measurement of the fibre tensile strength, single fibres were glued to a sample holder and tested at room temperature and 50% relative humidity in an Instron tester using a load rate of 0.02 cm/min and a full scale load of 50 or 100 g.

RESULTS AND DISCUSSION

As indicated earlier two methods of fibre formation have been studied experimentally:

A) Precipitation of cellulose by addition of non-solvent to the stirred cellulose solution.

B) Precipitation of cellulose by coagulation of droplets of cellulose solution in a stirred precipitant.

Since the two methods involve different mechanisms of fibre formation and yield fibres of different properties, it is convenient to separate them in the following.

Method A

Typical fibres produced by this method are shown in Figure 1. The cellulose was precipitated by the addition of 15.5% water to a 0.1% cellulose solution in DMSO/PF that was stirred at 900 rpm. The fibres have dimensions in the range of 0.5 to 2 cm in length and 100 to 500 μm in width; there are no non-fibrous coagula present. The crystal structure of the fibres was found to be that of cellulose II. The influence of the stirring speed on the fibre dimensions is shown in Table 1. It can be seen that the length and the width of the fibres decrease with higher stirring speeds. The origin of this behaviour is not understood at present. The influence of the amount of precipitant added and the concentration of the cellulose solution on the dimensions of the fibres was also examined. Although variations in the fibre dimensions were observed there were no obvious systematic trends.

In order to get some information on the structure of the fibres, studies

Figure 1
Darkfield optical micrograph of cellulose fibres precipitated at a stirring speed of about 900 rpm from a 0.1% solution in DMSO/PF by addition of 15.5% water by volume. 3.4X.

TABLE 1

Properties of cellulose fibres obtained by method A at various stirring speeds from a solution of 0.12% cellulose in DMSO/PF after addition of 20% water. The orientation factor was calculated from eq. 2 using a value of $n_\alpha - n_\gamma = 0.055$.

Stirring Speed	Length Range	Length Mean	Width Range	Width Mean	Birefringence	Orientation Factor	Tensile Strength
rpm	mm	mm	μm	μm	-	-	10^6Pa
720	7 - 28	14	50 - 200	150	0.0095	0.173	62.8
920	11 - 21	16	40 - 220	120	0.0108	0.196	108.0
1170	6 - 33	12	40 - 120	60	0.0111	0.202	177.0
1440	3 - 8	5	15 - 35	25	0.0163	0.296	-

were carried out in the electron microscope. Figure 2 shows a transmission electron micrograph of a thin edge of a shadowed fibre preparation. It was found that the microfibrils on the surface of the fibres have a width of about 20 to 100 nm. They are preferentially oriented in the fibre axis direction, but their degree of orientation appears to be small. From investigations of ultrasonicated and negatively stained samples in the transmission electron microscope it was found that these microfibrils comprise 3.5 nm elementary fibrils as the smallest morphological units.

It is further of interest to investigate the degree of molecular orientation of the fibres because the orientation is closely related to the tensile strength of the fibres. The molecular orientation in the fibres was determined by birefringence measurements, which were carried out by measuring the difference in phase retardation, $\Delta\wp$, of plane polarized light penetrating the fibre with the vibration direction parallel and orthogonal to the fibre axis, and by determining the thickness, d, of the sample. The birefringence, Δn, is expressed by eq. 1,

$$\Delta n = \frac{\Delta\wp}{360}\frac{\lambda}{d} \qquad 1$$

where λ is the wavelength of the monochromatic light. Having determined Δn, the orientation factor f is given[19] by eq. 2,

$$f = \frac{\Delta n}{n_\alpha - n_\gamma} \qquad 2$$

where $n_\alpha - n_\gamma$ is the birefringence of fully oriented cellulose II, given by Hermans[19] as 0.055. A value of $f = 1$ is an indication of perfect orientation. When the birefringence is measured at different positions across a fibre, a birefringence profile is obtained. The birefringence varies across the width of the fibre suggesting that the orientation is non-uniform. The mean values

Figure 2

Transmission electron micrograph of a thin edge of a shadowed fibre preparation showing preferential but low orientation in the fibre axis direction. The arrow indicates the fibre axis direction. 86,000X.

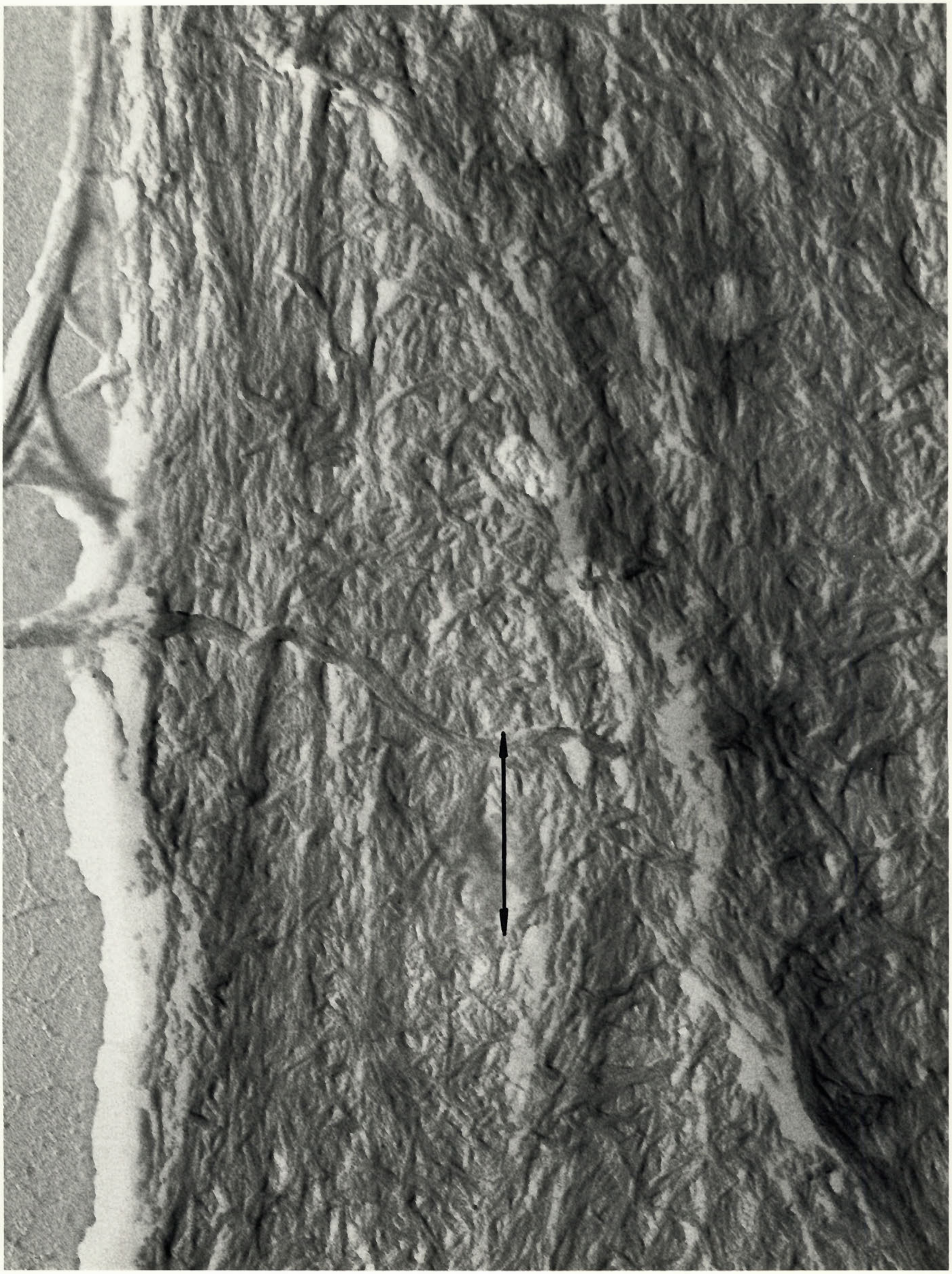

of the birefringence, averaged over the profile and over a number of 10 to 20 fibres, from different sample preparations yield with eq. 2 the orientation factor. The birefringence and the orientation factor are shown in Table 1. It can be seen that the orientation of the fibres is generally low, but increases with the stirring speed. Also shown in Table 1 is the average of the tensile strength of three series of single fibres. The tensile strength increases with the stirring speed as can be expected from the increase in orientation. For comparison it may be noted that the tensile strength of typical regenerated cellulose fibres (viscose textile rayon) lies in the range[20] of (200 to 500) x 10^6 Pa.

Wide angle X-ray diffraction patterns on single fibres also disclosed that the molecular orientation of the fibres is low. This result was inferred from the large angular spread of the arcs formed by the reflections in the diffraction pattern.

In the following an attempt is made to elucidate the mechanism of fibre formation for the fibres produced by method A. In this connection it was of interest to investigate the structure of cellulose precipitated under quiescent conditions, since this might give information about the initial step of fibre formation, immediately after the precipitant is added. For this purpose, water (about 50%) was carefully added to a dilute cellulose/DMSO/PF solution (about 0.01% cellulose) and the thus formed precipitate was examined in the electron microscope after slight ultrasonication and negative staining of the specimen. From the electron micrograph shown in Figure 3 it can be seen that the precipitation of cellulose under quiescent conditions resulted in a spontaneous formation of elementary fibrils having a width of approximately 3 to 4 nm. Since the same dimensions of the elementary fibrils were found for the fibres produced under stirring, it may be concluded that the flow field has

Figure 3

High resolution electron micrograph of cellulose precipitated under quiescent conditions and observed after slight ultrasonication and negative staining of the specimen. 132,000X.

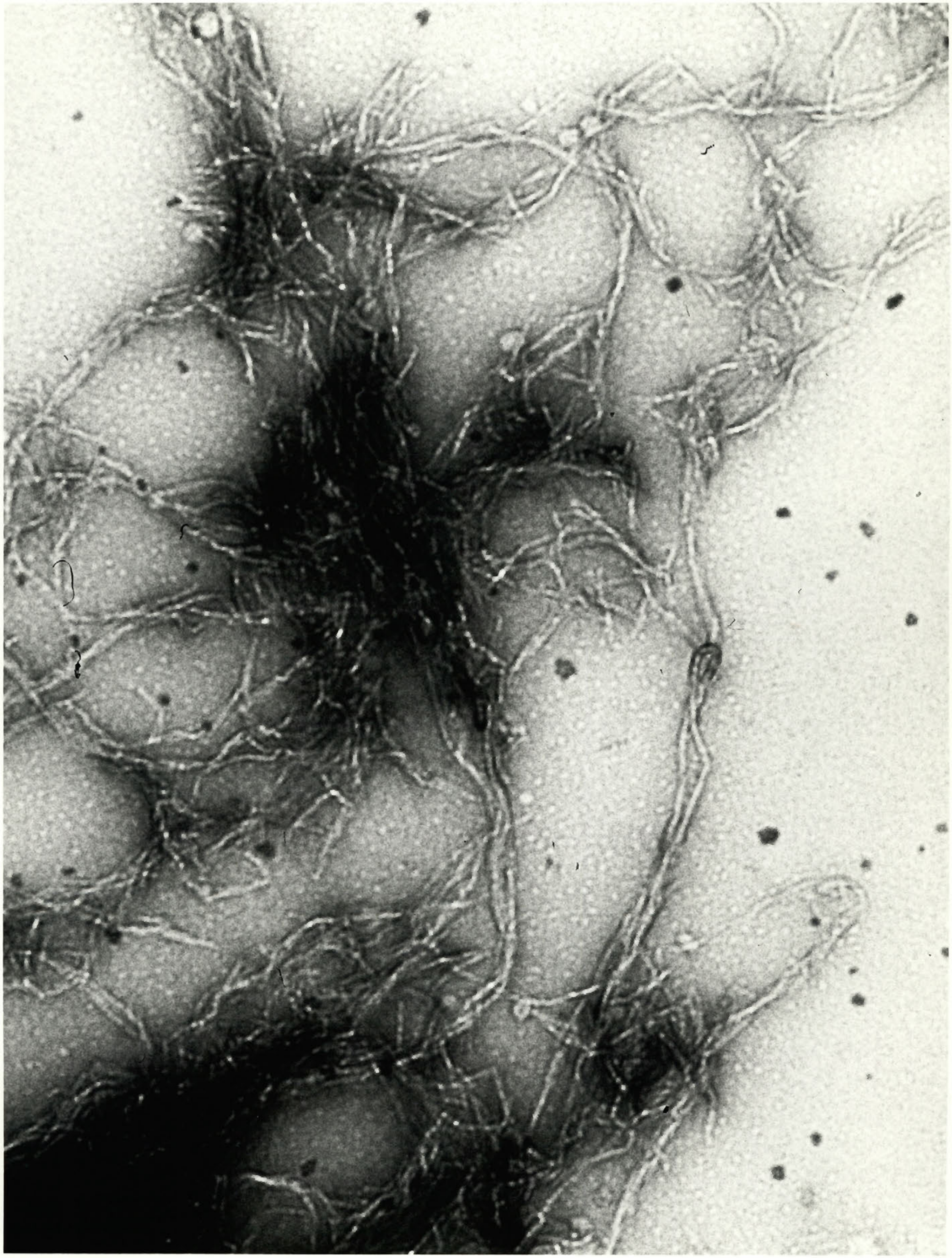

no influence on the formation of elementary fibrils. Further information about the subsequent organization of the elementary fibrils into fibres was obtained by observations in the optical microscope which were made at an early stage of fibre formation, shortly after the precipitant was added. Figure 4 is an optical micrograph in phase contrast, taken about 2 min after addition of 20% water to a 0.12% cellulose solution in DMSO/PF stirred at 920 rpm. The total precipitation time for this preparation was more than one hour and the final fibres had a width of over 100 μm. It can be seen in Figure 4 that the fibrous aggregates consist of microfibrils of 8 μm and less in width which apparently are in the process of being bundled together to form larger fibres. According to this and the other observations made above, the mechanism of fibre formation is thought to be as follows. As illustrated in Figure 5, the macromolecules precipitate from solution after addition of the coagulant and crystallize as 3.5 nm elementary fibrils. Subsequently, these elementary fibrils, which can be seen from Figure 3 to be relatively long and rigid structures, are aligned by the action of the flow field and aggregate into larger microfibrils that are about 20 to 100 nm in width. Eventually these microfibrils are themselves aligned to form the final macrofibre.

In this proposed fibre formation mechanism, unoriented cellulose materials may also be formed in regions where the flow field is very weak. These unoriented coagula that consist of elementary fibrils are also incorporated into the macrofibre. Thus the degree of orientation obtained in the fibres depends on the amount of unoriented cellulose present and also on the way the microfibrils coagulate to form macrofibres.

Figure 4

Optical micrograph with phase contrast showing the fibrillar structures formed in the early stage of formation (i.e. 2 min after the precipitant has been added). The small fibrils organize and form larger fibrous structures. 680X.

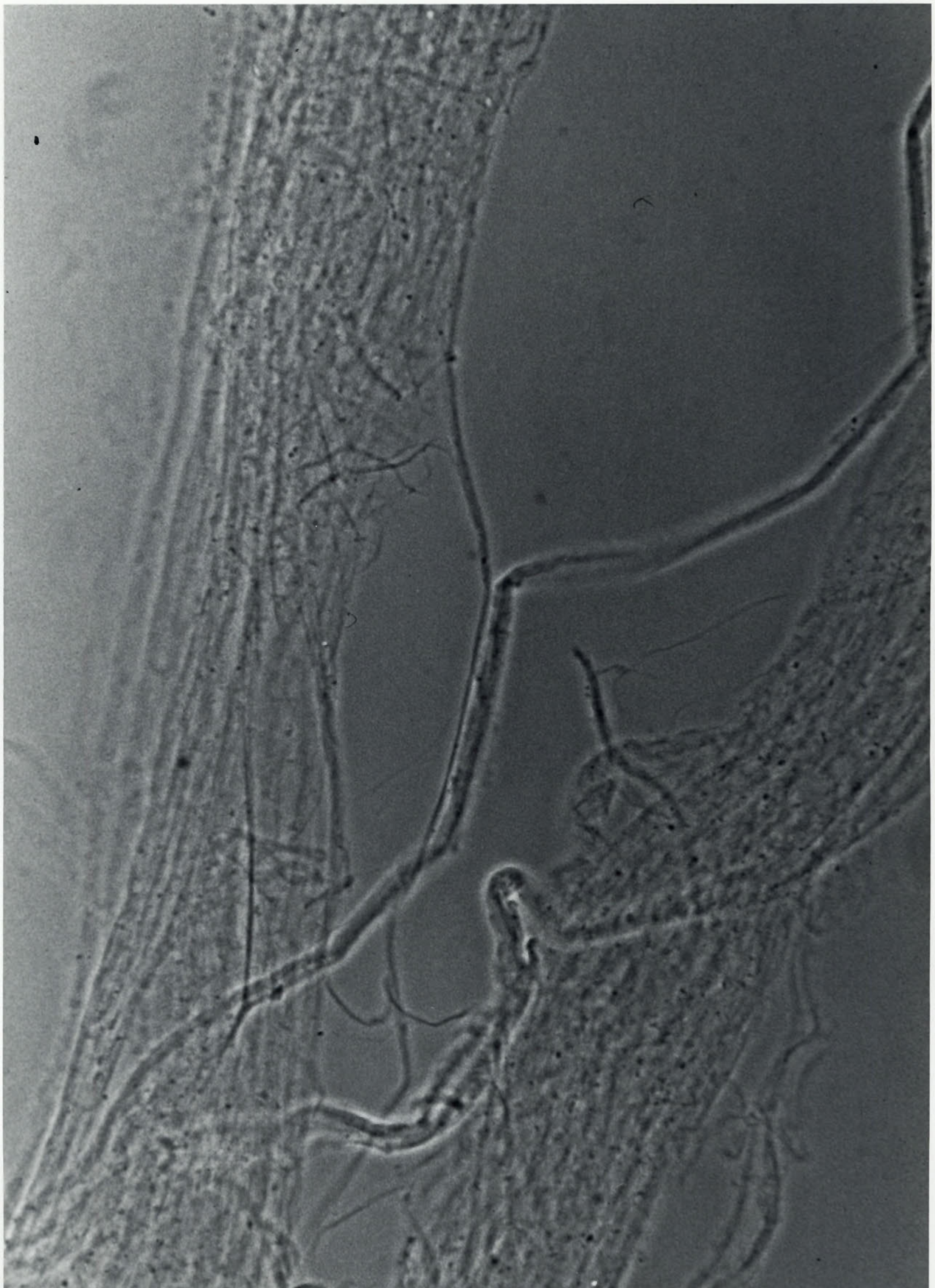

Figure 5

Illustration of the proposed fibre formation mechanism for method A. Due to the action of the flow field the crystallized elementary fibrils become extended and aligned and form microfibrils. Eventually these microfibrils are themselves aligned to form the final macrofibre. For simplicity non-fibrous coagula have not been included in the figure.

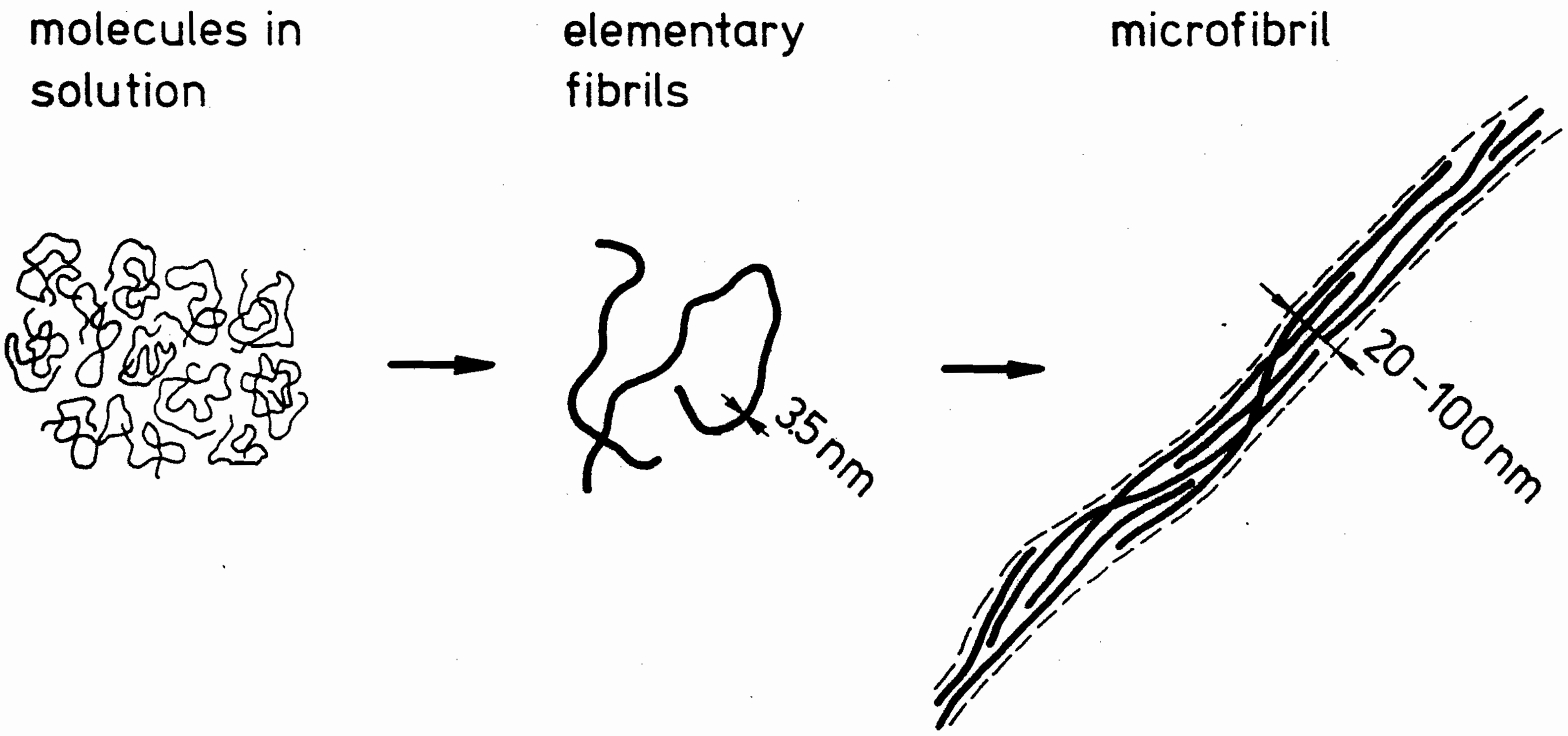
molecules in solution
elementary fibrils
microfibril
3.5 nm
20-100 nm

FIGURE 5

Method B

Method B deals with the preparation of cellulose by coagulation of drops of cellulose solution in a stirred precipitant. As already indicated, Allen et al[9] studied a similar method using cellulose xanthate precipitated from aqueous sodium sulfate and zinc sulfate solutions. We therefore thought it expedient to repeat their experiments, with slight alterations in the preparation of the cellulose xanthate solution and the precipitation process. Figure 6 shows a characteristic example of the fibres that were thus obtained. These cellulose xanthate fibres may subsequently be regenerated to give pure cellulose fibres which are shown in Figure 7. The fibres in Figures 6 and 7 seem to be flat in cross-section and have long tapered ends. According to Allen et al[9] the mechanism of formation of the fibres involves the dispersion of the viscous cellulose xanthate solution into droplets which become deformed by the action of the flow field. As will be seen shortly, the same mechanism seems to be operative in the system cellulose/DMSO/PF.

The fibres produced by the coagulation of drops of cellulose/DMSO/PF in stirred methanol either adhered to the stirrer as a network, similar to the observations with polyethylene[21], or were found as single fibres in the coagulant solution. Figure 8 shows an optical micrograph of a typical fibre preparation. The larger fibres in particular seemed to be ribbon-like in appearance. Various experimental observations, some of which are not detailed here, indicated that the dimensions and properties of the fibres depended on the cellulose concentration, the stirring speed and the strength of the coagulant. The fibre length lay in the range of 0.1 to 1.5 cm while the width varied from about 1 μm to several hundred micrometers.

The degree of orientation of the fibres was determined from birefrin-

<u>Figure 6</u>

Optical micrograph of cellulose-xanthate fibres precipitated in a mixture of 0.25M sodium sulphate, 0.12M zinc sulphate and 9% glucose stirred at 720 rpm. The glucose was added to increase the viscosity of the coagulant. 64X.

<u>Figure 7</u>

Optical micrograph of cellulose fibres produced by regeneration of the xanthate fibres shown in Figure 6. 148X.

Figure 8

Brightfield photomicrograph of a typical fibre preparation produced by the introduction of droplets of a 0.14% cellulose solution in DMSO/PF into methanol, stirred at 900 rpm. 64X.

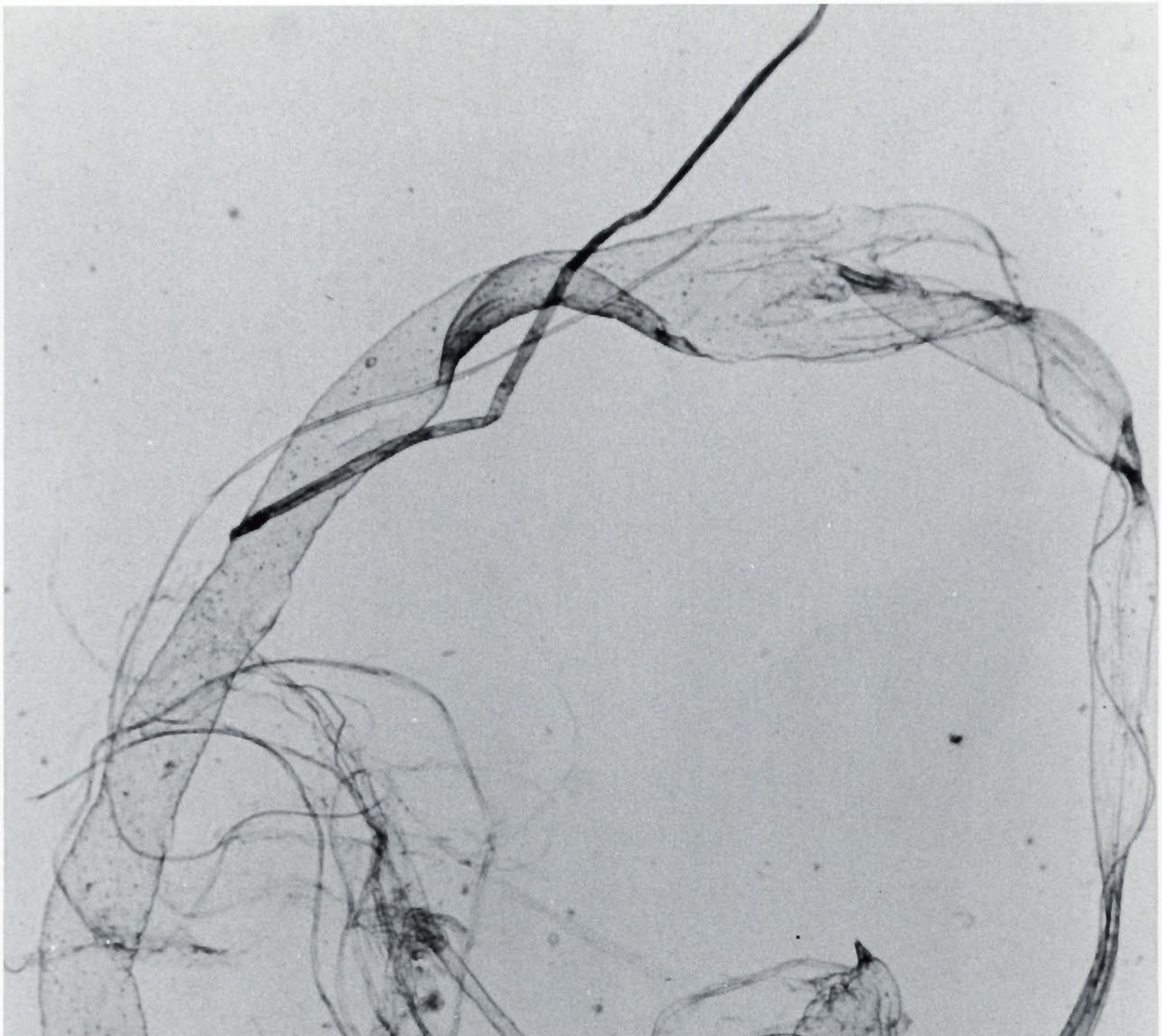

gence measurements (see method A). Some typical values of the birefringence and the orientation factor for fibres with different thickness are given in Table 2. It is seen that the f values cover a wide range with some of the finest fibres having close to perfect orientation.

The surface topography of a well oriented fibre can be seen in the scanning electron micrograph shown in Figure 9. A typical surface replica of such a fibre at high magnification in the transmission electron microscope is presented in Figure 10. The smallest microfibrils observed have a width in the range of 10 to 20 nm and are preferentially aligned in the fibre axis direction. In further transmission electron microscope observations of ultrasonicated samples the texture of the fibres was also revealed as fibrous, the microfibrils being further constituted of the 3.5 nm elementary fibrils which have been suggested to be the fundamental constituents of all cellulose fibres[22].

As in method A, wide angle X-ray diffraction patterns disclosed that the crystal structure of the fibres is that of cellulose II.

In discussing the possible mechanism of fibre formation it is important to note the following observation. When a droplet of viscous cellulose solution is added to a stirred coagulant it is observed that the drop is elongated, the elongation being greater the higher the stirring speed. It is essential to call attention to the fact that the droplet is not completely dispersed.

On the strength of these visual observations a mechanism of fibre formation similar to that proposed by Allen et al[9] can be envisaged: when the cellulose solution is introduced into a rapidly stirred coagulant, it is dispersed into smaller drops. These droplets are extended into long liquid threads in domains of extensional flow and finally solidify when sufficient coagulant has diffused across the boundary between cellulose solution and

TABLE 2

Some typical values for the birefringence and orientation factor for cellulose fibres formed by method B. To obtain these measurements two different fibre preparations were used. Three fibres were selected at random from one preparation (specimens 1 to 3, produced by addition of drops of cellulose solution with a concentration of 0.14% cellulose to methanol stirred at 720 rpm) and five from another (specimens 4 to 8, produced as above, but at a stirring speed of 540 rpm). Because of experimental difficulties the tensile properties were not measured. The orientation factor was calculated from eq. 2 with $n_\alpha - n_\gamma = 0.055$.

Specimen	Thickness µm	Birefringence -	Orientation Factor -
1	0.52	0.038 ± 0.004	0.69
2	3.4	0.029 ± 0.002	0.53
3	11.1	0.008 ± 0.002	0.15
4	0.49	0.044 ± 0.002	0.80
5	1.33	0.058 ± 0.005	1.0
6	2.13	0.050 ± 0.001	0.91
7	2.36	0.053 ± 0.001	0.96
8	5.0	0.024 ± 0.001	0.44

<u>Figure 9</u>

Scanning electron micrograph of the surface of a well oriented fibre produced by method B. 11,500X.

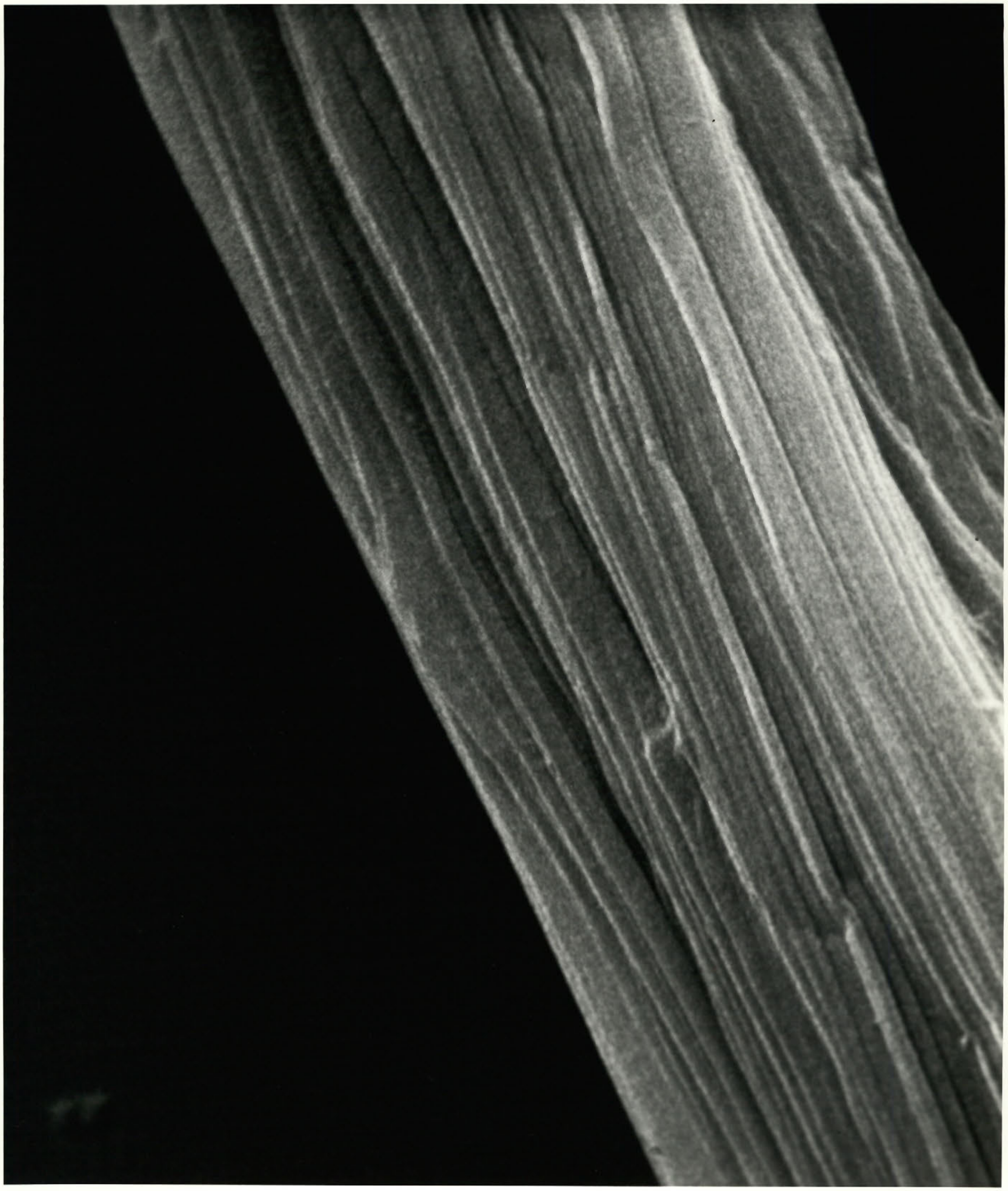

Figure 10

Surface replica of a fibre produced by method B showing that the smallest microfibrils observed are 10 to 20 nm in width. When these fibres are ultrasonicated in water they are found to be composed ultimately of 3.5 nm elementary fibrils. The arrow indicates the fibre axis direction. 134,000X.

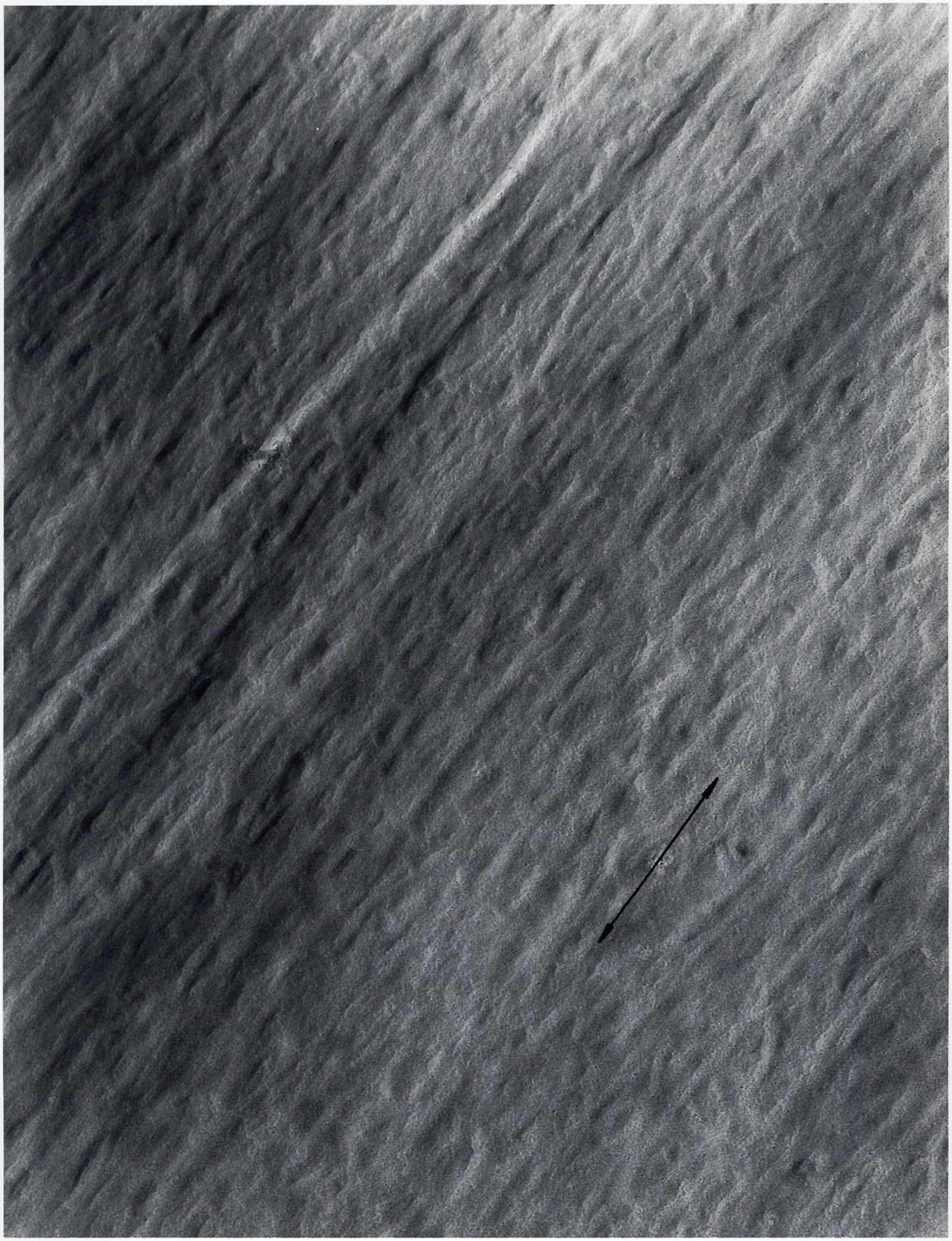

coagulant.

An example of a simple droplet deformation mechanism is shown in Figure 11. Drop and dispersing medium (coagulant) are assumed to have the same viscosity, and zero interfacial tension (in real systems there exists a very small and transient interfacial tension between miscible liquids[23]). The drop therefore deforms at the same rate as the surrounding liquid. An extensional flow field as supplied by a four-roller-mill[24-27] was chosen. Here there is two-dimensional hyperbolic flow in the XY plane with extension along the X-axis. Every fluid particle in this droplet deformation process follows hyperbolic streamlines, thus the shape of the drop can be constructed by simple geometrical considerations at any time of deformation. It is seen in Figure 11, which shows the drop in the Y-X and Z-X plane, that the originally spherical drop becomes extended to fibre dimensions with increasing times $t_o < t_1 < t_2$. The deformed drops in this two-dimensional flow field are flat in cross-section. If the conditions for coagulation are selected so that the liquid fibre solidifies at certain elongations, fibres of any dimensions may be produced.

It may also be noted that for drops that differ in their viscosity from that of the continuum, the deformation can be calculated according to Taylor's droplet deformation theory[24], though only for small deformations. No theories are yet available that describe the high droplet deformations occurring in this fibre formation mechanism.

Figure 11

Illustration of the proposed mechanism of fibre formation for method B. The drops of cellulose solution become increasingly elongated by the action of the extensional flow field with increasing time $t_o < t_1 < t_2$. The upper part of the figure shows the top view and the lower the side view of the deforming drop.

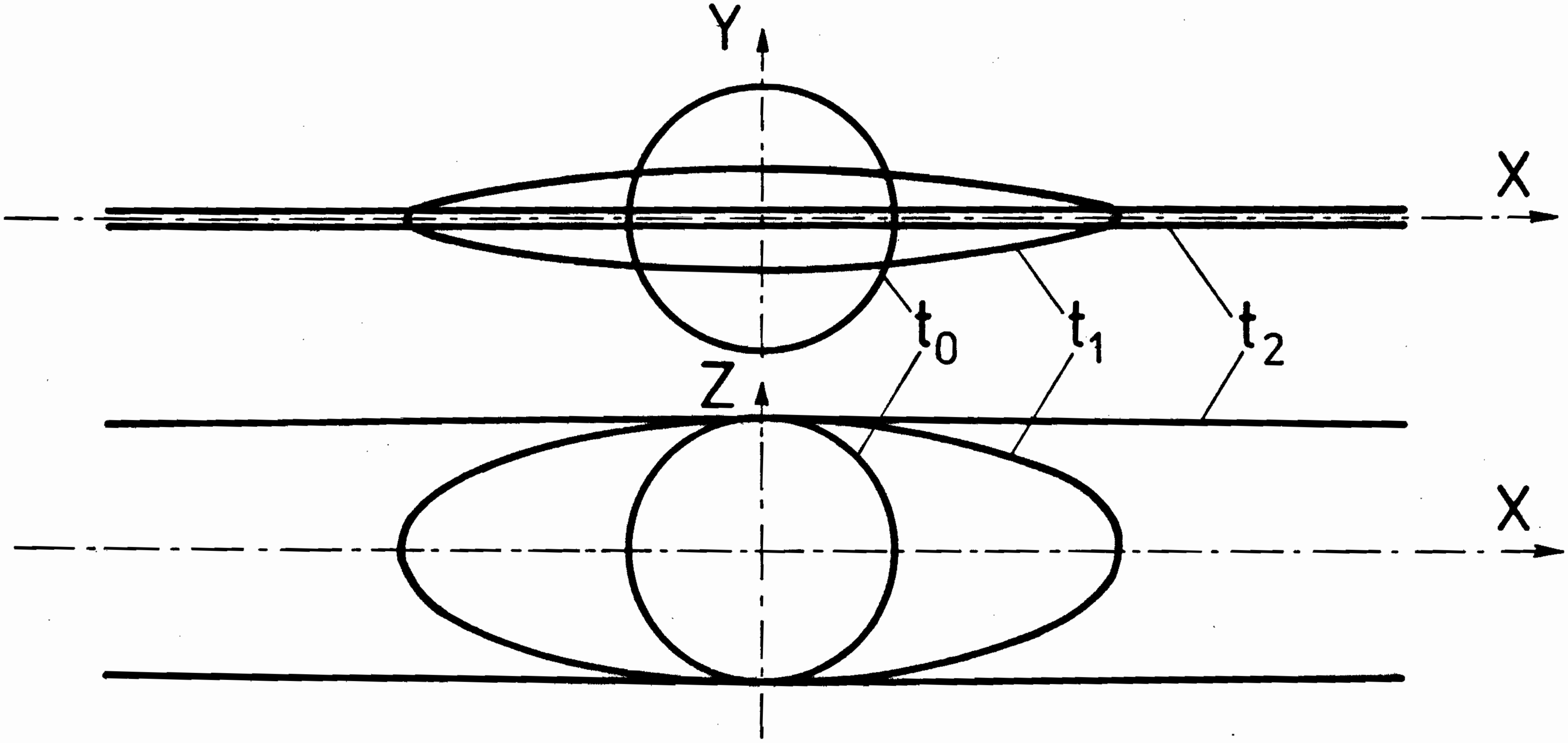

FIGURE 11

CONCLUSION

In fibre formation by method A, it is thought that elementary fibrils of cellulose are precipitated by the addition of coagulant. These elementary fibrils then become extended and aligned in regions of extensional flow in the turbulent flow field, and subsequently form microfibrils which aggregate further as macrofibres. Fibres produced by this method exhibit properties that depend on the stirring speed, the concentration of the cellulose solution, and the amount of water added. The dimensions clearly decrease while the orientation increases with the stirring speed. The samples produced by this method are free of non-fibrous coagula, but the fibres have a low degree of orientation. At present this mechanism of fibre formation does not appear to be amenable to a theoretical analysis.

In method B, where the cellulose solution is added to the stirred coagulant, the fibres form as a result of the dispersion of the introduced cellulose solution as droplets, followed by deformation of the droplets and their subsequent coagulation. Coagulation sets in when sufficient coagulant has diffused into the deforming drop. The fibres produced by this mechanism are less uniform in their size throughout the sample than those from method A, but the degree of orientation is higher particularly for fibres with smaller lateral dimensions; the orientation factor is unity for some of the finest fibres.

These findings indicate that method B is very promising for producing highly oriented fibres. Furthermore, the droplet deformation mechanism seems to be accessible for theoretical studies which may yield information about the conditions for obtaining fibres of high orientation and may permit predictions of the fibre length to be expected under given experimental conditions. In subsequent chapters[28] we will therefore concentrate on method B.

Finally it is interesting to note that the shish-kebab structures frequently observed with synthetic polymers do not form in the case of cellulose. This may be related to the fact that high molecular weight cellulose does not crystallize from solution in lamellar form; it crystallizes as 3.5 nm elementary fibrils[22]. Only very low molecular weight cellulose (degree of polymerization approximately 30) can form lamellar crystals from solution[7]. Accordingly, the lamellar overgrowth, that is a typical morphological constituent of shish-kebabs, cannot be formed and only smooth fibres are observed.

REFERENCES

1. Wikjord, A.G., and Manley, R.St.John, J. Macromol. Sci. (Phys.) B4, 397 (1970).

2. Pelzbauer, Z., and Manley, R.St.John, J. Macromol. Sci. (Phys.) B4, 761 (1970).

3. Pennings, A.J., and Kiel, A.M., Kolloid Z.u.Z. Polymere 205, 160 (1965).

4. Pennings, A.J., J. Polym. Sci.: Polym. Symp. 59, 55 (1977).

5. Keller, A., and Willmouth, F.M., J. Macromol. Sci. (Phys.) B6, 493 (1972).

6. Peterlin, A., Polymer Preprints - ACS 16, 315 (1975).

7. Buléon, A., Chanzy, H., and Roche, E., J. Polym. Sci. (Phys.) 14, 1913 (1976).

8. Bolhuis, H.H., and Pennings, A.J., J. Macromol. Sci. (Phys.) B11, 455 (1975).

9. Allen, S.L., Turvey, R.W., and Bolker, H.I., Appl. Polym. Symp. 28, 903 (1976).

10. Parrish, E., McCartney, J.R., and Morgan, P.W. (to du Pont), U.S. 2,988,782, June 20, 1961.

11. Parrish, E. (to du Pont), U.S. 3,114,747, Dec. 17, 1963.

12. Kohne, Jr., H.F., Kurrle, F.L., and Li, F.S. (to Westvaco), U.S. 3,597,312, August 3, 1971.

13. Voith, J.M., GmbH, Brit. 1,205,509, Sept. 16, 1970.

14. Morgan, P.W. (to du Pont), U.S. 2,999,788, Sept. 12, 1961.

15. Johnson, D.C., Nicholson, M.D., and Haigh, F.C., Appl. Polym. Symp. 28, 941 (1976).

16. Swenson, H.A., Appl. Polym. Symp. 28, 945 (1976).

17. Kline, E., in "High Polymers", Ott, E., and Spurlin, H.M., Eds., Interscience, N.Y., 1971, Vol. V, Part II, Page 959.

18. Clark, D'A.J., Pulp Paper Can. 63, T-53 (1962).

19. Hermans, P.H., "Physics and Chemistry of Cellulose Fibres", Elsevier, N.Y., 1949.

20. Wooding, N.S., in "Fibre Structure", Hearle, J.W.S., and Peters, R.H., Eds., Textile Institute and Butterworths, Manchester, 1963, Page 455.

21. Pennings, A.J., van der Mark, J.M.A.A., and Booij, H.C., Kolloid Z.u.Z. Polymere 236, 99 (1970).

22. Manley, R.St.John, J. Polym. Sci. A-2, 9, 1025 (1971).

23. Freundlich, H., "Colloid and Capillary Chemistry", Methuen & Co., London, 1926.

24. Taylor, G.I., Pro. Roy. Soc. (London), A, 146, 501 (1934).

25. Torza, S., J. Polym. Sci. (Phys.) 13, 43 (1975).

26. Crowley, D.G., Frank, F.C., Mackley, M.R., and Stephenson, R.G., J. Polym. Sci. (Phys.) 14, 1111 (1976).

27. Pope, D.P., and Keller, A., Colloid Polym. Sci. 255, 633 (1977).

28. Chapters III, IV and V.

CHAPTER III

FIBRE FORMATION BY DEFORMATION OF DROPLETS AT LOW EXTENSIONAL FLOW RATES

ABSTRACT

Taylor's droplet deformation theory and Cox's slender body theory have been used to derive expressions for small and high deformations of droplets with negligible interfacial tension between drop and suspending medium. The theory applies for deformations in extensional flow at small strain rates and yields expressions for the time dependence of the droplet deformation. On the basis of experimental studies which were carried out on a four-roller-mill, semi-empirical equations were obtained describing the whole range of small to very large deformations. The theory predicts that the strain rate inside the drop increases with time and becomes equal to that of the flow outside (G/2) when large deformations are reached, and furthermore,that Gt is the main deformation parameter comprising the time. The theory is shown to apply for viscosity ratios between 1 and about 20. The significance of the results of the present study for the fibre formation processes involving deformation of polymer drops in flowing coagulants is discussed.

LIST OF SYMBOLS

A, B, C = coefficients in the parabolic deformation function

a, b, c = ellipsoidal semi-axes in the x, y, and z-direction respectively

a', b', c' = ellipsoidal semi-axes in the x, y, and z-direction respectively, when the z-dimensions of the ellipsoid change

$F(x)$ = force per unit length acting on a slender body at the position x in the x-direction

G; $G/2$ = shear rate; strain rate

$G\bar{t}$ = time coordinate of the point of intersection of tangent and asymptote drawn on the deformation curves

k = strain rate of hyperbolic flow inside the drop

ℓ; ℓ_o = length of deformed drop; diameter of spherical drop

N = speed of rotation of the rollers in rpm

$\underline{n}$ = normal unit vector for ellipse

p = pressure

r_o = initial radius of drop

t; t' = time; time needed to extend drop to $\alpha = 3$

$\underline{t}$ = tangential unit vector for ellipse

$\underline{U}_1$ = velocity field inside the drop

u, v, w = velocity components in the x, y, and z-direction respectively for the external flow

u_1, v_1, w_1 = velocity components in the x, y, and z-direction respectively for the internal flow

u_s, v_s, w_s = velocity components at the surface of the drop

x, y, z = coordinates outside the drop

x_1, y_1, z_1 = coordinates inside the drop

α; α' = length ratio ℓ/ℓ_o; α at $t = t'$

β = coefficient

δ_{ij} = Kronecker's delta

λ; λ' = viscosity ratio, μ_1/μ; viscosity ratio for corrected theory

μ, μ_1 = viscosities of continuum and drop respectively

ν, ν_1 = kinematic viscosities of continuum and drop respectively

ϕ, θ = spherical coordinates

ρ, ρ_1 = densities of continuum and drop respectively

τ_t, τ_{t1} = tangential stress due to external and internal flow field respectively

τ_{ij} = stress tensor

INTRODUCTION

The formation of fibres by precipitation from vigorously stirred cellulose solutions has been described previously[1,2]. The mechanism proposed is that the viscous cellulose solution is first dispersed as droplets in the precipitant; a droplet deformation process then occurs in regions of the system where extensional flow prevails. Subsequently, coagulation occurs when sufficient coagulant has diffused across the boundary between the deformed drop and the suspending medium and yields a solid fibre. The two steps, the droplet deformation step and the coagulation step, proceed simultaneously, but, because of the complexity in describing them mathematically, it is convenient to study them separately. This chapter will mainly be concerned with the droplet deformation step, while the coagulation step will be studied in chapter V.

Since the flow of polymer solutions is the main factor determining the orientation of the molecules[3-5] and therefore the properties of the fibres, a theoretical study of the hydrodynamics involved is of interest. Flowing polymer solutions are normally characterized by the variation of the viscosity with the shear rate[6] and the appearance of elongational viscosity[3,7,8]. These effects, however, exist only to a very small extent at low shear rates in these non-Newtonian liquids and can be neglected in the present investigation. Theoretical and experimental studies can therefore be carried out with Newtonian liquids.

Existing knowledge[9-19] of the deformation and burst of drops in pure and simple shear have recently been reviewed by Acrivos[20]. These studies are mainly for systems with interfacial tension between drop and suspending medium. However, the systems under investigation in the present work have only a negligible interfacial tension because the solvent for the polymer and the coagulant are miscible. Taylor[10] and Cox[11] considered such systems as a special case in their derivations, but only for very small deformations. Accordingly, it was of interest to derive a theory which applies for high deformation, since a fibre is actually a solidified and highly extended liquid thread. The present work deals with the process of droplet deformation at negligible interfacial tension, covering the whole range of small and high deformations.

It is well known that surface tension tends to retain droplets in a spherical shape, and has therefore to be overcome by large hydrodynamic forces when liquid threads are to be obtained. Moreover, the burst of drops[10] is to be avoided in the present context, since it yields smaller droplets instead of fibres. Because of both effects of the surface tension, namely, the resistance to deformation and the possibility of bursting, fibre forming processes that are based on droplet deformation should only involve systems with very low or zero surface tension. Of course, when the viscous forces in a system are much higher than the surface tension contribution, the surface tension may be unimportant.

The studies in this chapter will be carried out at low strain rates, allowing the flow to be described by the relatively simple slow motion equation. Although the orientation of the molecules is favoured by the presence of high strain rates[3,4], the underlying mechanism for the fibre formation can be described completely by studies at low strain rates. Moreover, the use of small strain rates opens the possibility of performing experiments on droplet deformations in order that the theoretical predictions can be tested.

THEORETICAL

Taylor's Theory for Small Deformations

The basic theory of droplet deformation for very small deformations in slow motion was established by Taylor[9,10]. He derived expressions for the velocity components at the surface of droplets without interfacial tension undergoing deformation in a hyperbolic flow field, defined by eqs. 1 to 3 for far distances from the drop.

$$u = \frac{G}{2}x \qquad 1$$

$$v = -\frac{G}{2}y \qquad 2$$

$$w = 0 \qquad 3$$

Here u, v, and w are the velocities in the x, y, and z-direction respectively; G/2 is the strain rate of the flow field outside the drop and G the shear rate. Taylor's expressions for the velocity components at the surface of the drop read

$$u_s = 2B_2 r_o \cos\phi \sin\theta \qquad 4$$

$$v_s = -\ 2B_2 r_o \sin\phi \sin\theta \qquad 5$$

$$w_s = 0 \qquad 6$$

$$B_2 = \frac{5G\mu}{4(2\mu_1 + 3\mu)}\ , \qquad 7$$

where r_o is the radius of the undeformed drop, μ_1 and μ are respectively the viscosities of the drop and the suspending medium. ϕ and θ denote the usual spherical coordinates and the index s represents the surface of the drop.

The interest in the present investigation lies especially in the length of the drop along the x-axis, corresponding to the major axis where

$\phi = 0$ and $\theta = 90^{o}$. The substitution of this and the viscosity ratio λ, which is the ratio of the viscosities of the drop and the suspending medium, ${}^{\mu}1/\mu$, lead to the deformation velocity in the x-direction, given by eq. 8.

$$u_s = \frac{5Gr_o}{2(2\lambda + 3)} \qquad 8$$

In these derivations Taylor neglected the additive term in the brackets and ended up with a formula that is only valid for high viscosity ratios. The present study, however, will also be concerned with small viscosity ratios, which makes it necessary to employ the full formula. Since u represents the time derivative of the semi major axis, the length of the drop as a function of time may be obtained by the integration of eq. 8 with respect to time. The result is given by the expression in eq. 9,

$$\frac{\ell}{\ell_o} = \frac{5Gt}{2(2\lambda + 3)} + 1 \qquad 9$$

where ℓ_o represents the diameter of the spherical drop.

It is advantageous, as will be shown later, to express the deformation of the drop by the natural logarithm of the length ratio.

With eq. 9 and recalling that

$$\ln(1 + x) = x + \mathcal{O}\{ - \frac{x^2}{2!} + \frac{2x^3}{3!} - \ldots\} , \qquad 10$$

the relative length of the drop can be approximated by eq. 11.

$$\ln\frac{\ell}{\ell_o} = \frac{5Gt}{2(2\lambda + 3)} \qquad 11$$

Theory for Large Deformations

Though the theories for droplet deformations at very small deformations are well established, no theoretical expressions have yet been derived for droplets with high deformations and zero surface tension. An attempt has therefore been made to develop a theory for high deformations, which is outlined in the following.

A schematic diagram of the arrangement of drop and flow field is shown in Figure 1, where a and b are the semi-axes of the drop in the x and y direction. The initially spherical drop with a radius c is deformed due to the shear that is applied from the flow field outside the drop. This flow field is plane and hyperbolic at far distances from the drop and can be described by eq. 2.

The flow field outside the drop and near to it is disturbed by the presence of the droplet, and will be characterized by expressions of Cox's slender body theory[21,22] which assumes slow motion conditions. The slow motion equation applies for very small Reynolds numbers, Re. It can therefore be used here to describe the flow field, because Re for typical experimental conditions is in the order of

$$Re = \frac{\ell \frac{\ell}{2} \frac{G}{2}}{\nu} \approx 2.5 \times 10^{-2}, \qquad 12$$

for $G = 1 \sec^{-1}$, $\ell = 1$ cm, and a kinematic viscosity $\nu = 10$ stokes.

In order to solve the problem, the flow field inside the drop must also be considered. The comparison of the tangential stresses from both flow fields at the interface will then yield an expression for the deformation of the drop. It is assumed that the flow field inside the drop follows the slow motion equation and can be expressed by eqs. 13 to 15,

Figure 1

Schematic diagram of drop and flow field. a and b are the semi-axes of the drop in the x and y-direction. The dashed circle corresponds to the initial drop diameter.

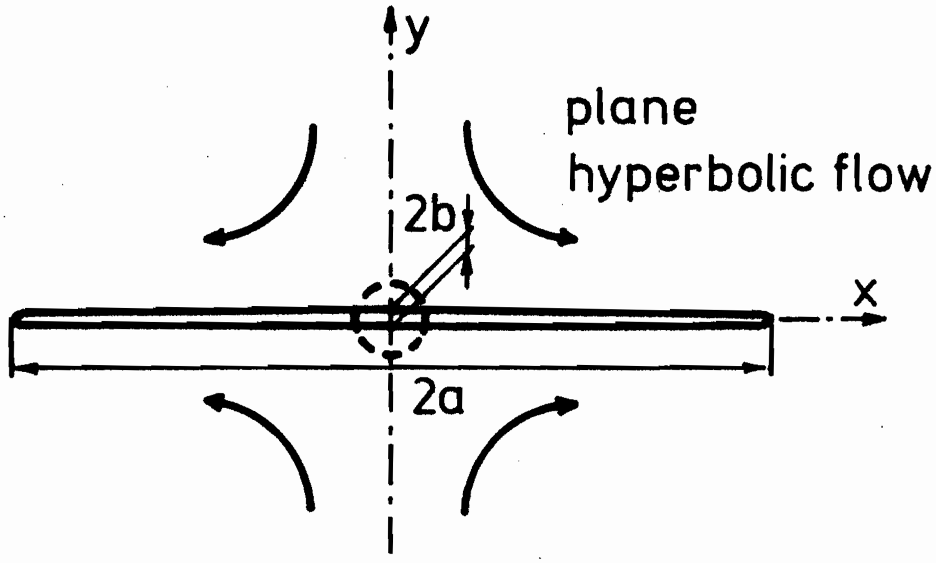

FIGURE 1

$$u_1 = kx_1 \qquad 13$$

$$v_1 = -ky_1 \qquad 14$$

$$w_1 = 0 \qquad 15$$

where k is a longitudinal velocity gradient to be determined and the index 1 indicates the flow inside the drop. Though eqs. 13 to 15 are limited in their application to high viscosity ratios and large deformations, as demonstrated in more detail in chapter IV, the results to be obtained will give good qualitative answers and can also describe the deformation mechanisms quantitatively when small modifications are made. The slow motion equation also applies here, since the viscosity of the drop is always greater than or equal to that of the continuum.

In the theory, the drop always remains an ellipsoid, because the equation for an ellipsoid retains its character when the time dependence of the semi-axes according to eqs. 13 to 15 is introduced:

$$\frac{x^2}{\left[c\exp\left({}_o\int^t k\,dt^*\right)\right]^2} + \frac{y^2}{\left[c\exp\left(-{}_o\int^t k\,dt^*\right)\right]^2} + \frac{z^2}{c^2} = 0 \; . \qquad 16$$

The z-dimension c is taken to be constant (this assumption will be tested experimentally later); it is therefore equal to the radius of the initially spherical drop.

In order to calculate the tangential stress exerted on the drop by the external flow, use has been made of Cox's slender body theory[21] which gives the tangential stress in the form of a force per unit length. It is shown in Appendix I that, for a deforming spheroid in hyperbolic flow, the expression for the force per unit length in the x-direction, F(x), takes the form of eq. 17.

$$F(x) = \frac{2\pi\mu(\frac{G}{2} - k)x}{\ln\frac{2a}{b} - \frac{3}{2}} + \mathcal{O}\{\frac{1}{(\ln\frac{b}{a})^3}\} \qquad 17$$

Here a represents the semi-major axis of the spheroid in the x-direction, and b is the radius of the circular cross-section. The second term is a measure of the error in F(x) for various axis ratios a/b.

The formula above can be modified according to Batchelor[23] for general ellipsoids with the semi-axes a, b, and c. Following his procedure, $\frac{1}{2}(b + c)$ is substituted for b in eq. 17. The force per unit length in the x-direction is then expressed by eq. 18.

$$F(x) = \frac{2\pi\mu(\frac{G}{2} - k)x}{\ln\frac{4a}{b + c} - \frac{3}{2}} \qquad 18$$

The condition for constant volume of the drop:

$$\frac{4\pi}{3}abc = \frac{4\pi}{3}c^3 = \text{constant}\ , \qquad 19$$

yields eq. 20.

$$b = \frac{c^2}{a} \qquad 20$$

The tangential stress from the flow outside the drop, τ_t, can be calculated by dividing F(x) by the circumference of the cross-section at the position x of the drop, and is expressed by eq. 21.

$$\tau_t = \frac{F(x)}{4c\left[1 - (\frac{x}{a})^2\right]^{\frac{1}{2}}} \qquad 21$$

Here, the assumption was made that τ_t is constant across the drop at a fixed position x. The root in the denominator accounts for the variation of the ellipsoidal cross-section with increasing x. Substitution of eqs. 18 and 20 in eq. 21 results in eq. 22.

$$\tau_t = \frac{\pi\mu(\frac{G}{2} - k)x}{2c\left\{1 - (\frac{x}{a})^2\right\}^{\frac{1}{2}}\left\{\ln\frac{4a^2}{c(c + a)} - \frac{3}{2}\right\}} \qquad 22$$

This equation describes the tangential force that is exerted on the deforming drop by the flow field outside the drop.

In order to obtain an expression for the tangential stress due to the flow inside the drop a procedure is employed that was suggested by Cox[24]. The flow inside the drop follows the slow motion equation:

$$\nabla p_1 = \rho_1 \nu_1 \nabla^2 \underline{U}_1 \ . \qquad 23$$

where $\underline{U}$ is the velocity vector, ρ and p are the density and the pressure respectively and the index 1 denotes the flow inside the drop. The stress tensor for incompressible fluids in slow motion is simply expressed by[25]

$$\tau_{ij} = -p\delta_{ij} + \rho_1\nu_1\left(\frac{\partial u_i}{\partial x_j} + \frac{\partial u_j}{\partial x_i}\right) . \qquad 24$$

Here i and j are 1, 2, 3 and solely represent the 3 coordinates in a different notation. δ_{ij} is Kronecker's delta being equal to 1 for $i = j$. For the hyperbolic and two-dimensional flow field that is given by the eqs. 13 to 15 the stress tensor is:

$$\tau_{ij} = \begin{vmatrix} -p + 2\rho_1\nu_1 k & 0 & 0 \\ 0 & -p-2\rho_1\nu_1 k & 0 \\ 0 & 0 & -p \end{vmatrix} . \qquad 25$$

This stress tensor now enables one to find the tangential stress when the geometry of the drop is defined. The drop here was assumed to be an ellipsoid with constant z-dimensions and in this case the calculation for the tangential stress reduces to that for an elliptic cylinder, given by

$$\frac{x_1^2}{a^2} + \frac{y_1^2}{b^2} = 1 \; . \qquad 26$$

For the ellipse the normal ($\underline{n}$) and tangential ($\underline{t}$) unit vectors are

$$\underline{n} = \left(1 + \frac{y_1^2 a^4}{x_1^2 b^4}\right)^{-\frac{1}{2}} \begin{pmatrix} 1 \\ \dfrac{y_1 a^2}{x_1 b^2} \\ 0 \end{pmatrix} , \qquad 27$$

$$\underline{t} = \left(1 + \frac{x_1^2 b^4}{y_1^2 a^4}\right)^{-\frac{1}{2}} \begin{pmatrix} 1 \\ -\dfrac{x_1 b^2}{y_1 a^2} \\ 0 \end{pmatrix} . \qquad 28$$

These unit vectors are multiplied by the stress tensor following eq. 29,

$$\tau_{t1} = \tau_{ij} n_i t_j \qquad 29$$

to yield the tangential stress due to the internal flow, given by eq. 30.

$$\tau_{t1} = \frac{4\rho_1 \nu_1 k x_1 b^2}{y_1 a^2 \left(1 + \dfrac{x_1^2 b^4}{y_1^2 a^4}\right)} \qquad 30$$

The surface coordinate y_1 in this formula can be expressed by:

$$y_1 = b\left(1 - \left(\frac{x_1}{a}\right)^2\right)^{\frac{1}{2}} . \qquad 31$$

In eq. 30, the additive term $x_1^2 b^4 / y_1^2 a^4$ will become very small for high axis ratios a/b and can therefore be omitted. With the condition for constant volume (eq. 20), the tangential stress for the flow inside then takes the form of eq. 32.

$$\tau_{t1} = \frac{4\mu_1 k x_1 c^2}{a^3\left(1 - \left(\frac{x_1}{a}\right)^2\right)^{\frac{1}{2}}} \qquad 32$$

Both flow fields may now be combined at the interface, because the tangential stress for systems without slip and without interfacial tension is continuous across the interface. By setting $\tau_t = \tau_{t1}$, $x = x_1$ and $\alpha = a/c$, the following expression can be derived:

$$\frac{2k}{G} = \frac{1}{\frac{8\lambda}{\pi}\frac{1}{\alpha^3}\left(\ln\frac{4\alpha^2}{\alpha+1} - \frac{3}{2}\right) + 1} \; . \qquad 33$$

This equation describes the variation of the longitudinal velocity gradient, k, inside the drop as a function of λ and α for constant values of G/2, the velocity gradient in the continuum. As indicated by eq. 17, the error involved in the calculations for the flow outside, by considering the drop as a slender body, may be deduced from the axis ratio of the drop. The error is about 9.5% for $\alpha = 3$, and results in an error of 4% in 2k/G. No smaller axis ratios than 3 will be allowed here.

The time dependence of the deformation is derived from eq. 13 for $x_1 = a$:

$$\frac{da}{dt} = ka \; , \qquad 34$$

and is expressed by eq. 35.

$$G(t - t') = 2\int_{\alpha'}^{\alpha} \frac{d\alpha^*}{\frac{2k}{G}\alpha^*} \qquad 35$$

Here α' corresponds to the deformation at t'. Figure 2 and Figure 3 illustrate the time dependence of the strain rate ratio and the natural logarithm of the

Figure 2

Theoretical result for the strain rate ratio 2k/G as a function of the dimensionless time G(t - t') for various viscosity ratios, λ.

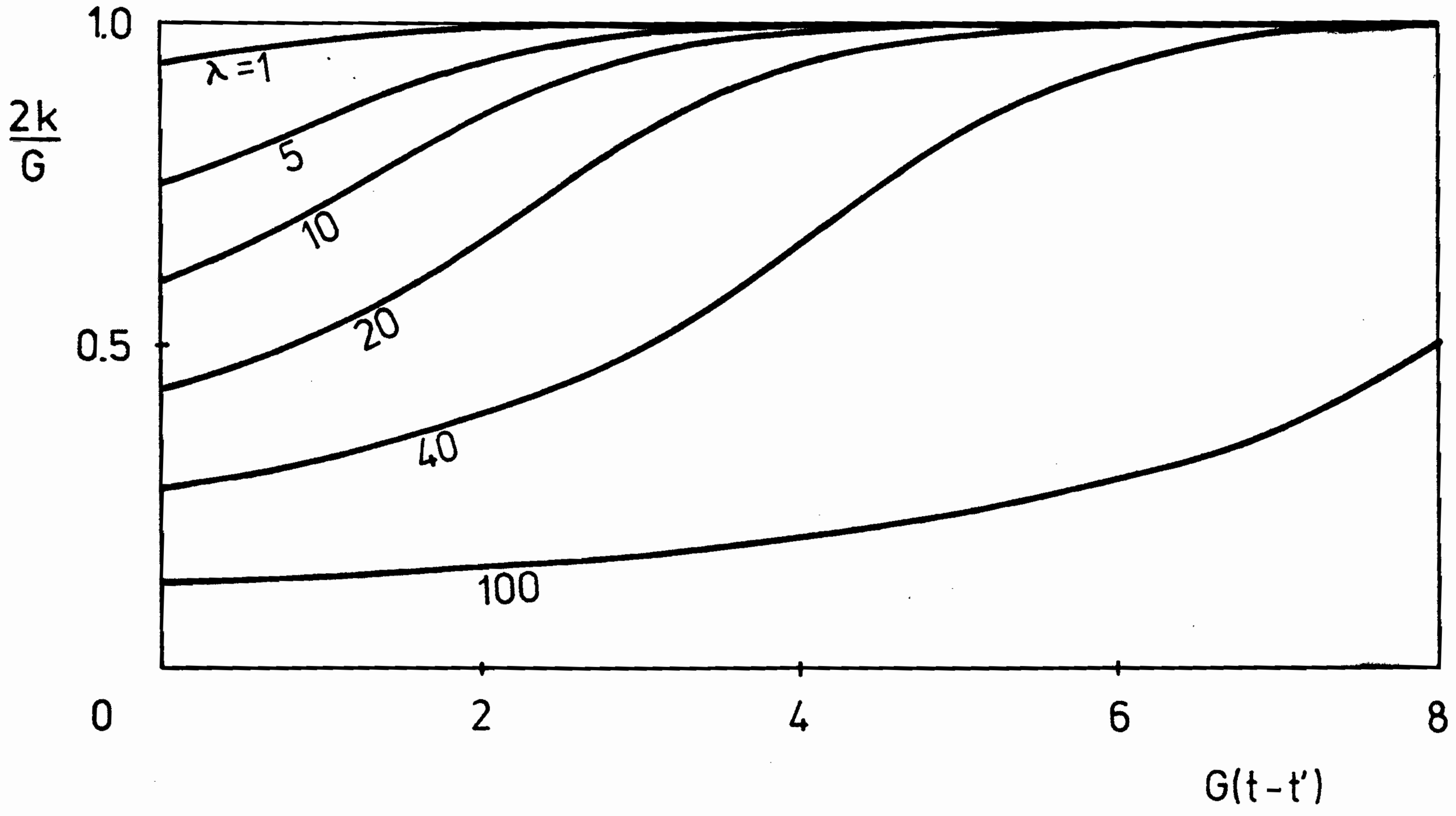

FIGURE 2

Figure 3

Theoretical result for the variation of the logarithm of the length ratio, $\ln\alpha$, as a function of the dimensionless time, $G(t - t')$, for various viscosity ratios, λ.

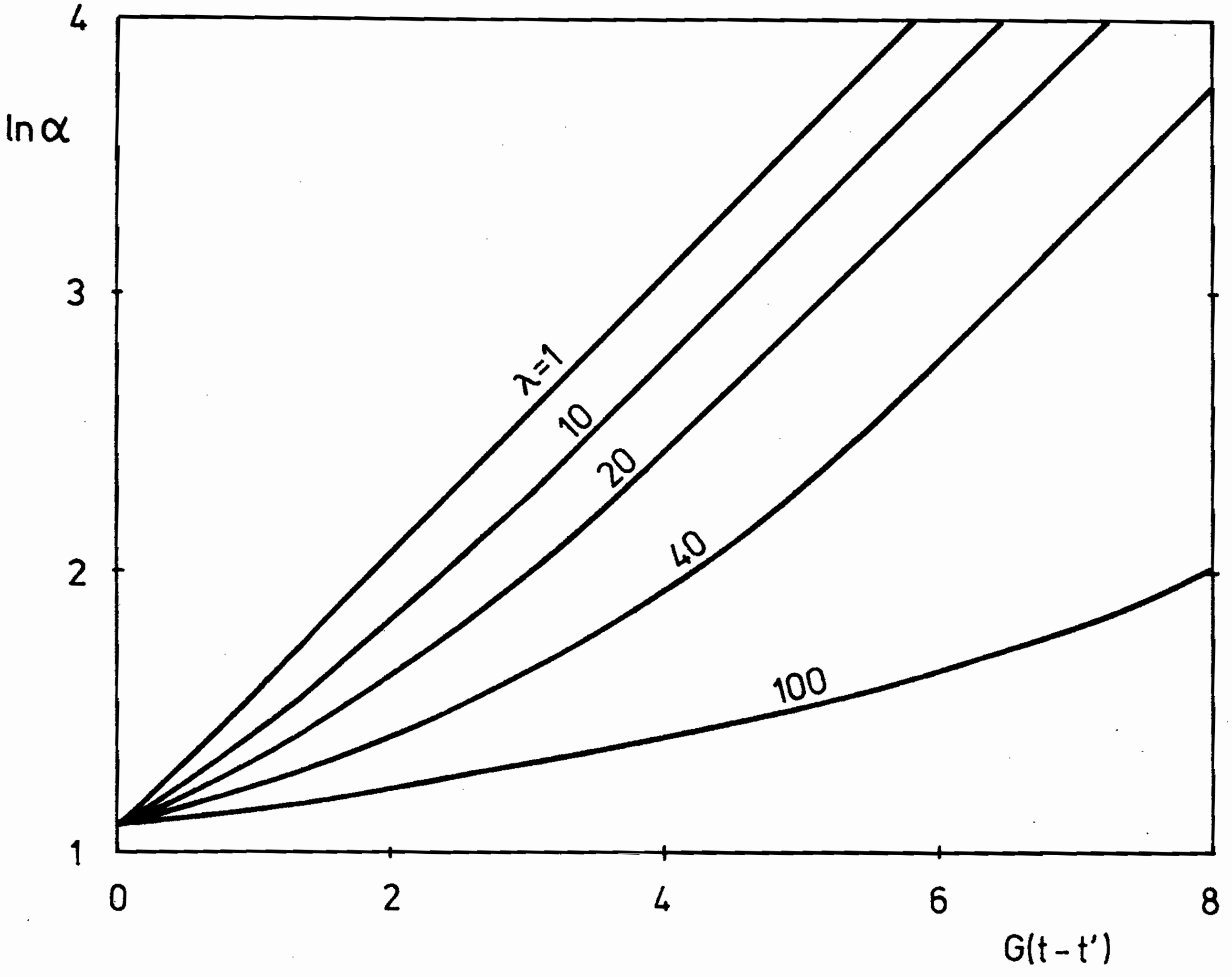

FIGURE 3

axis ratio $\ln\alpha$ for various viscosity ratios and for $\alpha' = 3$. The axis ratio is at the same time the length ratio of the drop, since c is constant. It can be seen in Figure 2 that all deformation curves are of the same general appearance and are shifted towards higher times by an amount that is determined by the viscosity ratio. Further, the strain rate ratio reaches $2k/G = 1$ within increasing time intervals for increasing viscosity ratios. The strain rate ratio of $2k/G = 1$ means that both flow fields have the same velocity gradient and the liquid drop has reached the maximum obtainable rate of extension. The same can be concluded form Figure 3, where the curves straighten with increasing time and become parallel to the deformation curve of $\lambda = 1$. Finally, it can be seen from Figure 2 that for the curve with $\lambda = 1$, $2k/G$ deviates from unity at low Gt. However, for this case, i.e. $\lambda = 1$, $2k/G$ must always be unity since the droplet is only imaginary. Thus the theory is obviously not exact at low Gt. Nevertheless, it is apparent from Figure 3 that the error in the theory at $\lambda = 1$ is small because the curve for $\lambda = 1$ is essentially a straight line.

In concluding the theoretical part of this chapter, it may be said that there exist two theories of droplet deformation in viscous flow for systems without interfacial tension; both are restricted in their application. The theory of Taylor applies for very small deformations, while the theory developed above is valid for very high deformations. There still remains a range of intermadiate deformations which has not been covered theoretically. In the following, the applicability of the theories will be tested experimentally and an attempt will be made to describe the whole range of small, medium and large deformations by semi-empirical expressions.

EXPERIMENTAL

The experiments on droplet deformation in extensional flow fields with systems of zero interfacial tension were carried out in a so-called four-roller-mill,[10,16,26-28] as illustrated in Figure 4. The rollers were made of aluminium and were 40 mm in diameter, and 100 mm in length. They were immersed in the continuum which was retained in a square-shaped Plexiglass container, 110 mm deep and 205 mm wide. The possible end-effects that could result from the drag of the rollers by the bottom of the container were avoided by floating the continuous phase (silicone oil in the present study) on a layer of an immiscible liquid with higher density and a much lower viscosity (e.g. water). For the observation of the droplet, a 16 mm Bolex cine camera was mounted above the centre of the flow field. The film speed of the camera was calibrated in order to permit accurate time dependent recordings. A light source behind a frosted glass screen supplied the necessary illumination.

The calibration of the four-roller-mill for the dependence of the shear rate on the roller speed was carried out according to the method suggested by Taylor[10]. Small tracer particles in the suspending fluid were filmed as they passed along the hyperbolic streamlines. From the distances travelled in known time intervals at certain roller speeds, the shear rate can be found as a function of the roller speed. The calibration function is

$$G = 31.7 \times 10^{-3} \times N \, , \qquad 36$$

where G is expressed in $\sec^{-1}$ and the speed, N, in rpm.

Single drops (diameter of about 0.3 cm) of coloured silicone oil with higher viscosities than the continuum were introduced into the apparatus through the open top. Colour (Calco Oil Scarlet B, supplied by American Cyanamid) was

Figure 4

Schematic diagram of the four-roller-mill and the experimental arrangement used in the deformation measurements.

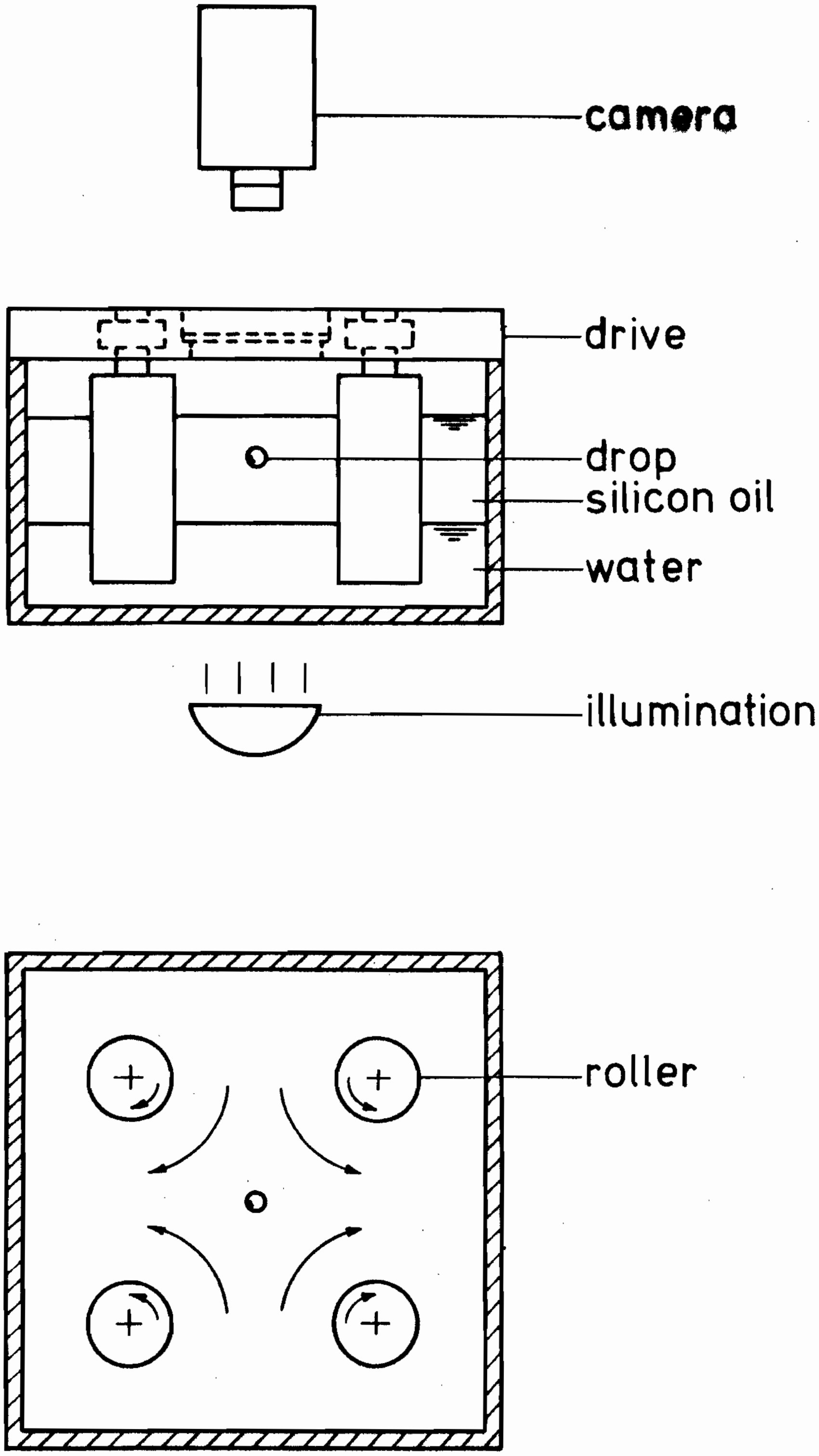

FIGURE 4

added in small amounts, just sufficient to provide the necessary contrast for the photographic recordings of the droplets. After placing the drop properly in the centre of the flow field the deformation process was filmed. At the end of all experiments, the drop was removed in order to avoid contamination of the suspending fluid.

The silicone oils (Dow Corning Fluid 200) used are tabulated with their viscosities and densities in Table 1. The viscosities were measured with a calibrated falling-ball viscometer at a constant temperature of 21°C. The molecular weight of these polymeric silicone fluids is low. Hence their viscosities commence to change only at a shear rate that is far higher than that applied in the experiments and were therefore assumed to be constant.

The recorded films were analyzed by projecting the image of the films on a transparent screen and by measuring the length of the drop as a function of time.

Table 1

Densities and viscosities of the silicone oils used for continuum and droplets at a temperature of 21°C.

Fluid	Density g/cm^3	Viscosity centipoise	Viscosity ratio with respect to fluid 1000
1000	0.974	1047.6	1.0
2000	0.974	2149.8	2.05
5000	0.975	5134.6	5.07
10000	0.975	12265.0	11.70
20000	0.975	19523.0	18.6
40000	0.975	40577.0	38.7

RESULTS AND DISCUSSION

The droplet deformation experiments were carried out at different shear rates within a range of 0.25 and 1.78 sec^{-1} and viscosity ratios ranging from 2.05 to 38.7. Errors, due to changes in viscosity and volume which are caused by the diffusion between the silicone oils of the droplet and the suspending medium, could be neglected because it was found that no changes occured in the deformation behaviour within deformation times of 1 min. The deformation times involved in the experiments were always shorter than 1 min.

Typical results of the droplet deformation measurements are shown in Figures 5 and 6. Here the length ratio α is given as a function of the time for two different viscosity ratios, $\lambda_1 = 5.07$ and $\lambda_2 = 11.70$ (Figure 5) and two different shear rates, $G_1 = 1.19\ sec^{-1}$ and $G_2 = 0.43\ sec^{-1}$ (Figure 6). It can be seen that α increases rapidly with increasing time. No accurate measurements could be made close to $t = 0$ due to errors in the shear rate arising from inertia effects of the motor, rollers and suspending liquid. The origin of the deformation curves at $t = 0$ in Figures 5 and 6 was therefore found by a straight line extrapolation. Such an extrapolation is allowed according to eq. 9 which was derived from Taylor's theory for small deformations. Proof for the applicability of Taylor's theory will be given later.

In Figure 7, the most significant experimental data are collected. Here the change of the logarithm of the length ratio, $\ln\alpha$, is shown as a function of the dimensionless time Gt for various viscosity ratios λ. By plotting the data in this way, a comparison with theory is facilitated. A qualitative agreement with the theory may be recognized immediately from the straightening of the deformation curves into lines parallel to that of a drop

Figure 5

Experimental data showing the length ratio of the deforming drop, α, as a function of the time for two different viscosity ratios, $\lambda_1 = 5.07$ and $\lambda_2 = 11.70$, at a constant shear rate $G = 1.19\ \text{sec}^{-1}$.

Figure 6

Experimental data showing the length ratio of the deforming drop, α, as a function of the time for two different shear rates, $G_1 = 1.19\ \text{sec}^{-1}$ and $G_2 = 0.434\ \text{sec}^{-1}$, at a constant λ of 5.07.

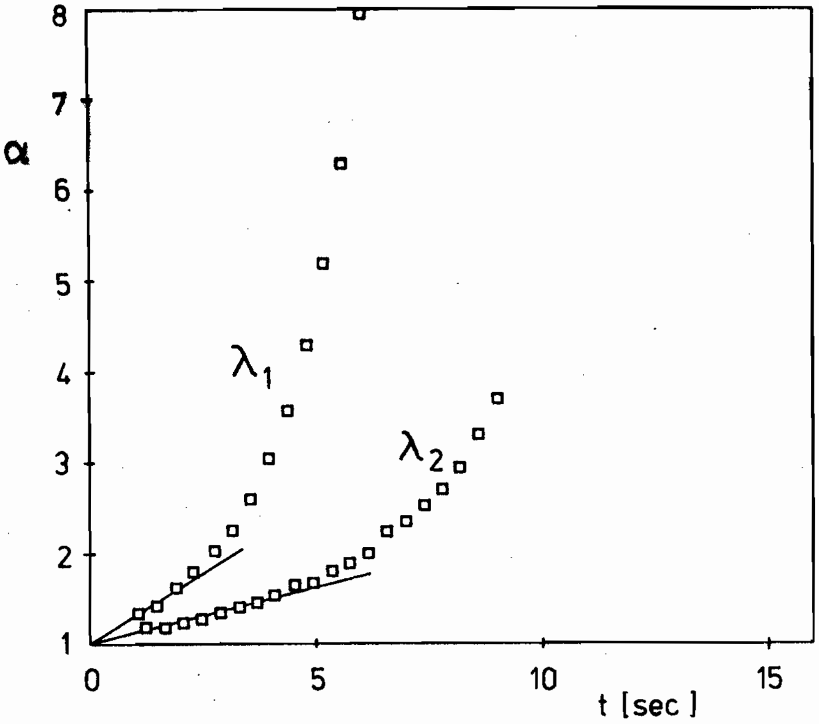

FIGURE 5

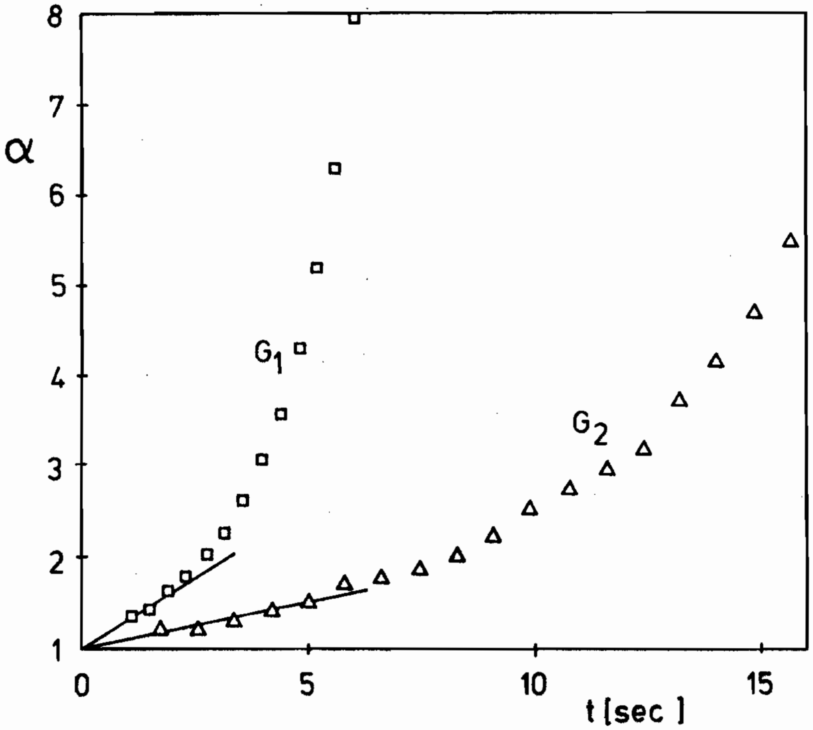

FIGURE 6

Figure 7

Experimental data plotted as the logarithm of the length ratio, lnα, versus the dimensionless time, Gt, for various viscosity ratios, λ. The dashed line for $\lambda = 1$ corresponds to the deformation of a drop of the same fluid as the continuum and the full lines represent the theoretical result by Taylor for small deformations (eq. 11).

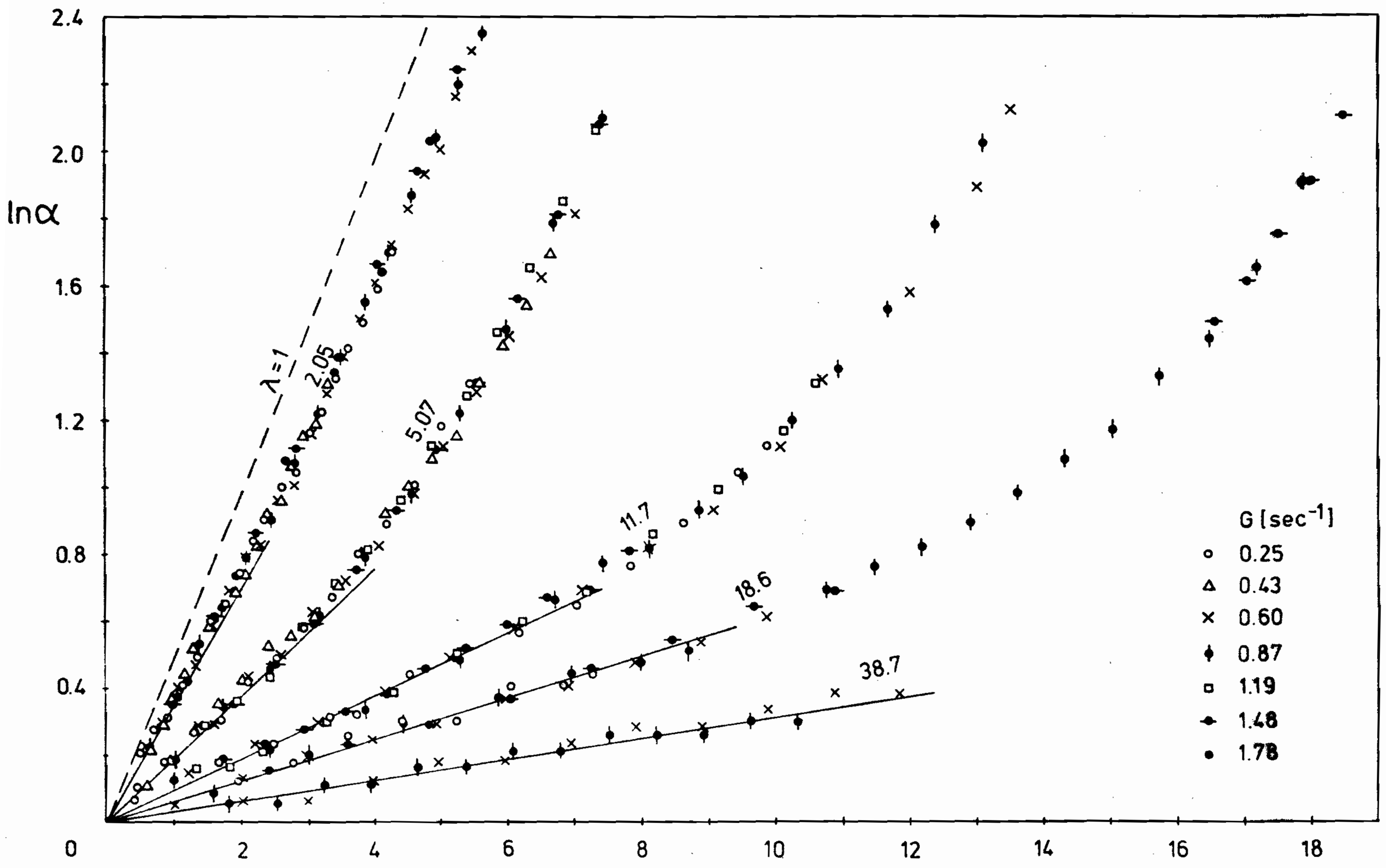
lnα
2.4
2.0
1.6
1.2
0.8
0.4
0
2
4
6
8
10
12
14
16
18
Gt
λ=1
2.05
5.07
11.7
18.6
38.7
G [sec⁻¹]
○ 0.25
△ 0.43
× 0.60
● 0.87
□ 1.19
● 1.48
● 1.78

FIGURE 7

with $\lambda = 1$ (see Fig. 3). The dashed line for $\lambda = 1$ corresponds to the deformation of a drop of the same fluid as the continuum. It can be clearly seen that, when $\ln\alpha$ is plotted as a function of Gt, the deformation data at different shear rates fall on the same curve. This behaviour confirms the theoretical prediction that Gt is the main deformation parameter comprising the time. The start of the deformation curves was again found by a straight line extrapolation employing eq. 11. Eq. 11 was derived from Taylor's theory and its agreement with the experiments may be analyzed by comparing the slope of the tangent to the experimental points close to the origin with the slope of the line given by eq. 11. For very small times, the velocity gradient inside the drop, k, is constant and the deformation of a drop in hyperbolic flow may be written as:

$$\ln\alpha = kt \; . \qquad 37$$

Comparison with eq. 11 yields for the slope $k = 5G/2(2\lambda + 3)$ and for the strain rate ratio:

$$\frac{2k}{G} = \frac{5}{2\lambda + 3} \; . \qquad 38$$

Accordingly, when the slope of the extrapolation line near the origin is divided by G/2 and plotted against $5/(2\lambda + 3)$, a linear relationship should be obtained. This is confirmed in Figure 8. Here, the strain rate ratio 2k/G is given as a function of λ (to show the influence of λ) as well as of $5/(2\lambda + 3)$ for $G = 0.25$ to 1.78 sec^{-1}. The circles are the average slopes of the tangents to the experimental curves. In this figure the close agreement between the experimental data and the theoretical curve proves that eq. 11 and eq. 38, derived from Taylor's theory, are applicable.

The high deformation theory was found to be qualitatively in full agreement with the experiments. Figure 9 shows the dependence of $\ln\alpha$ on Gt for

Figure 8

Comparison of Taylor's theoretical result (full curve) with the experimental results (circles). The data given by the strain rate ratio, 2k/G, versus the viscosity ratio, λ, were obtained as the slope of the tangent on the experimental points close to the origin (Figure 7). The bars indicate the distribution of the values of the slope.

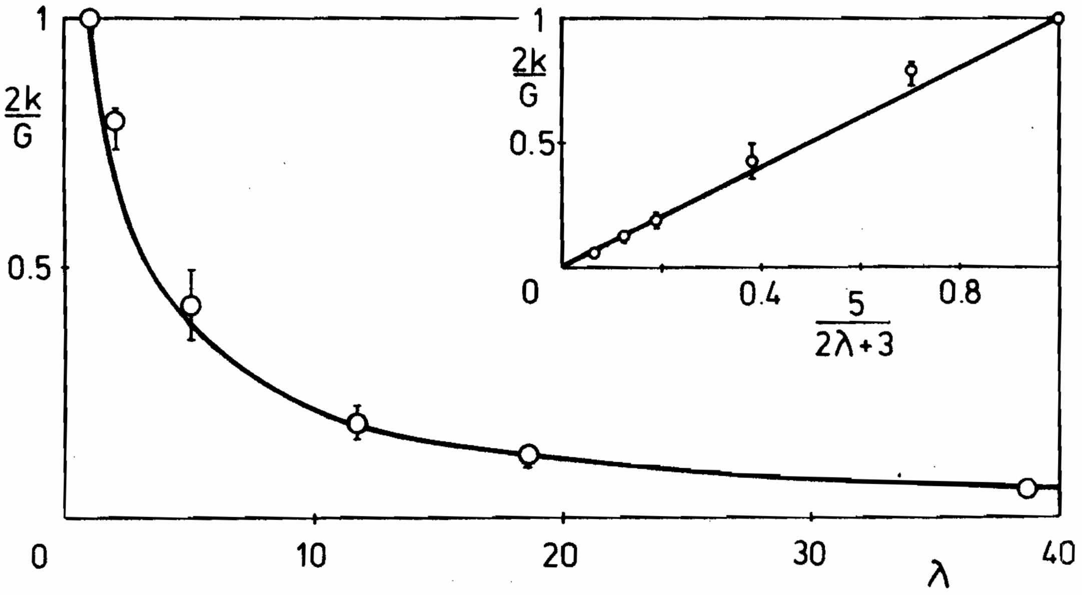

FIGURE 8

Figure 9

The logarithm of the length ratio, $\ln\alpha$, is plotted as a function of the dimensionless time, Gt, for $\lambda = 18.6$. The derived high deformation theory (full curve) agrees only qualitatively with the experimental data (points). The dashed curve shows the validity of the corrected theory.

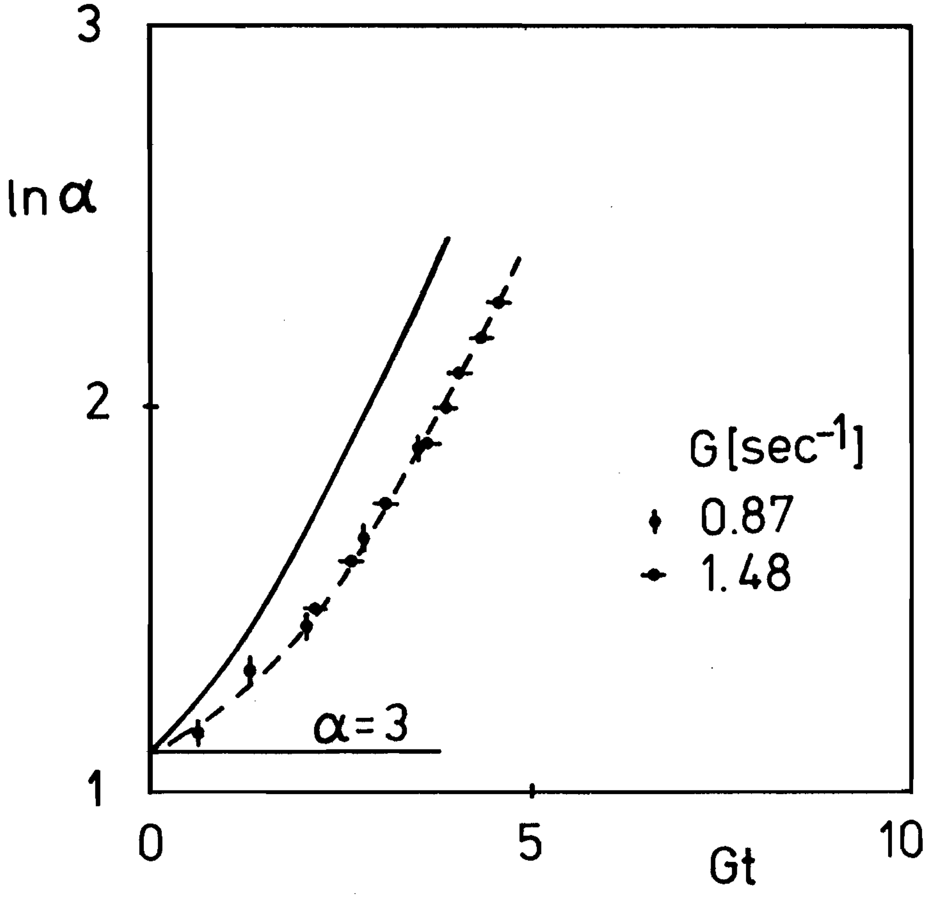

FIGURE 9

$\lambda = 18.6$ and for $\alpha \geq 3$. The full curve corresponds to the theoretical result for the same λ. The quantitative agreement is poor due to the use of the slender body theory, as well as simplifying assumptions that were made. Some of these assumptions are: negligible effects of the drop-ends, hyperbolic flow field inside the drop, and the drop always has an ellipsoidal shape. As shown later, the assumption of constant z-dimension of the drop causes only small errors. Since it appears that the quantitative validity of this theory commences at higher length ratios than expected, a simple correction can be made. This correction was performed by introducing the following expression for λ:

$$\lambda' = 1.75\lambda - 0.75 \,. \qquad 39$$

Eq. 39 was derived from the best fit to the experimental data for $\lambda = 2.05$ to 18.6, and it shows that every theoretical deformation curve has to be exchanged for one that is calculated for an up to 75% higher viscosity ratio. The then achieved quantitative agreement between experiments and theory is good and is shown in Figure 9 by the dashed curve.

In the theoretical section dealing with high deformations, the assumption was made that the z-dimensions of the drop do not change. To find out whether this assumption has any effect on the theoretical results, an analysis of the variation of the drop dimensions was made. In addition to the length, the width of a few deformed drops was also measured. The change in the z-dimensions can then be calculated by eq. 40,

$$\frac{c'}{c} = \frac{c^2}{a'b'} \qquad 40$$

which is derived from the condition for constant volume of the ellipsoid (eq. 19). Here a', b', and c' represent the actual dimensions of the ellipsoidal semi-axes. Figure 10 shows the variation of c'/c with increasing length ratios α, for two examples of highly deformed drops. The shear rates related to these

Figure 10.

The variation of the relative z-dimension, c'/c, of the drop calculated by eq. 40 from the experimental data (× for $G = 0.6$ sec^{-1} and $\lambda = 38.6$; and ● for $G = 1.48$ sec^{-1} and $\lambda = 18.6$) and plotted as a function of the length ratio, α. The full curve represents the best least square fit of the data (×) by the analytical function given in eq. 41.

Figure 11.

Relationship between $G\bar{t}$, the position on the time scale of the point of intersection of tangent and asymptote drawn to the experimental deformation curves, and the viscosity ratio, λ. The full line corresponds to the best least square fit of the experimental points and is expressed by eq. 42.

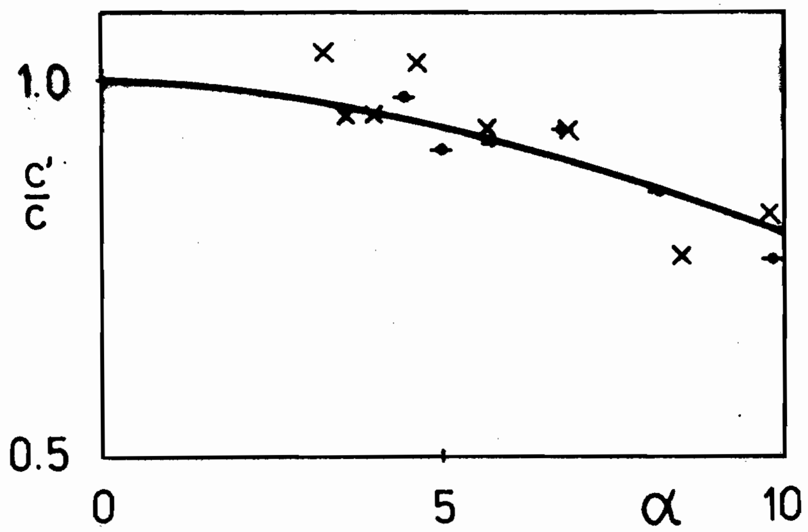

FIGURE 10

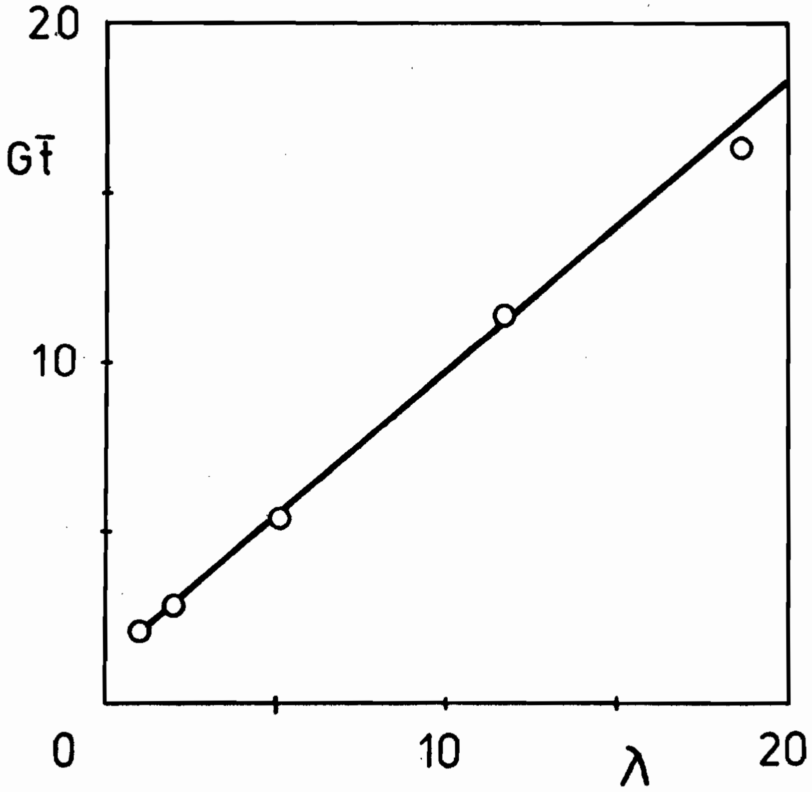

FIGURE 11

results were 0.6 and 1.48 $\sec^{-1}$, and the viscosity ratios amounted to 38.6 and 18.6 respectively. As can be seen from Figure 10, there is a decrease in the z-dimension of the drop at high elongations. The effect of this decrease on the theory was checked by introducing an analytical function that fits the experimental data and is expressed by eq. 41,

$$\frac{c'}{c} = \frac{1}{1 + \alpha^2 \beta} \qquad 41$$

where β is a coefficient with a magnitude of 0.0028. This magnitude was obtained by the best least square fit of the data for $G = 0.6 \sec^{-1}$ and $\lambda = 38.6$. The full curve in Figure 10 shows the analytical approach to the data. It was found that the error made in the theory by assuming that the z-dimensions are constant is smaller than 2% for α up to about 10, and is therefore of no significance.

Thus far it has been shown that two regions of the deformation curves can be described mathematically. One is the range of very small deformations, the other that of high deformations. Small droplet deformations are approximated by the tangent to the actual deformation curve, whereas high droplet deformations can be described by a corrected high deformation theory for $\alpha \geq 3$. Because of the complexity of the problem, the range of intermediate deformations cannot be covered mathematically at present, but it may be approximated by a second order parabola with respect to the semi-logarithmic coordinates. The position and shape of the parabola are determined by: its fixed position at the origin of the coordinates, its slope at the origin that is given by Taylor's theory (derivative of eq. 11 with respect to Gt), and the connection point to the curve of the high deformation theory at $\alpha = 3$. The connection point may be found from the experimental data in the following way. The tangent at $\ln\alpha = 0$ and the asymptote at large $\ln\alpha$'s to the experimental deformation curves intersect very close to $\ln\alpha = 1.1$ ($\alpha = 3$) at $\overline{Gt}$. $\overline{Gt}$ depends on the viscosity ratio as shown in Figure 11 (open circles). The full line in this figure represents the best least square fit to the data and is expressed by

$$\overline{Gt} = 1.344 + 0.856\lambda \ . \qquad 42$$

Since the asymptote is parallel to the deformation line for $\lambda = 1$ and $\overline{Gt}$ is known, the connection point of the parabola with the high deformation curve may be obtained by calculating the high deformation curve from large $\ln\alpha$'s back to $\ln\alpha = 1.1$. This results in eq. 43,

$$(Gt)_{\alpha\,=\,3} = 1.344 + 0.856\lambda + 5.724 - \int_{3}^{52.5} \frac{2d\alpha}{\frac{2k}{G}\alpha} \qquad 43$$

where the upper limit for the integral which theoretically should be infinity was however approximated to 52.5, since this was chosen as the highest value in the numerical calculation. The boundary conditions for the parabola are therefore:

$$\ln\alpha = 0 \quad : \quad Gt = 0, \quad \frac{d\ln\alpha}{dGt} = \frac{5}{2(2\lambda + 3)} \ , \qquad 44$$

$$\ln\alpha = 1.1 \quad : \quad Gt = (Gt)_{\alpha\,=\,3} \ . \qquad 45$$

Finally, the equation for the parabola can be written as eq. 46,

$$Gt = -A(\ln\alpha)^2 + B\ln\alpha + C \qquad 46$$

where the constants can be determined by the use of eqs. 44 and 45. It can be shown that the constants have the form:

$$A = \frac{-1}{1.207}\left[7.068 + 0.856\lambda - \int_{3}^{52.5} \frac{2d\alpha}{\frac{2k}{G}\alpha} - 1.1\,B\right] \qquad 47$$

$$B = 2(2\lambda + 3)/5 \tag{48}$$

$$C = 0 \ . \tag{49}$$

A computer programme was used to describe the full deformation process of the droplet as defined by eqs. 43 and 35. In Figure 12, where the variation of $\ln\alpha$ is shown as a function of Gt for different λ's, the good agreement of the curves obtained semi-empirically with the experimental data is demonstrated. In this figure the experimental data are represented by dashed curves and the theoretical results are given by full curves.

The semi-empirical equations are the first to describe the droplet deformation for all extensions and are of considerable importance for the coagulation process that is treated in chapter V.

Figure 12

Comparison of semi-empirical and experimental deformation curves. The dashed curves represent the experimental and the full curves the theoretical deformation behaviour.

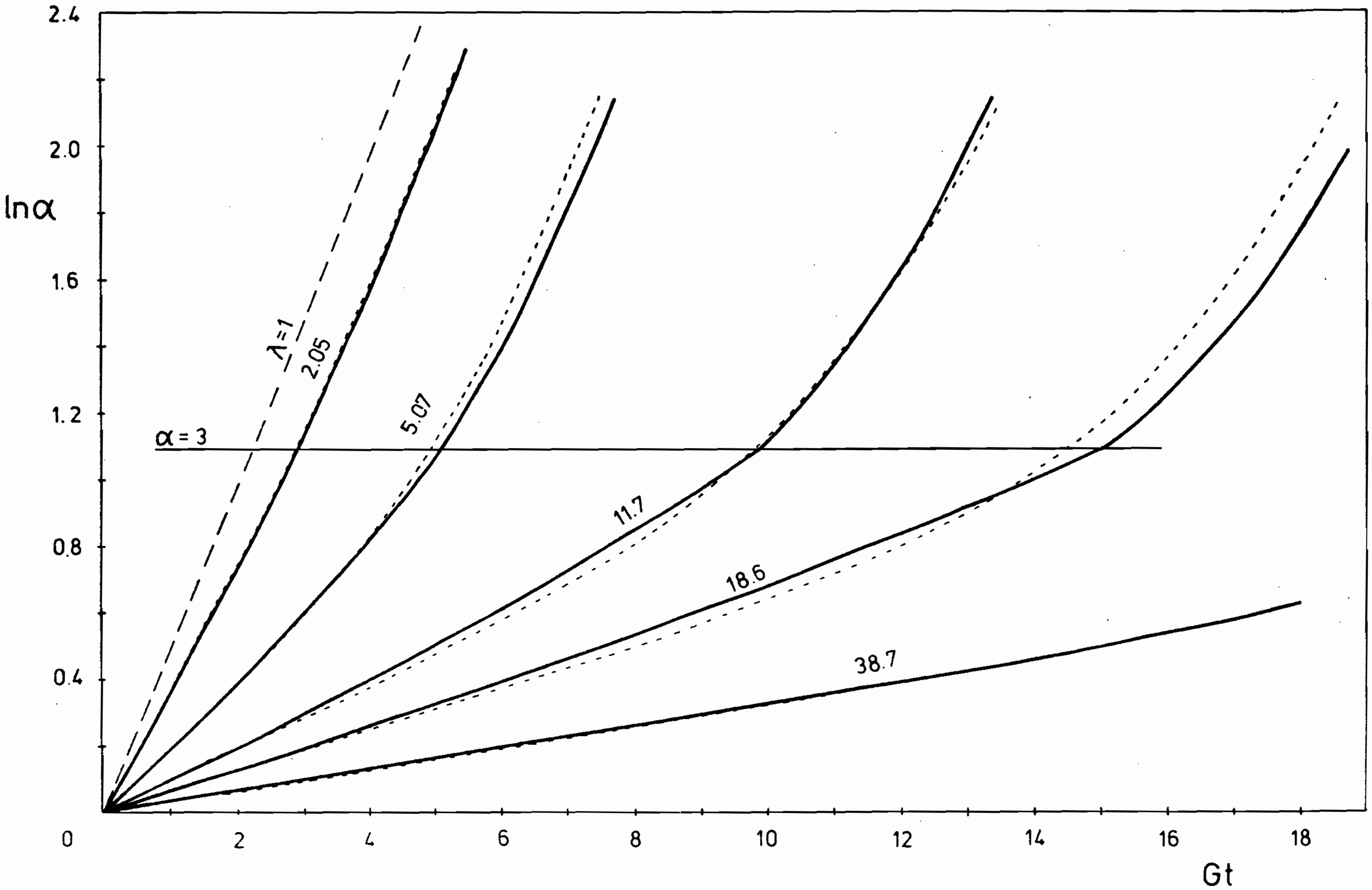

lnα
2.4
2.0
1.6
1.2
0.8
0.4
0
2
4
6
8
10
12
14
16
18
Gt
$\alpha = 3$
$\lambda = 1$
2.05
5.07
11.7
18.6
38.7

FIGURE 12

CONCLUSION

It was found that Taylor's theory for small deformations and negligible surface tension agrees with the present experimental data at small deformations. There is quantitative agreement between the corrected theory for high deformations and the experiments. The deformation behaviour between $\alpha = 1$ and $\alpha = 3$ was approximated by eq. 46, while the deformation behaviour for $\alpha \geq 3$ is given by eq. 35 together with eqs. 33 and 39. These expressions now describe the deformation of droplets from zero up to very large length ratios in hyperbolic flow fields and systems without interfacial tension. The presently available experimental data do not allow conclusions to be drawn about the applicability of these equations at higher viscosity ratios than about 20 and lower than 1.

The theory and the experiments show that the shear rate and the viscosity ratio are the main factors influencing the rate of droplet deformation. It may be noted that the product of the shear rate and the time (Gt) is the main time dependent parameter. All deformation diagrams therefore contain Gt as abscissa and show deformation curves which coincide for all shear rates at a constant viscosity ratio.

The theory describes the deformation of droplets in extensional flow fields with small strain rates and contributes important information to the underlying mechanism of fibre formation. The theory indicates for instance that the strain rate inside the drop increases with higher deformations and approaches the strain rate of the flow outside, when $\ln\alpha = 2$ to 3. Thus, in order to obtain highly oriented fibres, the coagulation should only commence when sufficient high strain rates inside the fibres are achieved.

These theoretical results explain some previous experimental findings[2], where it was shown that the fibres, which were precipitated in a stirred coagulant, exhibited great variations in size and orientation. It was found that the finer fibres possessed much higher degrees of orientation than the thicker ones. According to the theory, these high degrees of orientation are explainable by the high strain rates reached inside the drop when they become highly extended and very thin.

There is no doubt that the theory also describes the deformation of high polymer droplets, as long as the strain rate stays so small that the high polymers show Newtonian behaviour. The theory can also give important qualitative information even when non-Newtonian liquids are involved.

It is noteworthy that the experiments and the theory in the present chapter are a basis for the high shear rate studies to be carried out in chapter IV.

REFERENCES

1. Allen, S.L., Bolker, H.I., and Turvey, R.W., Appl. Polym. Symp. 28, 903 (1976).
2. Chapter II.
3. Peterlin, A., Polym. Eng. Sci. 16, 126 (1976).
4. Marrucci, G., Polym. Eng. Sci. 15, 229 (1975).
5. Pennings, A.J., van der Mark, J.M.A.A., and Booij, H.C., Kolloid Z.u.Z. Polymere 236, 99 (1970).
6. Peterlin, A., in "Advances in Macromolecular Chemistry", W.M. Pasika Ed. Academic Press, N.Y., 1968, Vol. 1, Page 225.
7. Bird, R.B., Hassager, O., and Abdel-Khalik, S.I., A.I.Ch.E.J. 20, 1041 (1974).
8. Williams, M.C., A.I.Ch.E.J. 21, 1 (1975).
9. Taylor, G.I., Proc. Roy. Soc. (London) A, 138, 41 (1932).
10. Taylor, G.I., Proc. Roy. Soc. (London) A, 146, 501 (1934).
11. Cox, R.G., J. Fluid Mech. 37, 601 (1969).
12. Barthès-Biesel, D., and Acrivos, A., J. Fluid Mech. 61, 1 (1973).
13. Buckmaster, J.D., J. Fluid Mech. 55, 385 (1972).
14. Buckmaster, J.D., J. Appl. Mech. E, 40, 18 (1973).
15. Bartok, W., and Mason, S.G., J. Colloid Sci. 13, 293 (1958).
16. Rumscheidt, F.D., and Mason, S.G., J. Colloid Sci. 16, 210 (1961).
17. Rumscheidt, F.D., and Mason, S.G., J. Colloid Sci. 16, 238 (1961).
18. Torza, S., Cox, R.G., and Mason, S.G., J. Colloid Interface Sci. 38, 395 (1972).
19. Grace, H.P., Eng. Foundation 3rd Res. Conf. on Mixing, Andover, New Hampshire (1971).
20. Acrivos, A., Proc. Int. Colloquium Drops and Bubbles, Pasadena, Ca., Vol. II 390 (1974).
21. Cox, R.G., J. Fluid Mech. 44, 791 (1970).

22. Cox, R.G., J. Fluid Mech. 45, 625 (1971).

23. Batchelor, G.K., J. Fluid Mech. 44, 419 (1970).

24. Cox, R.G., private communication.

25. Batchelor, G.K., "An Introduction to Fluid Dynamics", Cambridge University Press, 1967.

26. Torza, S., J. Polym. Sci.-Phys. 13, 43 (1975).

27. Crowley, D.G., Frank, F.C., Mackley, M.R., and Stephenson, R.G., J. Polym. Sci.(Phys.)14, 1111 (1976).

28. Pope, D.P., and Keller, A., Colloid Polym. Sci. 255, 633 (1977).

CHAPTER IV

THEORY OF FIBRE FORMATION BY DEFORMATION OF DROPLETS AT HIGH EXTENSIONAL FLOW RATES

ABSTRACT

A theory is derived for high droplet deformations in extensional flow of high strain rates and predicts the time dependence of the droplet deformation. The flow outside the drop is described by the boundary layer equations, and that for the inside by the creeping flow equation. The theory generally applies for high viscosity ratios of drop and suspending medium, but at low viscosity ratios the error is small as long as high deformations are considered. It was found that the strain rate of the flow inside the drop increases with time and at high deformations approaches that of the flow outside, in time intervals that mainly depend on the viscosity ratio. This result can meet the requirement of high strain rates for good molecular orientation of polymers and is similar to that obtained earlier for the deformation of drops at small strain rates. The implications of the theory for fibre formation processes involving coagulation of polymer solutions are discussed.

LIST OF SYMBOLS

a, b, c = ellipsoidal axes in the x, y and z-direction respectively
$a_0, a_1, a_2, a_3 \ldots$ = coefficients in the series expansion for f
C_1, C_2 = integration constants
f, f_1 = $f(\eta)$, $f_1(\eta)$, dimensionless variables describing the velocity outside the drop
$G, G/2$ = shear rate and strain rate respectively of the flow outside the drop
k = strain rate of the internal flow
$\ell; \ell_o$ = length of the drop on the x-axis; diameter of spherical drop
n = integer
p, p_1 = pressure of the flow outside and inside the drop respectively
Re = Reynolds number
$t; t'$ = time; integration constant
$\underline{U}_1$ = velocity field inside the drop
u, v, w = velocity components outside the drop
u_1, v_1, w_1 = velocity components inside the drop
x, y, z = coordinates outside the drop
x_1, y_1, z_1 = coordinates inside the drop
β = deformation coefficient, dimensionless
δ = boundary layer thickness
η = dimensionless coordinate, defined by eq. 16

λ = viscosity ratio, μ_1/μ

μ, μ_1 = viscosity of drop and suspending medium respectively

ν, ν_1 = kinematic viscosity of drop and suspending medium respectively

ρ, ρ_1 = density of drop and suspending medium respectively

τ, τ_{t1} = tangential stress at the drop surface due to external and internal flow respectively

INTRODUCTION

When a viscous solution of cellulose is added to a vigorously agitated coagulant, it is dispersed as droplets which become deformed into thin threads that subsequently coagulate forming fibres[1,2]. To obtain a detailed understanding of the mechanism of fibre formation, a theory for high droplet deformations at low strain rates was developed and tested experimentally[3]. It was shown that the strain rate inside the deforming droplet increases with the time of deformation and eventually becomes equal to that outside the drop. This increase in the strain rate can promote molecular extension and orientation[4-6] when the strain rate becomes high enough; the optimal magnitude depends on the molecular properties of the respective systems. Good orientation in most practical systems can, however, only be achieved when the strain rate of the internal flow field is high. Therefore, to be able to consider such systems, it is necessary to study the deformation of droplets at high strain rates of the flow field outside and inside the drop this is the subject of the present chapter.

Theoretical studies on droplet deformation with Newtonian fluids have been carried out earlier[7-12] and were reviewed by Acrivos[13]. The few deformation studies on drops of a viscoelastic fluid were summarized by Zana and Leal[14]. Nevertheless, none of these studies apply for the present conditions.

At small shear and strain rates, the behaviour of polymer solutions can be approximated by that of Newtonian liquids. At high shear and strain rates, however, polymer solutions exhibit non-Newtonian (for instance viscoelastic) behaviour[15]; the theories describing it may become extremely complex[16,17]. Hence, the studies in the present chapter are performed with

Newtonian liquids.

Finally, it should be noted that the theory to be outlined applies for high deformations of droplets, because a fibre can be considered to be a highly deformed and solidified drop. Furthermore, since low interfacial tension between drop and suspending medium is a prerequisite for good fibre formation (as already stated earlier[3]), only systems with negligible interfacial tension are considered.

THEORETICAL

Description of the Problem

The problem of finding exact solutions for the flow of a deformable particle, such as a drop, is mathematically complex. Existing theories[7-12] are of limited applicability and do not describe large deformations of drops in flow fields of high velocities or velocity gradients. The theory developed in the present chapter is therefore derived for these conditions and, as will be seen, provides information, for example, as to how the droplet length and the strain rate inside the drop change with time.

Consider a drop undergoing deformation in an extensional flow field. A schematic diagram of the drop and the flow field is shown in Figure 1, where a and b are the semi-axes of the drop in the x and y-direction. The initially spherical drop (dashed circle) is deformed into a long ellipsoidal thread by the action of the extensional flow field. This flow field is at far distances from the drop equal to the undisturbed flow field (without drop) and is given by eqs. 1 to 3,

$$u = \frac{G}{2}x \qquad 1$$

$$v = -\frac{G}{2}y \qquad 2$$

$$w = 0 \qquad 3$$

where u and v are the velocities in the x and y-direction; G/2 is the strain rate, and G the shear rate in the continuum. The flow field is thus hyperbolic and two-dimensional, having no velocity component in the z-direction. It is further assumed that the shear rate is high, of the order of 100 $\sec^{-1}$, the viscosity of the continuum is low (for example, 0.01 poise) and that of the drop is high (10 to 100 poise). There is no interfacial tension between drop and suspending medium. These assumptions correspond roughly to possible

Figure 1

Schematic diagram of drop and flow field. a and b are the semi-axes of the drop in the x and y-direction. The dashed circle corresponds to the initial drop diameter.

Figure 2

Illustration reflecting the assumption of the rectangular velocity profile inside the drop and the coordinates chosen. The two parallel horizontal lines represent the highly extended drop. Due to high viscosity ratios and the continuous tangential stress across the interface, the velocity gradient inside, $\left(\frac{\partial u_1}{\partial y_1}\right)_s$, is much smaller than that outside the drop, $\left(\frac{\partial u}{\partial y}\right)_s$.

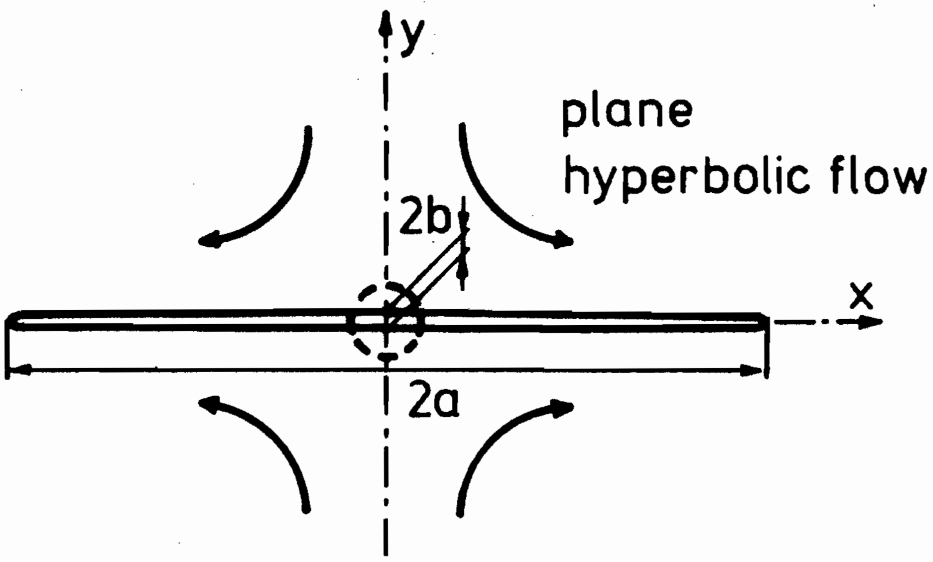

FIGURE 1

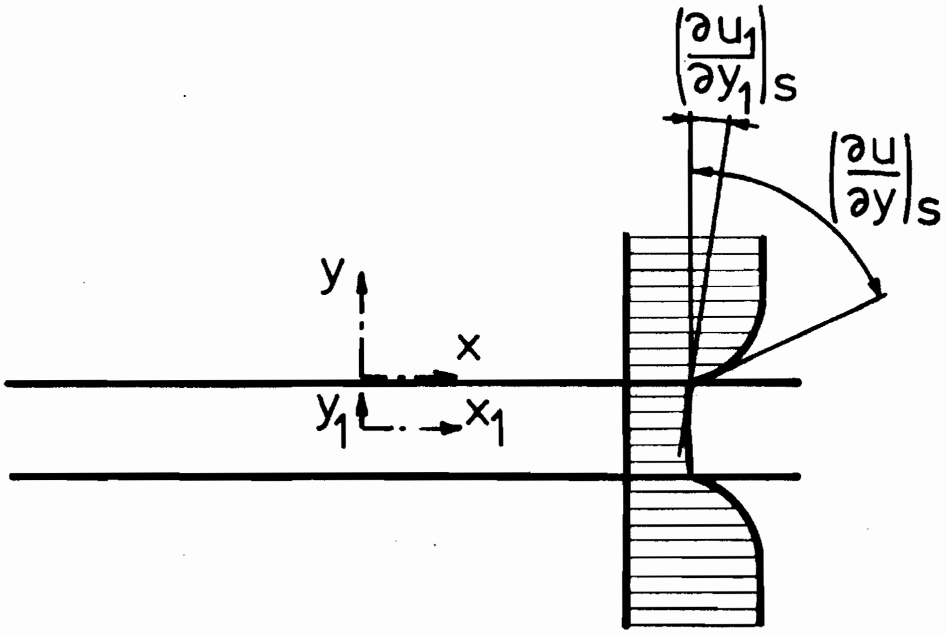

FIGURE 2

practical conditions.

In order to solve the problem, two flow fields have to be considered separately. First, that outside the drop, in a fluid of low viscosity. Secondly, the flow inside the drop in a fluid of high viscosity, following equations to be established. Both flow fields are combined at the interface according to the condition of equal tangential stress; this is permissable because the surface tension is negligible due to the miscibility of both liquids. The comparison of the tangential stresses from both flow fields then yields an expression for the deformation of the drop.

For the flow field outside the drop, having the viscosity and the shear rate given above, the Reynolds number Re will be large

$$Re \simeq \frac{\ell \frac{\ell}{2} \frac{G}{2}}{\nu} \simeq 2500, \qquad 4$$

for a drop that has a length, ℓ, of about 1 cm; ν denotes the kinematic viscosity of the medium. The thickness of the laminar boundary layer, δ, is of the order of:

$$\delta \simeq \left(\frac{2\nu}{G}\right)^{\frac{1}{2}} \simeq 1.4 \times 10^{-2} \text{ cm} . \qquad 5$$

The high Reynolds number and the fact that the thickness of the laminar boundary layer is relatively small, justify the use of the boundary layer equations for the flow outside[18,20].

The flow inside the drop is assumed to be characterized by eqs. 6 to 8,

$$u_1 = kx_1 \qquad 6$$

$$v_1 = -ky_1 \qquad 7$$

$$w_1 = 0 \qquad 8$$

where k is a longitudinal velocity gradient and the index 1 denotes the flow inside the drop. Equations 6 to 8 satisfy the creeping flow equation since for $k \approx 5$ to $50\ \mathrm{sec}^{-1}$, $\ell \simeq 1$ cm and $\nu \approx 10$ to 100 stokes, the Reynolds number is small:

$$Re \simeq \frac{k\frac{\ell}{2}\ell}{\nu} \simeq 0.25\ .$$

These equations are not very realistic at small deformations, but they closely approximate the flow at high deformations and high viscosities, for which the velocity profile inside the drop is nearly rectangular, as illustrated in Figure 2. That the velocity profile inside the drop is rectangular can be seen from the following considerations. The tangential stresses, τ_t and τ_{t1}, at the interface are equal and are defined by the product of the viscosity, μ or μ_1, and the transverse velocity gradient, as shown in eqs. 10 and 11,

$$\tau_t = \tau_{t1} \qquad 10$$

$$\mu\left(\frac{\partial u}{\partial y}\right)_s = \mu_1\left(\frac{\partial u_1}{\partial y_1}\right)_s \qquad 11$$

where s indicates the surface of the drop. Accordingly, the velocity gradient inside the drop $\left(\frac{\partial u_1}{\partial y_1}\right)_s$ must be very small for large viscosity ratios, which indicates an essentially rectangular velocity profile. The viscosity ratio is defined by the ratio of the viscosities of the drop and that of the suspending medium.

It should be noted that under the flow given by eqs. 6 to 8, the deforming drop will retain an ellipsoidal character, as has already been shown earlier[3]. However, since the z components of the velocity for both flow fields are zero, the drops may be considered in the theory as an elliptic cylinder.

The Flow Outside the Drop

The flow outside the drop is described by the boundary layer equations, which have to be solved for the present boundary conditions. Of interest here is especially the velocity gradient at the interface that is directly related to the tangential stress at the interface. The boundary layer equations have been solved for problems with the flow along or towards flat plates[19] and other non-deforming solid bodies[20,21]. In the present investigation, however, the body consists of a fluid that deforms according to eqs. 6 to 8 and the solution therefore turns out to be different. Since the highly deformed drop has only a small curvature along the x-axis, the boundary layer equations for flat plates will be used. These boundary layer equations are represented by eqs. 12 and 13, while eq. 14 is the continuity equation,

$$\frac{\partial u}{\partial t} + u\frac{\partial u}{\partial x} + v\frac{\partial u}{\partial y} = -\frac{1}{\rho}\frac{\partial p}{\partial x} + \nu\frac{\partial^2 u}{\partial y^2} \qquad 12$$

$$\frac{\partial p}{\partial y} = 0 \qquad 13$$

$$\frac{\partial u}{\partial x} + \frac{\partial v}{\partial y} = 0 \qquad 14$$

where ρ and p represent the density and the pressure. In eq. 12, $\frac{\partial u}{\partial t}$ becomes negligible when the rate of change of k with respect to time is small. Considering the equations for the flow at far distances from the drop (eqs. 1 to 3), a possible solution of eqs. 12 to 14 may be described by:

$$u = \frac{G}{2}\, x\, f'(\eta) \ , \qquad 15$$

where f' is the derivative of f with respect to η. f is a variable depending on η, while η is the usually used dimensionless coordinate described by:

$$\eta = y\left(\frac{G}{2\nu}\right)^{\frac{1}{2}} . \qquad 16$$

With the assumption that the pressure inside the boundary layer does not change with y (see eq. 13), $\partial p/\partial x$ can be written in terms of the velocity at far distances from the drop (u_∞) as in eq. 17.

$$\frac{\partial p}{\partial x} = -\frac{1}{2}\rho u_\infty \frac{\partial u_\infty}{\partial x} \qquad 17$$

The substitution of eqs. 15 and 17 in eqs. 12 and 14 yields for the boundary layer equation:

$$f''' - f'^2 + ff'' + 1 = 0 , \qquad 18$$

and the corresponding boundary conditions are:

$$\eta = 0 \quad : \quad f = 0,\ f' = 2k/G , \qquad 19$$

$$\eta = \infty \quad : \quad f' = 1 . \qquad 20$$

A possible form for the solution of eq. 18 for small η is a series expansion given by eq. 21.

$$f = a_0 + a_1\eta + a_2\eta^2 + a_3\eta^3 + \ldots \qquad 21$$

A problem that now arises is that the last boundary condition (eq. 20), for which η is infinite, cannot be incorporated in the series expansion. A method of circumventing this problem has been suggested by Homan[20]. He used a series expansion for small values of η and developed another solution coming from infinity. Both solutions were then linked together at an intermediate value of $\eta = \eta_0$. First, however, the coefficients of the series expansion have to be found. One of them will remain unknown because of the missing boundary condition (eq. 20). The coefficients can be determined by introducing f from eq. 21 and its derivatives into eq. 18 and making use of the first two boundary conditions (eq. 19). The coefficients are then the following:

$$a_0 = 0 \tag{22}$$

$$a_1 = 2k/G \tag{23}$$

$$a_2 \text{ (see below)}$$

$$a_3 = \frac{1}{6}(a_1^2 - 1) \tag{24}$$

for n = even

$$a_n = \frac{1}{n(n-1)(n-2)} \sum_{i=1}^{(n-2)/2} \left\{2i(n-i-1)-(n-i-1)(n-i-2)-i(i-1)\right\} a_i\ a_{(n-i-1)} \tag{25}$$

for n = odd

$$a_n = \frac{1}{n(n-1)(n-2)} \sum_{i=1}^{(n-3)/2} \left\{2i(n-i-1)-(n-i-1)(n-i-2)-i(i-1)\right\} a_i\ a_{(n-i-1)}$$

$$+ \{(n-1)^2/4 - \frac{n-1}{2}\left(\frac{n-1}{2}\right)-1\}\ a_{(n-1)/2}\ . \tag{26}$$

It turns out that it is a_2 which will remain undetermined for the present.

The solution of the differential equation (eq. 18) for the case of large η may be derived from the asymptotic behaviour of f when η goes to infinity, where $f \simeq \eta$ and $f' \simeq 1$. Setting

$$f = \eta + f_1 \tag{27}$$

and

$$f' = 1 + f_1' , \tag{28}$$

with f_1 always small compared to η, eq. 18 takes the form of eq. 29,

$$f_1''' + \eta f_1'' - 2f_1' = 0 \tag{29}$$

where the second order terms in f_1 have been neglected. Eq. 29 represents a second order differential equation that can be solved by known methods. It can be shown (see Appendix II, where $\phi = f'$) that the solution is given by eq. 30,

$$f_1 = C_1 \int_{\infty}^{\eta} \left[(\eta'^2 + 1) \int_{\infty}^{\eta'} \frac{e^{-\eta^{*2}/2}}{(\eta^{*2} + 1)^2} \, d\eta^* \right] d\eta' + C_2 \qquad 30$$

where the boundary condition of $f_1' = 0$ for large η has been used. With $f = \eta + f_1$, the solution coming from infinity is finally given by eq. 31.

$$f = \eta + C_1 \int_{\infty}^{\eta} \left[(\eta'^2 + 1) \int_{\infty}^{\eta'} \frac{e^{-\eta^{*2}/2}}{(\eta^{*2} + 1)^2} \, d\eta^* \right] d\eta' + C_2 \qquad 31$$

Both solutions of the boundary layer equations (eqs. 21 and 31) and their derivatives are now equated at the connection point η_o.

$$a_1\eta_o + a_2\eta_o^2 + a_3\eta_o^3 + \ldots = \eta_o + C_1 \int_{\infty}^{\eta_o} \left[(\eta'^2 + 1) \int_{\infty}^{\eta'} \frac{e^{-\eta^{*2}/2}}{(\eta^{*2} + 1)^2} \, d\eta^* \right] d\eta' + C_2 \qquad 32$$

$$a_1 + 2a_2\eta_o + 3a_3\eta_o^2 + \ldots = 1 + C_1 \left[(\eta_o^2 + 1) \int_{\infty}^{\eta_o} \frac{e^{-\eta^{*2}/2}}{(\eta^{*2} + 1)^2} \, d\eta^* \right] \qquad 33$$

$$2a_2 + 6a_3\eta_o + \ldots = C_1 \left[\frac{e^{-\eta_o^2/2}}{(\eta_o^2 + 1)} + 2\eta_o \int_{\infty}^{\eta_o} \frac{e^{-\eta^{*2}/2}}{(\eta^{*2} + 1)^2} \, d\eta^* \right] \qquad 34$$

The connection point at $\eta_o = 2.5$ has been found by trial and error to be most suitable here and the system of 3 equations and 3 unknowns is left to be solved. The unknowns are a_2, C_1 and C_2 and the best way to calculate them is numerically. The resulting dimensionless velocity profiles (f') are shown in Figure 3 as a function of η for values of 2k/G equal to 0.0, 0.25, 0.5, 0.75, and 1.0. The actual velocities can be calculated by eq. 8. As can be seen, f' has an initial value equal to 2k/G and with increasing η approaches asymptotically the value of f' = 1, where the flow field is described by eqs. 1 to 3. For illustrative purposes, Figure 3 also shows f and f" as a function of η for 2k/G = 0.

The tangential stress exerted on the drop from the flow outside the drop is given by:

$$\tau_t = \rho\nu\left(\frac{\partial u}{\partial y}\right)_s \quad . \tag{35}$$

Using eq. 15, the shear stress at the interface can finally by expressed in terms of the dimensionless velocity gradient f"(0) by eq. 36.

$$\tau_t = \rho\nu\frac{G}{2}\left(\frac{G}{2\nu}\right)^{\frac{1}{2}} \times f''(0) \tag{36}$$

f"(0) is a measure of the velocity gradient at the surface of the drop where η = 0. It follows from eq. 21 that f"(0) equals $2a_2$.

It is interesting to note that for the special case of a solid particle, for which 2k/G = 0, f" has a value of 1.232. This is in agreement with the value given by Howarth[20] which is derived for the flow towards a stagnation point at a solid body, a case for which the same flow equations were applied.

Figure 3

Diagram showing the velocity profile outside the drop in dimensionless form (f') with respect to the dimensionless coordinate η for various values of 2k/G. f' corresponds to the velocity in x-direction, while f is related to the velocity in the y-direction and f" to the gradient of the velocity in the x-direction. f" and f are given for 2k/G = 0.

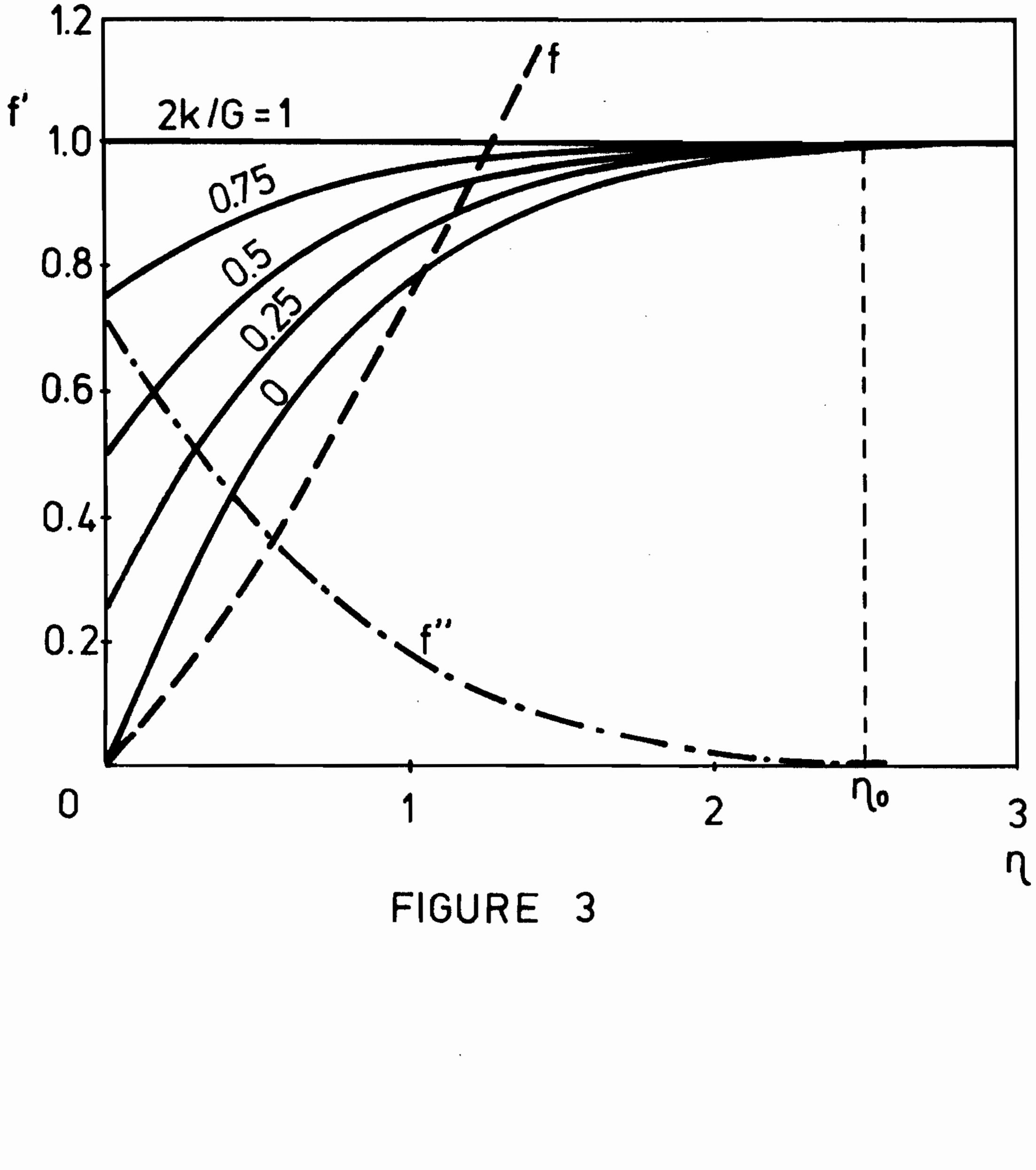

FIGURE 3

The Flow Inside the Drop

As in the previous chapter[3], the flow inside the drop follows the slow motion equation:

$$\nabla p_1 = \rho_1 \nu_1 \nabla^2 \underline{U}_1 \, , \qquad 37$$

where $\underline{U}$ is the velocity vector and the index 1 denotes the flow inside the drop. The derivation of the tangential stress on the basis of eqs. 6 to 8 and for the case of a cylindrical drop with an elliptic cross-section defined by

$$\frac{x_1^2}{a^2} + \frac{y_1^2}{b^2} = 1 \qquad 38$$

was outlined earlier[3,22]. It was demonstrated that the tangential stress can be expressed as eq. 39.

$$\tau_{t1} = \frac{4\rho_1 \nu_1 k x_1 b^2}{y_1 a^2 \left(1 + \frac{x_1^2 b^4}{y_1^2 a^4}\right)} \qquad 39$$

If the second term in the brackets in this equation is neglected, because its magnitude will be small when the semi-axis a becomes large, and substituting b for y_1, eq. 39 reduces to:

$$\tau_{t1} = 4\rho_1 \nu_1 k x_1 \frac{b}{a^2} \, . \qquad 40$$

Further, the condition of constant volume for the drop yields for b:

$$b = \frac{c^2}{a} \, , \qquad 41$$

where c is the constant semi-axis in the z-direction.

The tangential stress is finally expressed by eq. 42

$$\tau_{t1} = 4\rho_1 \nu_1 k x_1 \frac{c^2}{a^3} \, . \qquad 42$$

The Combination of the Two Flow Fields at the Interface

Provided that no slip occurs, the two flow fields can be combined mathematically by the condition of equal tangential stress at the interface of the drop, and an expression may be derived for the dimensions of the drop as a function of time. The tangential stresses τ_t and τ_{t1} according to eqs. 36 and 42 are therefore equated. Rewriting and setting $x = x_1$ leads to eq. 43.

$$\frac{2k/G}{f''(0)} = \frac{\rho \, a^3}{\rho_1 c^2} \left(\frac{G}{2}\right)^{\frac{1}{2}} \frac{\nu^{1/2}}{4\nu_1} \qquad 43$$

As will be seen later, it is advantageous to define a coefficient β that is the cube root of the expression on the left hand side in the equation above and is written in eq. 44.

$$\beta = \left(\frac{2k/G}{f''(0)}\right)^{\frac{1}{3}} \qquad 44$$

From eqs. 43 and 44 the length ($\ell = 2a$) of the drop can be calculated and is given by eq. 45.

$$\ell = 2\beta \left(\frac{\rho^2}{\rho_1^2} \frac{G\nu}{32\nu_1^2 c^4}\right)^{-\frac{1}{6}} \qquad 45$$

Taking the equation for the velocity at the tip of the drop in the hyperbolic flow where x = a:

$$\frac{da}{dt} = ka \, , \tag{46}$$

and substituting eq. 45 for a (bearing in mind that $\ell = 2a$) finally yields eq. 47 after integration.

$$G(t - t') = 2 \int_{\beta_o}^{\beta} \frac{d\beta^*}{\frac{2k}{G}\beta^*} \tag{47}$$

This equation describes the time dependence of the droplet deformation. t' is an integration constant that can be chosen arbitrarily, since it only adjusts the position of the time scale. It can be seen from eqs. 44 and 47 that β is a dimensionless deformation coefficient that depends on the product of shear rate and time. The variation in its magnitude can be calculated universally from eqs. 44 and 47 for all initial drop sizes and all viscosity ratios at any instant of time. Figure 4 shows the variation of the deformation coefficient as a function of the dimensionless time G(t - t'). The position of the start of any deformation, where $\ell = \ell_o$ and $\beta = \beta_o$, has to be determined by calculating β_o from eq. 45 for any particular ρ, ρ_1, G, ν, ν_1, and c. The corresponding starting point Gt_o is then obtained from Figure 4. For small magnitudes of β_o, it will be convenient to use tabulated values of β, because the reading of Gt_o for a certain β_o might otherwise become difficult, due to the small slope of β versus G(t - t') in that region. In any case, the length of the drop at any instant after Gt_o is then expressed by eq. 45 together with the appropriate β at the time Gt.

The deformation behaviour calculated on the basis of the equations above is shown in Figures 5 and 6. In Figure 5 the ratio of the strain rates for the flow inside and outside the drop, 2k/G, is plotted against G(t - t').

<u>Figure 4</u>

The universal deformation coefficient, β, as a function of the dimensionless time, $G(t - t')$.

<u>Figure 5</u>

The variation of the strain rate ratio, $2k/G$, as a function of the dimensionless time, $G(t - t')$.

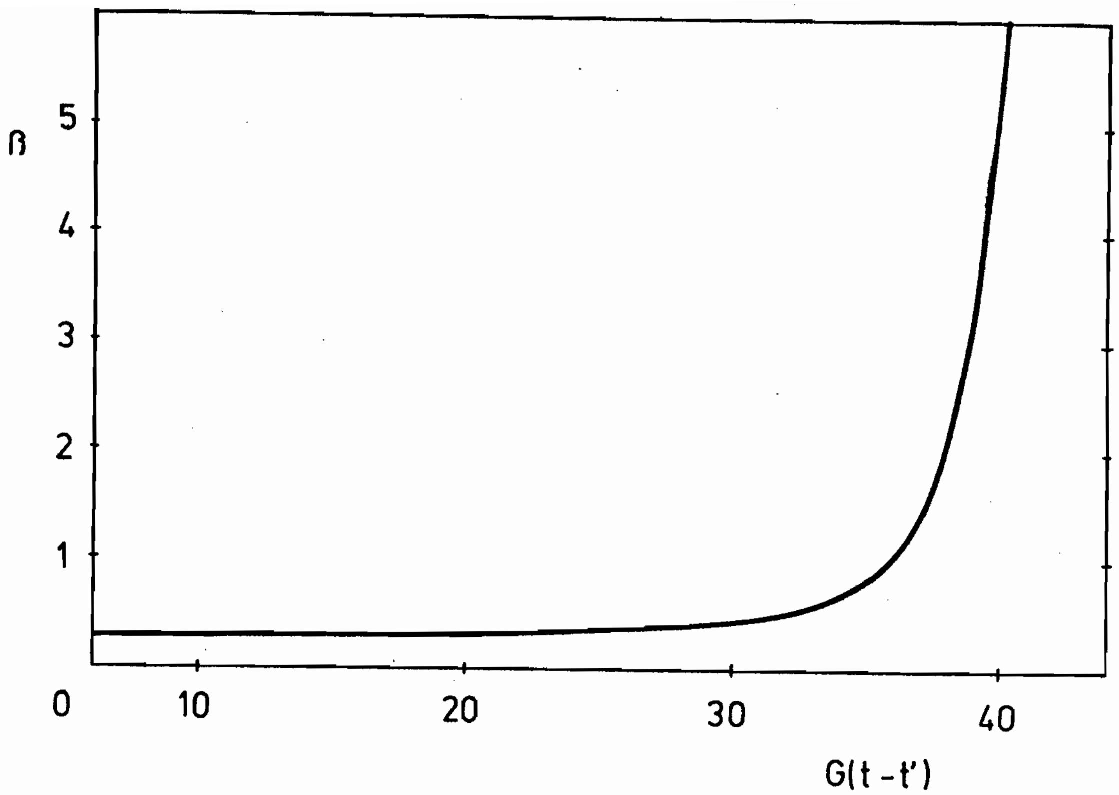

FIGURE 4

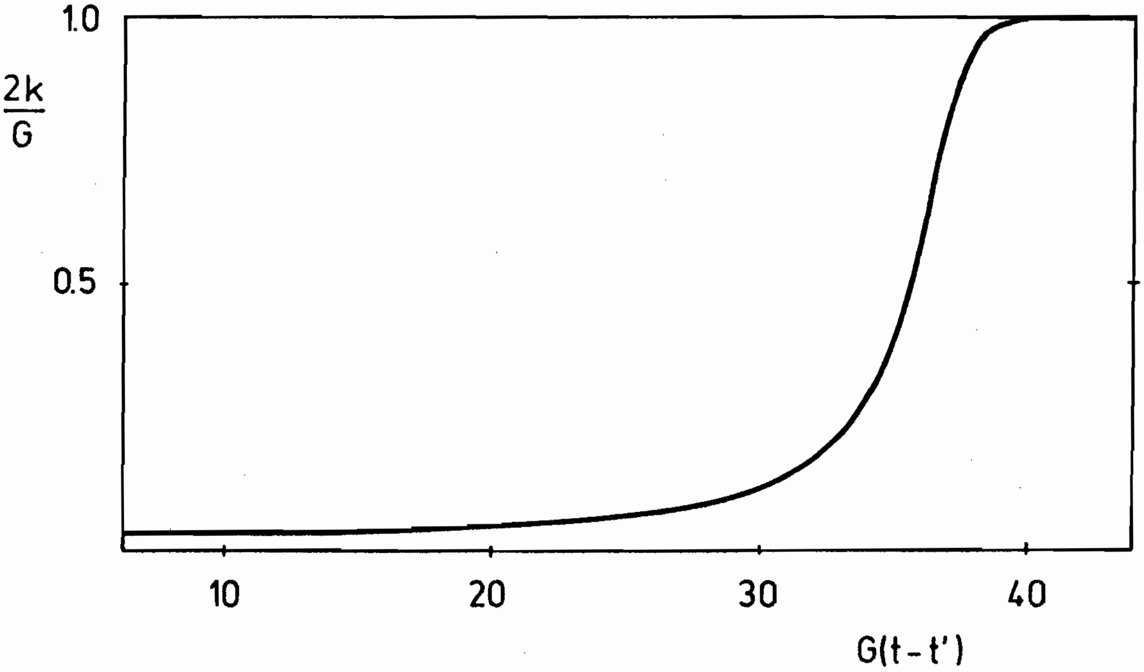

FIGURE 5

Figure 6

The logarithm of the length ratio of the drop, $\ln \ell/\ell_o$, is plotted against the dimensionless time, $G(t - t')$, for various viscosity ratios, λ. The calculations have been made with constant values of $\ell_o = 0.3$ cm and $\nu = 0.1$ stokes. The theory is expected to be valid for $\ell/\ell_o \geq 3$.

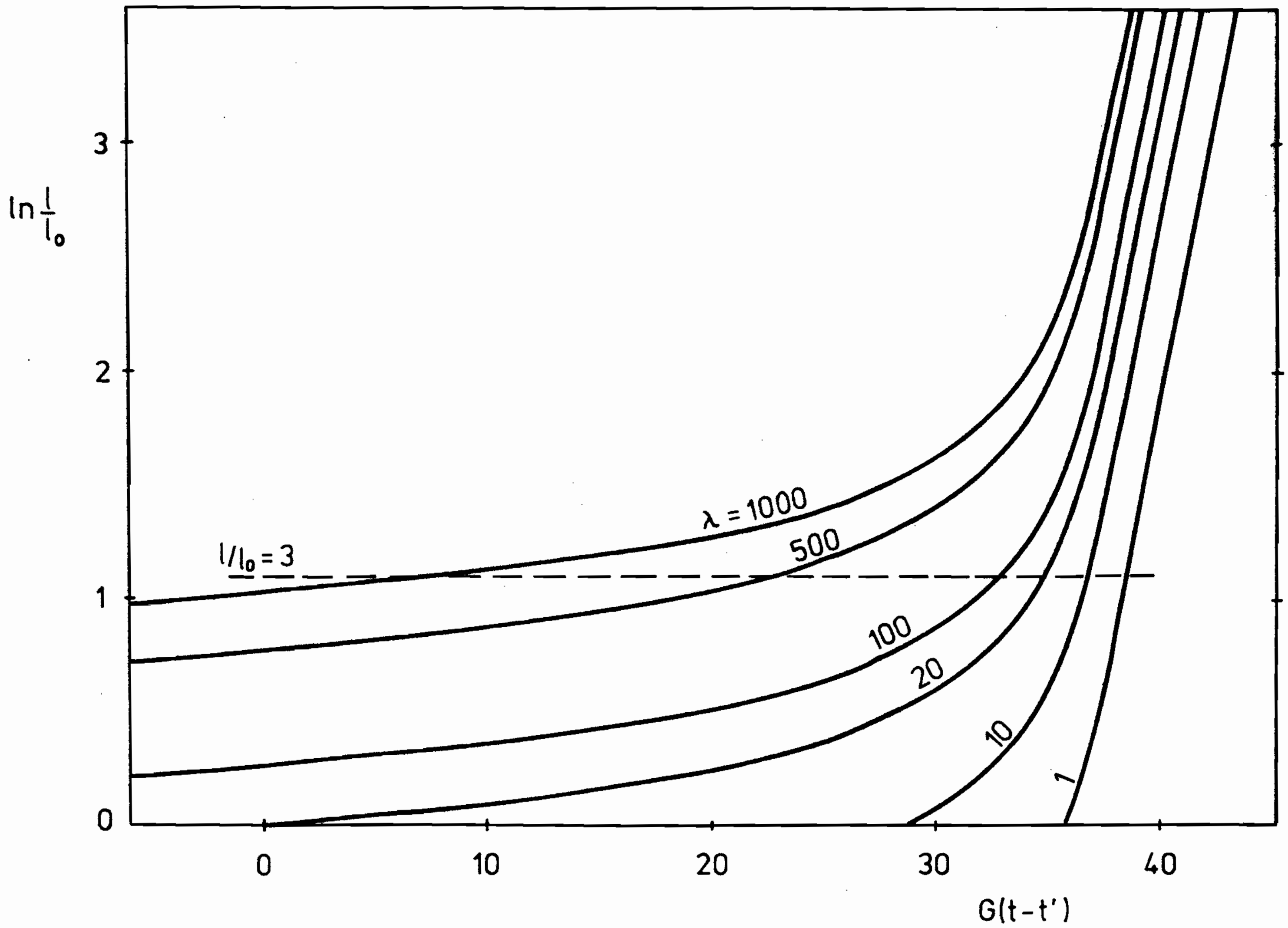

$\ln \frac{I}{I_0}$
3
2
1
0
0
10
20
30
40
$G(t-t')$
$I/I_0=3$
$\lambda = 1000$
500
100
20
10
1

FIGURE 6

Since G is generally kept constant, the figure expresses the time dependence of the strain rate inside the drop. The change of the droplet length with time is indicated in Figure 6. Here, the natural logarithm of the ratio of the droplet lengths, ℓ/ℓ_o, where ℓ_o is the original diameter of the drop, is shown as a function of $G(t - t')$ for various viscosity ratios, λ, where $\lambda = \nu_1/\nu$. In these calculations, ρ was chosen equal to ρ_1, $\ell_o = 0.3$ cm and $\nu = 0.1$ stokes as being representative for practical systems.

The present theory is expected to be valid at length ratios $\ell/\ell_o \geq 3$.

DISCUSSION

From the theory developed above, the change in the length of the drop with time can be explained and calculated for various viscosity ratios and shear rates; a graphical interpretation is given in Figure 6. The use of the universal deformation coefficient β allows the determination of the length of the drop for any instant of time, viscosity ratio (within the limits), original droplet size, shear rate and density of the media.

According to the assumptions made, the theory is expected to apply mainly for high deformations and high viscosity ratios. However, the error in the deformation of a drop with $\lambda = 1$ is surprisingly small, as can be recognized by the slight deviation of the deformation curve from a straight line at small deformations of the drop. Therefore, in addition to the fact that the theory appears to be a good approximation for drops with high viscosity ratios at high deformations, it can possibly also serve as a rough approximation for drops with small viscosity ratios at low deformations.

It is also seen from Figure 6 that, for constant shear rates, the time needed for the drop to extend from spherical shape ($\ln\ell/\ell_o = 0$) to fibre dimensions ($\ln\ell/\ell_o = 2$ to 3) increases very quickly at higher viscosity ratios. Accordingly, there is an increasing time available for the diffusion of the coagulant into the drop of polymer solution. As indicated earlier[3], this time is important because it determines the amount of coagulant diffusing into the drop and therefore also the length of the fibre.

Another feature in Figure 6 is the straightening of all curves into parallel lines at values of $G(t - t')$ in the range of 30 to 40. This is the same region where $2k/G$ reaches unity, as shown in Figure 5, and implies that the elongation rate of the drop approaches that of the flow outside (which is high) and is practically equal to it at $G(t - t') \approx 38$. This is the most significant result of the theoretical work because this behaviour meets the requirement of high strain rate conditions for good molecular orientation.

The theory developed above is valid for Newtonian liquids (for example monomers and solutions of polymers with low molecular weights) that are characterized by a viscosity which is constant with respect to the shear rate. Solutions of polymers with high molecular weights, however, deviate considerably from the Newtonian behaviour[15]. Though the theory applies quantitatively for solutions of polymers with low molecular weights, it also provides important qualitative information in the case of high polymers on the mechanism of droplet deformation, and describes parameters, such as the strain rate inside the drop. It allows conclusions to be drawn about the rate of deformation of drops containing high polymers. In this latter case the deformation rate will be smaller than that given in the theory for Newtonian liquids because of the appearance of large extensional viscosities[4,5] at high shear rates. Thus, in the case of non-Newtonian liquids, the theory gives a qualitative understanding of the general conditions that have to be satisfied to optimize the molecular orientation and extension.

Since the theory applies specifically at high shear rates, it will be difficult to test it experimentally because the deformation times involved are extremely short, and also because the continuum becomes turbulent at high stirring speeds. However, the theory does make the same general predictions as that derived earlier[3] for low strain rates, and since the latter has been verified experimentally, there is reason to believe that the present high strain rate theory is also correct.

REFERENCES

1. Allen, S.L., Bolker, H.I., and Turvey, R.W., Appl. Polym. Symp. 28, 903 (1976).
2. Chapter II.
3. Chapter III.
4. Peterlin, A., Polym. Eng. Sci. 16, 126 (1976).
5. Marrucci, G., Polym. Eng. Sci. 15, 229 (1975).
6. Pennings, A.J., van der Mark, J.M.A.A., and Booij, H.C., Kolloid Z.u.Z. Polymere 236, 99 (1970).
7. Taylor, G.I., Proc. Roy. Soc. (London) A 138, 41 (1932).
8. Taylor, G.I., Proc. Roy. Soc. (London) A 146, 501 (1934).
9. Chaffey, C.E., Brenner, H., and Mason, S.G., Rheol. Acta 4, 56 (1965).
10. Cox, R.G., J. Fluid Mech. 37, 601 (1969).
11. Barthès-Biesel, D. and Acrivos, A., J. Fluid Mech. 61, 1 (1973).
12. Buckmaster, J.D., J. Fluid Mech. 55, 385 (1972).
13. Acrivos, A., Proc. Int. Colloquium Drops and Bubbles, Pasadena, Ca., 2, 390 (1974).
14. Zana, E., and Leal, L.G., Proc. Int. Colloquium Drops and Bubbles, Pasadena, Ca., 2, 428 (1974).
15. Peterlin, A. in "Advances in Macromolecular Chemistry", Pasika, W.M., Ed., Academic Press, 1968, Vol. 1, Page 225.
16. Bird, R.B., Hassager, O., and Abdel-Khalik, S.I., A.I.Ch.E.J. 20, 1041 (1974).
17. Williams, M.C., A.I.Ch.E.J. 21, 1 (1975).
18. Batchelor, G.K., "An Introduction to Fluid Dynamics", Cambridge University Press, 1967.
19. Blasius, H., Z. Math. Phys. 56, 1 (1908).
20. Howarth, L., in "Encyclopedia of Physics", by Flügge, S., Ed., Springer, Berlin, 1959, Vol. VIII/1, Page 264.
21. Homan, F., Z.A.M.M. 16, 153 (1936).
22. Cox, R.G. private communications.

CHAPTER V

COAGULATION OF DROPLETS OF CELLULOSE SOLUTION IN EXTENSIONAL FLOW

ABSTRACT

The formation of cellulose fibres by coagulation of drops of cellulose solution in extensional flow was studied theoretically and experimentally. In the theory, which applies for slow motion conditions, homogenity of the drop is assumed. The drop deforms according to a previously established deformation mechanism and becomes solid when a critical concentration of coagulant is reached at a certain position inside the drop. The theoretical predictions of the variation of the fibre length with various parameters were tested experimentally in a four-roller-mill for the system cellulose/dimethyl sulfoxide/paraformaldehyde with glycerol as coagulant. In agreement with the theoretical predictions it was found that the fibre length increases with the shear rate, the original droplet size, and decreases with the diffusion coefficient of the coagulant in the cellulose solution. Fluctuations in the strain rate inside the deforming drop and in the apparent viscosity ratio (ratio of the viscosities of drop and suspending coagulant) were observed and could be interpreted in terms of skin formation and rupture during coagulation. The process studied can be applied to other polymer/coagulant systems.

LIST OF SYMBOLS

A, B = coefficients dependent on λ

a, b, c = ellipsoidal axes in the x, y and z-direction respectively

$c^*; c_1^*$ = coagulant concentration (w/w); coagulant concentration at the surface of the drop

D = diffusion coefficient

F_α = force per unit cross-sectional area in the x-direction

$G; Gt^*$ = shear rate; point of coagulation

k = strain rate inside the drop

Re, Re_1 = Reynolds number outside and inside the drop respectively

Sc, Sc_1 = Schmidt number outside and inside the drop respectively

$T_c; \Delta T$ = crystallization temperature; supercooling

$T(t)$ = dimensionless time function

$t; t'$ = time; time needed for the drop to reach $\alpha = 3$

t_c = time for coagulation

u, v, w = velocity components in the x, y and z-direction respectively

x, y, z = coordinates

Y = dimensionless y-coordinate ($Y = y/b$)

λ = viscosity ratio

λ_{app} = experimental apparent viscosity ratio

μ, μ_1 = viscosity of coagulant and drop respectively

τ_i = induction time for nucleation

INTRODUCTION

As discussed elsewhere[1,2] the formation of cellulose fibres by precipitation of cellulose solutions in a stirred coagulant is thought to proceed in two simultaneous steps. First, the dispersion of the cellulose solution as small droplets in the stirred coagulant and their elongation into thin liquid threads mainly in regions of extensional flow in the turbulent flow field. Secondly, there is the coagulation step that is governed by the diffusion of the coagulant into the cellulose solution. Theoretical and experimental studies on droplet deformation, the first step in the fibre formation process, have been carried out with an extensional flow field as produced by a four-roller-mill and were discussed in previous chapters[2,3]. It was shown[3] that Taylor's theory[4,5] for small deformations and small Reynolds numbers can be applied. Theories for high droplet deformations at small and large Reynolds numbers were then developed and the theory for small Reynolds numbers was tested experimentally. Following this the droplet deformation could be simulated by semi-empirical equations over the whole range of small and high deformations for small Reynolds numbers. It was found that the longitudinal velocity gradient inside the deforming drop increases rapidly and reaches that of the flow outside in time intervals that are mainly determined by the viscosity ratio. This behaviour meets the requirement of high extensional flow rates for good molecular orientation[6-8]. A crucial parameter was found to be the dimensionless time, Gt, during which the deformation proceeds. Gt is the product of shear rate, G, and time, t. The time is thought to be extremely important in the subsequent coagulation process, where it determines the amount of coagulant that diffuses into the extending drop. This coagulation process, the second simultaneous step, is the subject of the present chapter.

The diffusion of coagulants into cellulose-xanthate solutions has been studied earlier for the continuous fibre spinning process[9-11]. The magnitudes of the diffusion coefficients for various coagulants were derived by means of a mathematical formulation of the diffusion process. However, no further significant information is available.

Several patents[12-15] describe fibrous structures which are used for various applications in the paper and nonwoven industries. The structures are produced by coagulation of polymer solutions in highly sheared coagulants. A qualitative understanding of the coagulation of different polymer/coagulant systems was achieved from simple theoretical considerations and numerous experiments.

The present chapter establishes a mathematical model for the coagulation process in which idealized properties of the drops, as for instance homogenity, are selected. Special interest lies in the lengths of the fibres and the model allows predictions of the variation of the length with the change of various parameters. The agreement of these predictions with the experimentally obtained fibre lengths is illustrated. The experimental studies also allow conclusions to be drawn concerning the magnitude of the strain rate inside the drop and the change of the viscosity ratio of drop and suspending medium with time.

THEORETICAL

The mass transfer of coagulant into the deforming drop may occur by diffusion, convection or a combination of both and it is possible to ascertain which process is mainly involved from the magnitude of two dimensionless numbers[16]. These are the Reynolds number (Re) and the Schmidt number (Sc). By definition $Re = UL/\nu$ and $Sc = \nu/D$, where U and L are the characteristic velocity and length, and ν and D denote the kinematic viscosity and the diffusion coefficient respectively. When the product ReSc is very small, diffusional processes are dominant while very large values are an indication of convectional mass transfer.

Depending on the magnitude of Re and Sc and the geometry of the system, the mass transfer equation[17], given by eq. 1,

$$\frac{\partial c^*}{\partial t} + u\frac{\partial c^*}{\partial x} + v\frac{\partial c^*}{\partial y} + w\frac{\partial c^*}{\partial z} = D\left(\frac{\partial^2 c^*}{\partial x^2} + \frac{\partial^2 c^*}{\partial y^2} + \frac{\partial^2 c^*}{\partial z^2}\right) \qquad 1$$

can be considerably simplified. In eq. 1 u, v and w are the velocities in the x, y and z coordinate directions; t and c^* express the time and the concentration of the coagulant respectively. The simplest case to which eq. 1 can be reduced (i.e. mass transfer by diffusion only) is obtained when $ReSc << 1$. Then, for diffusional mass transfer in one dimension eq. 1 takes the form of eq. 2.

$$\frac{\partial c^*}{\partial t} = D\frac{\partial^2 c^*}{\partial y^2} \qquad 2$$

For the present experimental conditions Re and Sc may be estimated and yield for the inside of the drop:

$$Re_1 = \frac{k\, b\, 2b}{\nu_1} \simeq 0.5 \times 10^{-6} \qquad 3$$

$$Sc_1 = \frac{\nu_1}{D} \simeq 10^6 \qquad 4$$

$$Re_1 Sc_1 \approx 0.5, \qquad 5$$

since $k \simeq 0.25\ sec^{-1}$, $b \simeq 0.01$ cm, $\nu \simeq 100$ stokes and $D \simeq 10^{-6}$ to 10^{-5} cm^2/sec. Here k represents the longitudinal velocity gradient inside the drop and b the semi-axis in the y-direction. The dimensionless numbers for the outside of the drop similarly are:

$$Re = \frac{\frac{G}{2}\frac{\ell}{2}\ell}{\nu} \approx 0.5 \qquad 6$$

$$Sc = \frac{\nu}{D} \simeq 10^6 \qquad 7$$

$$ReSc \simeq 10^6, \qquad 8$$

where $G \simeq 1\ sec^{-1}$, $\ell \simeq 3$ cm and $\nu \simeq 5$ stokes. D is of approximately the same magnitude as for the inside of the drop. Here G denotes the shear rate of the external flow field and ℓ the length of the drop. Since $ReSc >> 1$ at the outside of the drop, the concentration boundary layer will be very small and the mass transfer at the outside of the drop is mainly governed by convection. It can further be seen that Re_1Sc_1 is close to unity, indicating that convection plays a role in the mass transfer process. However, to take convection into consideration poses a mathematically difficult problem. Therefore an approach will be made by using the relatively simple diffusion equation, i.e. eq. 2, with the assumption that the concentration of the coagulant at the drop surface is equal to that at far distances from the drop. This modification accounts for the facts that the surface concentration of the coagulant is high due to the flow outside the drop and that convection inside the drop results in an increased rate of mass transfer.

In order to solve eq. 2, the drop is considered to be a flat plate with a length of 2a and a thickness of 2b (a >> b); where a and b are the major and minor semi-axes of the approximately ellipsoidal drop in the x and y-direction respectively. The dimension 2c in the z-direction (c >> b) is assumed to be constant, as discussed previously[3]. The boundary conditions to be incorporated in the solution of eq. 2 are:

$$t = 0: \quad c^* = 0 \quad \text{for} \quad -b \leqslant y \leqslant b \qquad 9$$

$$c^* = c_1^* \quad \text{for} \quad y = \pm b \; ; \qquad 10$$

$$\text{all } t: \quad c^* = c_1^* \quad \text{for} \quad y = \pm b \; . \qquad 11$$

Here c_1^* is the coagulant concentration at the surface of the drop. The following definitions are made:

$$Y = \frac{y}{b} \qquad 12$$

$$dT(t) = \frac{D}{b^2}\, dt \; , \qquad 13$$

where Y represents the dimensionless coordinate and T(t) a time function.

Since

$$\frac{\partial c^*}{\partial t} = \frac{\partial c^*}{\partial T(t)} \frac{\partial T(t)}{\partial t} + \frac{\partial c^*}{\partial Y} \frac{\partial Y}{\partial t} \qquad 14$$

$$\frac{\partial c^*}{\partial y} = \frac{\partial c^*}{\partial T(t)} \frac{\partial T(t)}{\partial y} + \frac{\partial c^*}{\partial Y} \frac{\partial Y}{\partial y} \; , \qquad 15$$

which with eqs. 12 and 13 reduce to

$$\frac{\partial c^*}{\partial t} = \frac{\partial c^*}{\partial T(t)} \frac{D}{b^2} + \frac{\partial c^*}{\partial Y} y \left(-\frac{1}{b^2}\right) \frac{\partial b}{\partial t} \qquad 16$$

$$\frac{\partial c^*}{\partial y} = \frac{\partial c^*}{\partial Y} \frac{1}{b} , \qquad 17$$

the differential equation (eq. 2) takes the form of eq. 18.

$$\frac{\partial c^*}{\partial T(t)} - \frac{b}{D} \frac{\partial b}{\partial t} Y \frac{\partial c^*}{\partial Y} = \frac{\partial^2 c^*}{\partial Y^2} \qquad 18$$

The second term in eq. 18 is expected to be very small for highly extended drops, since:

$$\frac{b}{D} \frac{\partial b}{\partial t} << 1 \; . \qquad 19$$

Accordingly, the differential equation

$$\frac{\partial c^*}{\partial T(t)} = \frac{\partial^2 c^*}{\partial Y^2} \qquad 20$$

is left to be solved; its solution can be obtained by known mathematical procedures[17] and can be written as eq. 21.

$$c^* = c_1^* + c_1^* \sum_{m=1}^{\infty} e^{-\left(\frac{\pi(2m - 1)}{2}\right)^2 T(t)} \frac{4}{\pi} \frac{(-1)^m}{2m - 1} \cos\left(\frac{\pi}{2} (2m - 1)Y\right) \qquad 21$$

This relation describes the concentration of the coagulant inside the drop as a function of T(t) and the dimensionless coordinate Y. Recalling that for an ellipsoid of constant volume $b = c/\alpha$, where α denotes the length ratio of the drop, a/c, c being the constant semi-axis in the z-direction and also the initial droplet radius, T(t) can be expressed by eq. 22.

$$T(t) = \frac{D}{c^2}\int_o^t \alpha^2\, dt^* \qquad 22$$

The time dependence of α for slow motion conditions was determined elsewhere[3] and is given by the following expressions:

for $\alpha \leq 3$

$$\alpha = \exp\left[\frac{B}{2A} - \left\{(\frac{B}{2A})^2 - \frac{Gt}{A}\right\}^{\frac{1}{2}}\right] \qquad 23$$

with

$$A = \frac{-1}{1.207}\left[7.068 + 0.856\lambda - \int_3^{52.5}\frac{2d\alpha}{\frac{2k}{G}\alpha} - 1.1B\right] \qquad 24$$

$$B = \frac{2}{5}(2\lambda + 3) \qquad 25$$

$$\frac{2k}{G} = \left[\frac{14\lambda - 6}{\pi\alpha^3}\,(\ln\frac{4\alpha^2}{\alpha + 1} - \frac{3}{2}) + 1\right]^{-1} \qquad 26$$

for $\alpha \geq 3$

$$G(t - t') = 2\int_3^{\alpha}\frac{d\alpha^*}{\frac{2k}{G}\alpha^*} \qquad 27$$

with 2k/G from eq. 26.

In these expressions λ is the ratio of the viscosities of the drop and the suspending medium. The time t' is the time needed for the drop to elongate to $\alpha = 3$.

Since α is now fully described, the time function T(t) can be obtained by integrating eq. 22, which results for $\alpha \leq 3$ in eq. 28.

$$T(t) = \frac{DA}{2c^2G}\left\{\alpha^2\left[\left(\frac{B^2}{A^2} - \frac{4Gt}{A}\right)^{\frac{1}{2}} + 1\right] - 1 - \frac{B}{A}\right\} \qquad 28$$

Eq. 28 is valid for the case of constant A and B. A and B are constant when λ of the system does not change during the coagulation process, as is assumed in the present derivation. The validity of this assumption will be discussed in the experimental part. The same assumption is made for the range of $\alpha \geq 3$ where T(t) is described by eq. 29.

$$T(t) = \frac{2D}{Gc^2}\int_3^{\alpha} \frac{\alpha^* d\alpha^*}{\frac{2k}{G}} \qquad 29$$

The development of the profile of the coagulant concentration inside the deforming drop with time can then be calculated by means of eqs. 21 to 29. Typical concentration profiles for one half side of the drop are shown in Figure 1 for various times of deformation. The curves in the figure were calculated with $D = 2 \times 10^{-5}$ cm^2/sec, $G = 1$ sec^{-1}, $\lambda = 10$, $c = 0.15$ cm, and $c_1^* = 1.0$, values which were arbitrarily chosen as fairly representative of possible experimental systems. The numbers beside the curves indicate the times of deformation in seconds. It is evident that for any relative coordinate in the drop, the magnitude of the concentration of the coagulant, which is initially zero or very small, becomes increasingly greater in successive time intervals. This is further illustrated in Table 1, where the dimensions of the drop and the coagulant concentration at an arbitrarily chosen position on the x-axis in the drop are shown. It can be seen that the diffusion of the coagulant becomes more pronounced when the drop is highly extended, a fact which can be expected, because the thickness of the drop is very small and the surface is large. It may be noted that the change in concentration near the centre of

Figure 1

Typical coagulant concentration profiles with respect to $Y = y/b$ inside a deforming drop for one half side of the drop at various times of deformation.
$D = 2 \times 10^{-5}$ cm^2/sec, $G = 1$ sec^{-1}, $\lambda = 10$, $c = 0.15$ cm, and $c_1^* = 1$. At the times of deformation of $t = 5$, 10 and 12 sec the lengths of the fibres are 0.54, 1.26 and 2.69 cm respectively.

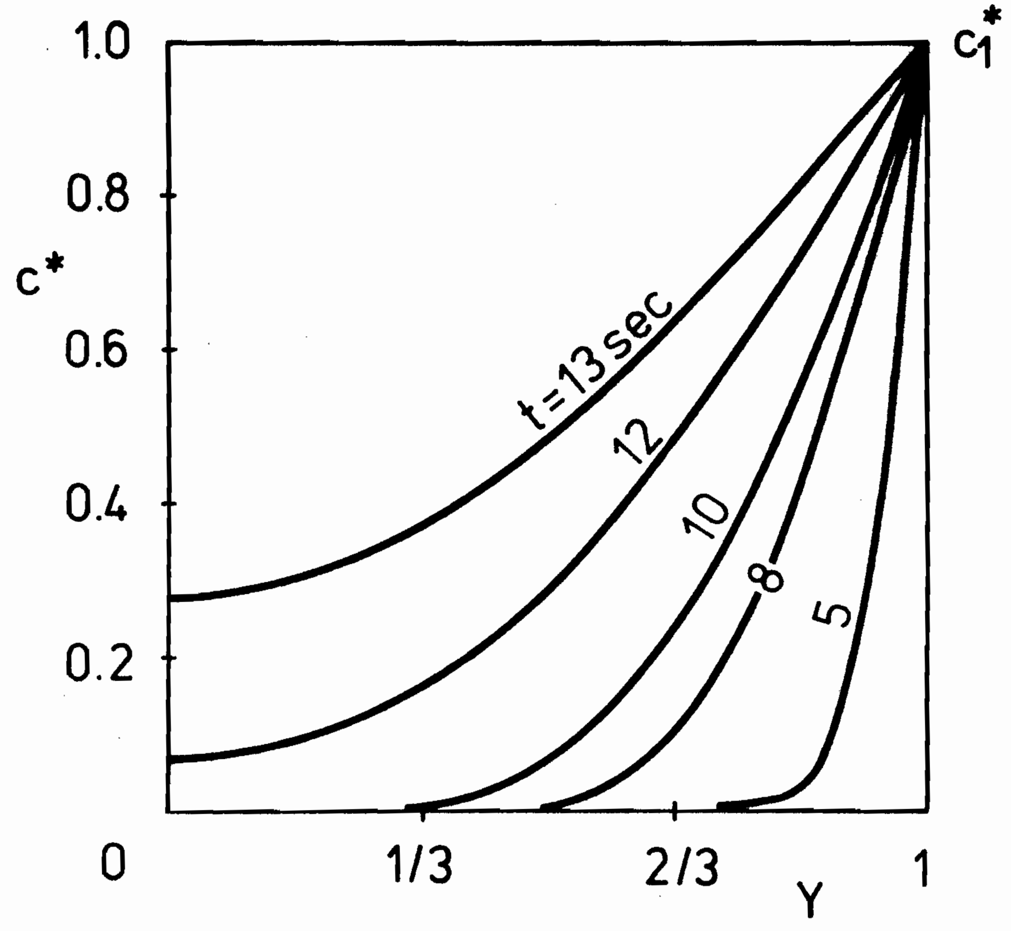

FIGURE 1

TABLE 1

Variation of the coagulant concentration at the centre of the drop and the drop dimensions as a function of time, with $D = 2 \times 10^{-5}$ cm^2/sec, $\lambda = 10$, $c = 0.15$ cm, $c_1^* = 1.0$, and $G = 1.0$ sec^{-1}.

Time t (sec)	Droplet thickness $2b$ (cm)	Droplet length ℓ (cm)	Coagulant concentration c^* (g/g)
0	0.3000	0.3000	0
1	0.2680	0.3358	0
2	0.2400	0.3750	0
3	0.2140	0.4206	0
4	0.1890	0.4762	0
5	0.1670	0.5389	0
6	0.1466	0.6139	0
7	0.1282	0.7020	0
8	0.1114	0.8079	0
9	0.0934	0.9636	0
10	0.0712	1.2640	0.001
11	0.0508	1.7717	0.010
12	0.0314	2.6946	0.068
13	0.0210	4.2857	0.279

the drop is small. The significance of this will become apparent shortly.

So far we have discussed the change of the coagulant concentration as a function of time and position in the drop. This information can now be used to determine the final length of the fibre as a function of various relevant parameters such as G, λ, D, c, and c_1^*. This final length may be obtained by considering that the deformation of the drop will cease as soon as the strength of the precipitated polymer is large enough to resist the hydrodynamic extension forces. Due to the concentration gradient within the drop the polymer precipitates at different locations at different times and inhomogeneity develops. The result is an increasing resistance towards deformation with time. To simplify the problem we assume that the deformation of the drop occurs normally, i.e. the deformation is not influenced by the diffusion of the coagulant (eqs. 22 to 27), until a certain critical concentration of the coagulant is reached. At this point the viscosity ratio suddenly changes to infinity, as illustrated in Figure 2, and the whole liquid thread has coagulated. It is of no great significance where exactly the coagulant concentration reaches its critical value, as long as the position lies close to the centre of the drop between about Y = -1/3 to 1/3, where the concentration profile is very flat. Figure 3 further illustrates the behaviour described above and shows qualitatively the deformation and coagulation of a drop with a viscosity ratio λ greater than unity as a function of the dimensionless time, Gt. Coagulation sets in at Gt^* where the deformation stops abruptly, and the fibre assumes its final length.

The theory described above can now be used to predict the effect of G, λ, D, c, and c_1^* on the final length of the fibre. The computations have been carried out numerically using eqs. 21 to 29. The resulting theoretical predictions for the influence of the various parameters on the fibre length are shown in Figure 4. It is demonstrated that G, D and c have the greatest effect

Figure 2

In the theory it is assumed that the viscosity ratio stays constant until a critical concentration, c^{*}_{crit}, is reached. At this point λ goes to infinity.

Figure 3

Qualitative illustration of the theoretically proposed fibre formation process for a constant viscosity ratio, λ. At Gt^{*} the deformation stops and the fibre assumes its final length.

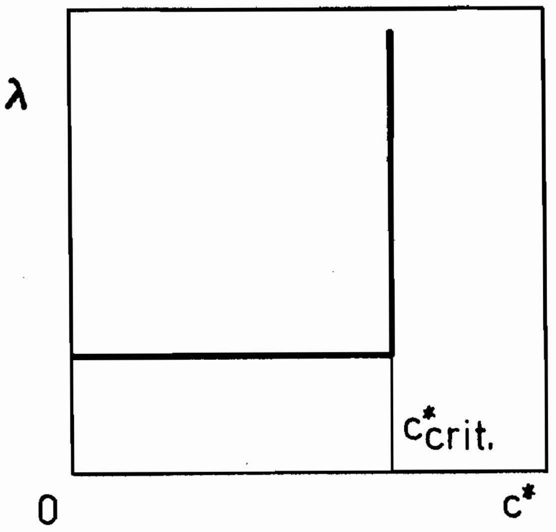

FIGURE 2

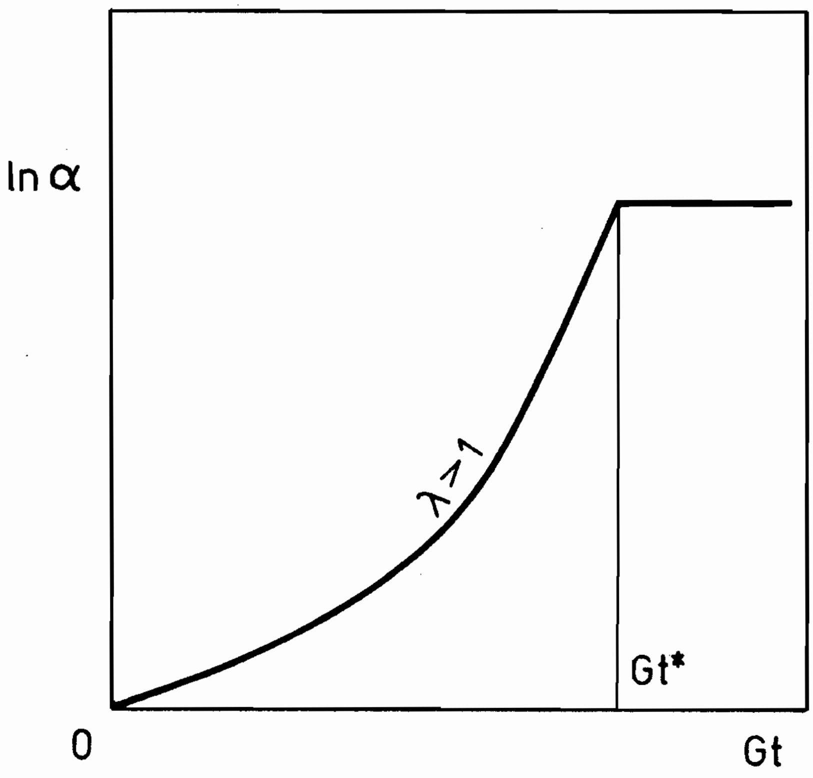

FIGURE 3

Figure 4

Theoretical predictions for the effects of the variation of different parameters as the shear rate (G), the viscosity ratio (λ), the diffusion coefficient (D), the original drop radius (c), and the surface concentration of the coagulant at the drop (c_1^*) on the fibre lengths. If not otherwise indicated, $G = 1\ \text{sec}^{-1}$, $\lambda = 10$, $D = 2 \times 10^{-5}\ \text{cm}^2/\text{sec}$, $c = 0.15$ cm and $c_1^* = 1.0$. It is shown that changes in λ have only small influences.

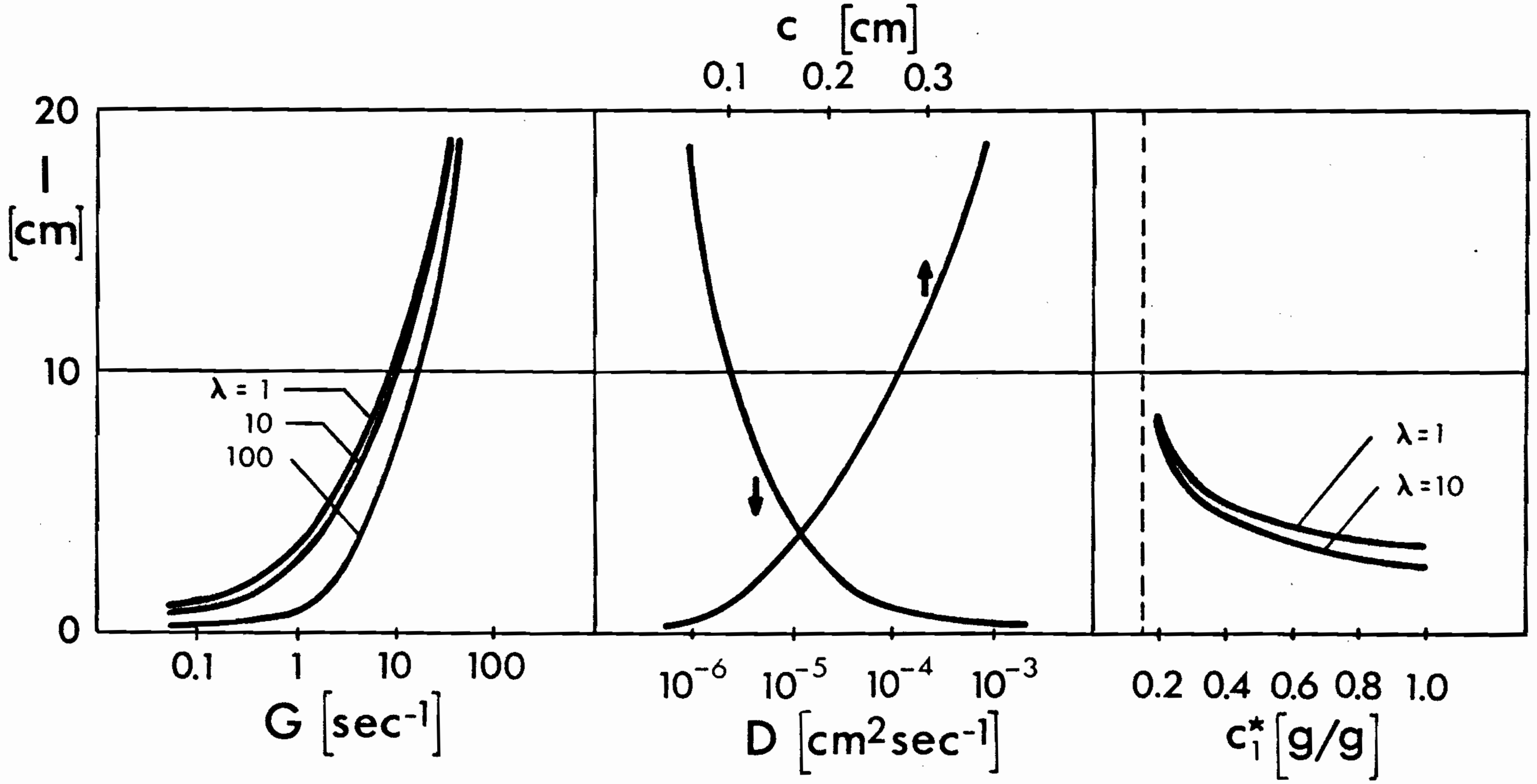

c [cm]
0.1
0.2
0.3
20
l
[cm]
10
0
λ = 1
10
100
0.1
1
10
100
G [sec⁻¹]
10^{-6}
10^{-5}
10^{-4}
10^{-3}
D [cm²sec⁻¹]
λ=1
λ=10
0.2
0.4
0.6
0.8
1.0
c_1^* [g/g]

FIGURE 4

on the fibre length, whereas the variation with λ is very small. In these calculations the deformation of the drops stopped when an assumed critical concentration of the coagulant of 15% (absolute) was reached at the position of $Y = 1/3$. This critical concentration is in fact close to the experimentally found value.

It may be noted that the position where the critical concentration is reached moves inwards and increases the thickness and strength of the coagulated layer. In practical systems with fast coagulants (e.g. viscose and $ZnSO_4$ solutions) the strength of the layer can increase very fast and may stop the deformation of the drop at an early stage, unless very high deformation rates are applied.

The variation of the fibre length may also be plotted as a function of a dimensionless parameter. From eqs. 22 to 27 it follows that

$$T(t) = \frac{D}{c^2 G} f(\lambda, Gt), \qquad 30$$

where f indicates a function, and from eqs. 12 and 23 to 27 that

$$Y = \frac{y}{c} f_1(\lambda, Gt) . \qquad 31$$

Further, eq. 21 can be expressed as:

$$\frac{c^*}{c_1^*} = f_2\left(T(t), Y\right) . \qquad 32$$

The fibre reaches its final length when $c^* = 0.15$ at $Y = 1/3$, therefore eq. 32 yields with eq. 30 the expression:

$$c_1^* = f_3\left(\frac{D}{c^2 G}, \lambda, Gt\right) , \qquad 33$$

or rewritten:

$$Gt = f_4\left(\frac{D}{c^2 G}, \lambda, c_1^*\right) . \qquad 34$$

Since $a = \alpha c$ and $\ell = 2a$ the length of the drop is given by

$$\ell = 2\alpha c \ , \tag{35}$$

or with eqs. 23 to 27:

$$\frac{\ell}{c} = f_5(\lambda, Gt) \ . \tag{36}$$

Eqs. 34 and 36 can then be combined in the form of eq. 37.

$$\frac{\ell}{c} = f_6\left(\frac{D}{c^2 G}, \lambda, c_1^*\right) \tag{37}$$

It can be seen from eq. 37 that the relative length, ℓ/c, of the fibre is now only dependent on the three parameters, D/c^2G, λ, c_1^*, instead of the original five. A plot of ℓ/c versus D/c^2G for various λ's and for $c_1^* = 1$ is shown in Figure 5. Plotting the data in this way is advantageous since the use of the dimensionless parameter D/c^2G in the graph allows coverage of a wide range of experimental conditions with respect to D, c and G. Figure 5 also shows, what was already evident from Figure 4, that the influence of λ on the fibre length is very small for small values of D/c^2G (i.e. in the upper part of the diagram).

It is clear that the theoretically outlined fibre formation process does not correspond exactly to the real situation, where skin formation occurs and results in the development of an inhomogeneous drop. In spite of the idealization of the process, it is thought that the theory gives a general qualitative description of the fibre formation process. It will be of interest to inquire, to what extent the skin formation causes a deviation of the droplet deformation and coagulation from the predicted behaviour.

Figure 5

The relative fibre length, ℓ/c, as a function of the dimensionless number D/c^2G is plotted for various viscosity ratios, λ, and constant c_1^*.

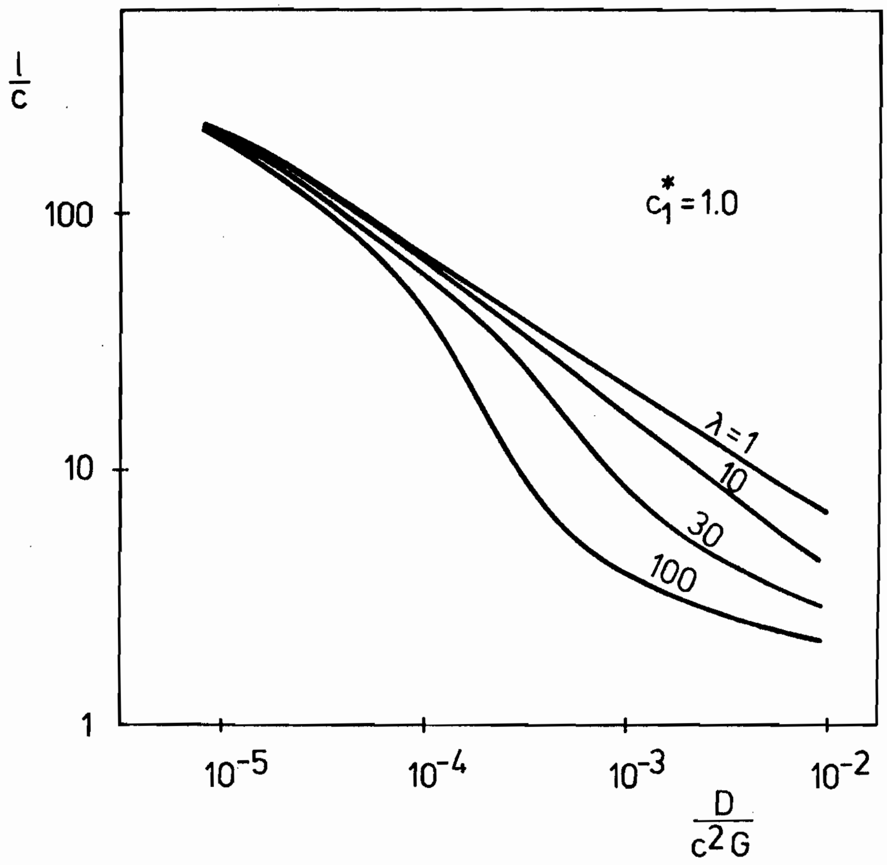

$\frac{l}{c}$
100
10
1
$c_1^* = 1.0$
$\lambda = 1$
10
30
100
10^{-5}
10^{-4}
10^{-3}
10^{-2}
$\frac{D}{c^2 G}$

FIGURE 5

EXPERIMENTAL

The cellulose sample used in the present investigation was cotton linters. It had an intrinsic viscosity of 14 dl/g in dimethyl sulfoxide/paraformaldehyde (DMSO/PF) corresponding to a degree of polymerization of about 1400 according to Swenson's relation[18]. The cellulose solutions were prepared at a concentration of 1.2% by dissolving the cotton linters in DMSO/PF according to procedures described previously[19,2]. Solutions of lower concentration were obtained by dilution with DMSO.

Viscosity measurements were carried out with a capillary viscometer. The measurements of the apparent diffusion coefficient were performed on a Zeiss diffusion interferometer employing sliding quartz cells. In this method, the displacement of the interference fringes in the diffusion interferometer is a measure of the change in the refractive index. The coagulant concentration is then related to the refractive index by a calibration curve, which was determined with an Abbe refractometer using samples of solution and coagulant with known concentrations. All measurements were made at 24°C.

The droplet deformation measurements were performed in a four-roller-mill as described elsewhere[3]. Glycerol was used as the coagulation medium because it was a suitably slow coagulant allowing the fibre formation to be followed photographically; it also provided the necessary high viscosity so that vibrations of the apparatus had no influence on the flow field. It may be noted in passing that the fibres obtained by coagulation with glycerol are rather gel-like in texture and only solidify after a very long period. Of course, more rapid solidification can be effected by a suitable choice of the coagulant.

The introduction of the droplet of cellulose solution into the flowing coagulant was accomplished by a syringe with a long steel needle. The needle, having an outer diameter of 1.2 mm, was placed in an upright position exactly in the centre of the flow field, with its end about 15 to 20 mm below the surface of the coagulant. The cellulose solution was injected in the form of single drops and was coloured with Congo Red using small amounts of the dye just sufficient to supply the necessary contrast for photographical purposes. The deformation process was filmed with a speed calibrated 16 mm Bolex cine camera positioned above the centre of the flow field. After each experiment the coagulated cellulose was removed in order to avoid contamination of the coagulant. It is noteworthy that the amount of coagulant was so large that the effect of the absorbed cellulose solvent on the properties of the coagulant could be neglected.

The cine films were analyzed by projecting the image on a transparent screen and measuring the length of the drop as a function of time.

RESULTS AND DISCUSSION

For analyzing the droplet deformation process and comparing the theoretical predictions with the experimental results, it was necessary to measure the critical coagulant concentration for coagulation of the cellulose solution, the diffusion coefficient of the coagulant into the cellulose solution, and the viscosity ratio of the cellulose solution and the coagulant.

The critical concentration of the coagulant was determined in a kinetic study of the coagulation of cellulose solutions. For this purpose the cellulose solution was carefully mixed with known amounts of glycerol and kept at a constant temperature of 24°C until coagulation occured. Figure 6a shows the time elapsed before the onset of coagulation (open circles) as indicated by a dramatic increase in the turbidity of the solutions and the subsequent separation of gel (full circles). As can be seen, under quiescent conditions the critical coagulant concentration for gelation lies in the range of 15 to 20% per weight of glycerol.

It should be noted that there exists a striking resemblance between the process of gelation as it occurs in the present work and nucleation in crystalline polymers. For example, for the crystallization of polyethylene from solution under Couette flow, it has been shown[20,21] that the induction time for nucleation (τ_i) increases with the crystallization temperature (T_c), or, in other words, decreases with the degree of supercooling (ΔT). A plot of $\tau_i^{-1/2}$ versus T_c or ΔT yielded a linear relationship. In the case of the gelation in the present work, a linear relationship is also obtained when the inverse square root of the coagulation time ($t_c^{-1/2}$) is plotted against the coagulant concentration c^* (see Figure 6b). Since the slopes of $\tau_i^{-1/2}$ versus

Figure 6a

The coagulation time as a function of the coagulant concentration measured at the onset of coagulation (open circles) and at the start of gel separation (full circles).

Figure 6b

Straight line relationship between the inverse root of the coagulation time and the coagulant concentration.

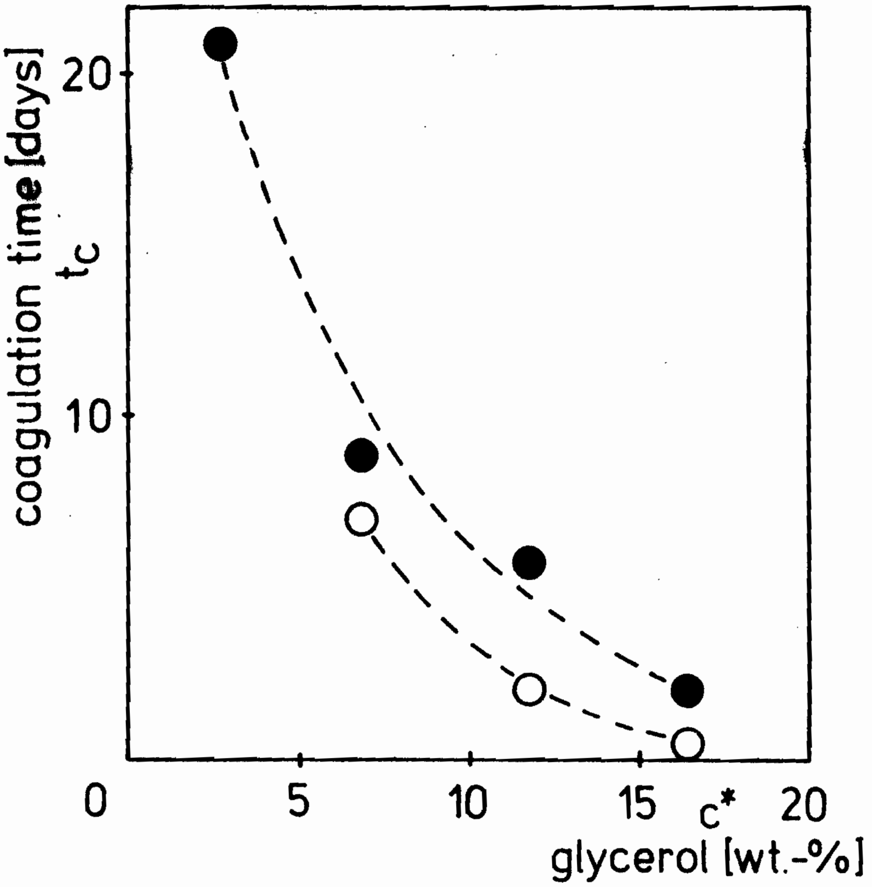

FIGURE 6a

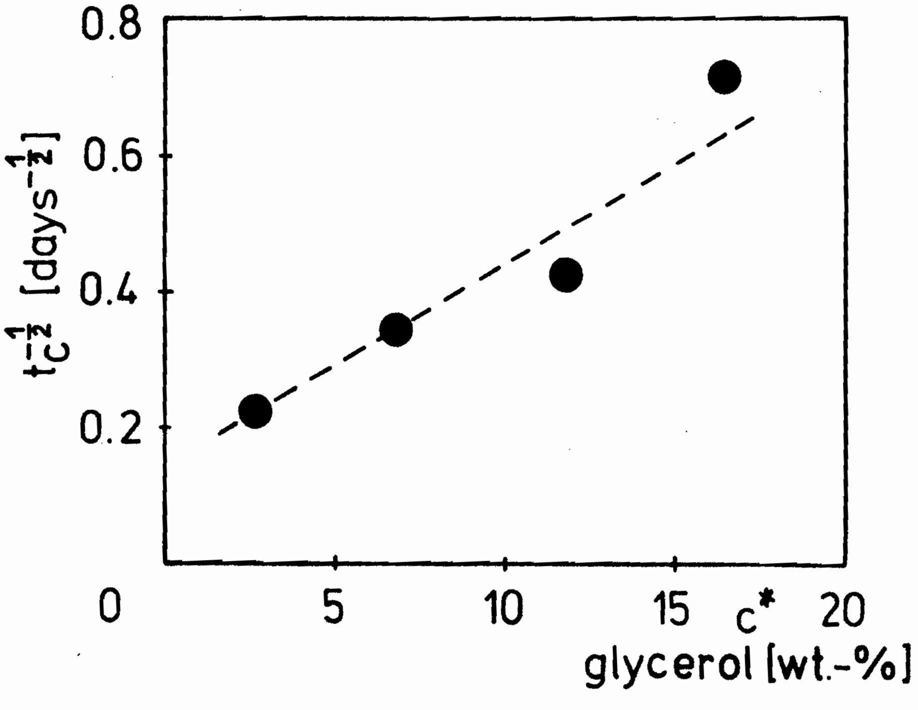

FIGURE 6b

ΔT for polyethylene and $t_c^{-1/2}$ versus c^* for the present system are both positive, the degree of supercooling and the coagulant concentration have similar influences. On the other hand, for polyethylene, $\tau_i^{-1/2}$ is also linearly related to the stirring speed in the Couette system. Therefore, on the basis of the hypothesis that nucleation and gelation are similar processes, it can be inferred that in gelation flow would have a similar effect as in polyethylene, namely, that the coagulation time should decrease with the magnitude of shear or strain applied. This effect has indeed been found experimentally for the gelation of aqueous poly (methacrylic acid) solutions under shear stress[22,23]. Since the coagulation time is dependent on flow, the critical concentration of the coagulant might also be influenced in the same way. However, no quantitative conclusions can be drawn and this subject remains open for further investigation.

The diffusion coefficient may vary with time and over the region where diffusion occurs, but for the sake of simplicity it is assumed that the diffusion coefficient is constant. The apparent diffusion coefficient in the present study for the diffusion of glycerol in a 1.2% cellulose/DMSO/PF solution was measured to be $(3.5 \pm 0.5) \times 10^{-6}$ cm^2/sec. The relatively high error in this measurement is due to the coagulation of the cellulose above the critical concentration of the coagulant; this causes a distortion of the straight interface between cellulose solution and coagulant. A straight interface is necessary for an accurate measurement in this method.

Experiments were also carried out to establish the dependence of the apparent diffusion coefficient on the concentration of the cellulose solution. These experiments were performed by allowing the coagulant to diffuse from both ends into a glass capillary filled with cellulose solution. The time needed for the coagulation boundaries, which appear as the interface between a turbid and a clear solution, to meet in the middle of the capillary is directly proportional to the apparent diffusion coefficient[17]. Two series of experiments with cellulose solutions of 0.7% and 1.2% by weight of cellulose, corresponding to the lowest and highest concentration used, were made. The measured times were about 10 to 15% less for the samples with the smaller cellulose concentration. The difference, however, lay within the range of the estimated error for the apparent diffusion coefficient and was therefore neglected.

The viscosities of the cellulose solutions used and the viscosity ratios of the solutions with respect to glycerol are shown in Table 2. In these viscosity measurements the shear rate was less that 0.5 $\sec^{-1}$. At such low shear rates the shear rate dependence of the viscosity is expected to be negligible.

The experiments on fibre formation were performed in the four-roller-mill at different shear rates (G) in the range of 0.44 and 1.21 $\sec^{-1}$ and viscosity ratios (λ) between 0.377 and 7.44. Typical results of the fibre formation process are shown in Figures 7 and 8. From the theory given earlier[3] and above, it can be shown that for deformations in which λ is unity or somewhat less, a plot of $\ln\alpha$ against Gt should increase almost linearly up to a certain value where $Gt = Gt^*$, after which it should remain constant, as illustrated in Figures 7 and 8 by the solid curves. When $\lambda > 1$, the increase of $\ln\alpha$ with Gt should be initially non-linear as shown in Figure 3. Comparing the observed deformation with the theoretical prediction, it can be seen that the observed deformation process is always slower than the predicted. This behaviour can be interpreted to mean that the viscosity ratio is not constant but increases with time, a point which will be discussed later on. Figure 8 also shows experimental data for a drop with $\lambda = 1.95$. The deformation in this case could not be completed because of the instability of the drop in the centre of the

TABLE 2

Viscosities and viscosity ratios of the cellulose solutions and the coagulant measured at 24^oC in a calibrated capillary viscometer.

Sample	Concentration wt-%	Viscosity poise	Viscosity ratio with glycerol λ -
cellulose in DMSO/PF	1.2	59.7	7.44
"	1.0	15.6	1.95
"	0.9	8.6	1.08
"	0.7	3.03	0.377
glycerol	99.0	8.02	1.0

Figure 7

The logarithm of the length ratio, $\ln\alpha$, as a function of the dimensionless time, Gt, for a viscosity ratio of $\lambda = 0.377$ and various shear rates, G; $c = 0.13$ cm. The points and the full curves correspond to the experimental and theoretical results respectively.

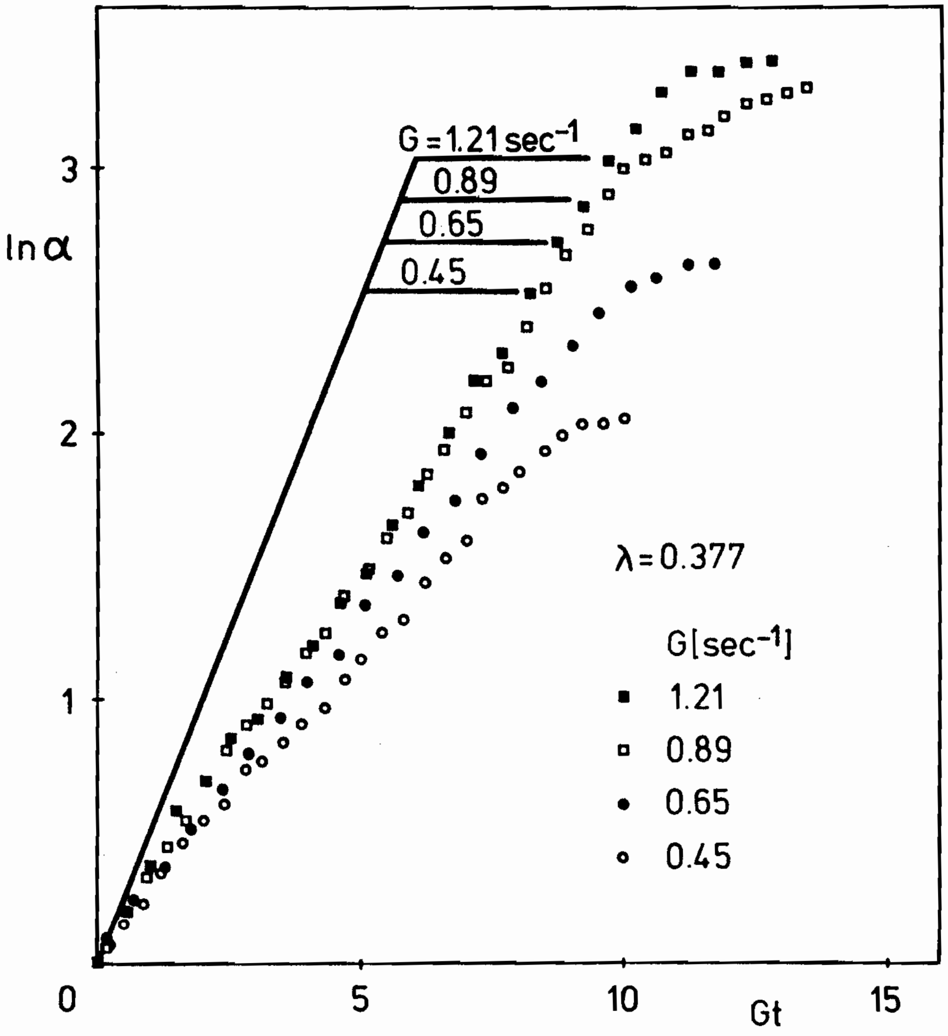

ln α
0
1
2
3
0
5
10
15
Gt
G = 1.21 sec⁻¹
0.89
0.65
0.45
λ = 0.377
G [sec⁻¹]
■ 1.21
□ 0.89
● 0.65
○ 0.45

FIGURE 7

Figure 8

The logarithm of the length ratio, $\ln\alpha$, as a function of the dimensionless time, Gt, for two viscosity ratios, λ, and various shear rates, G. $c = 0.14$ cm. The points and the full curves correspond to the experimental and theoretical results respectively.

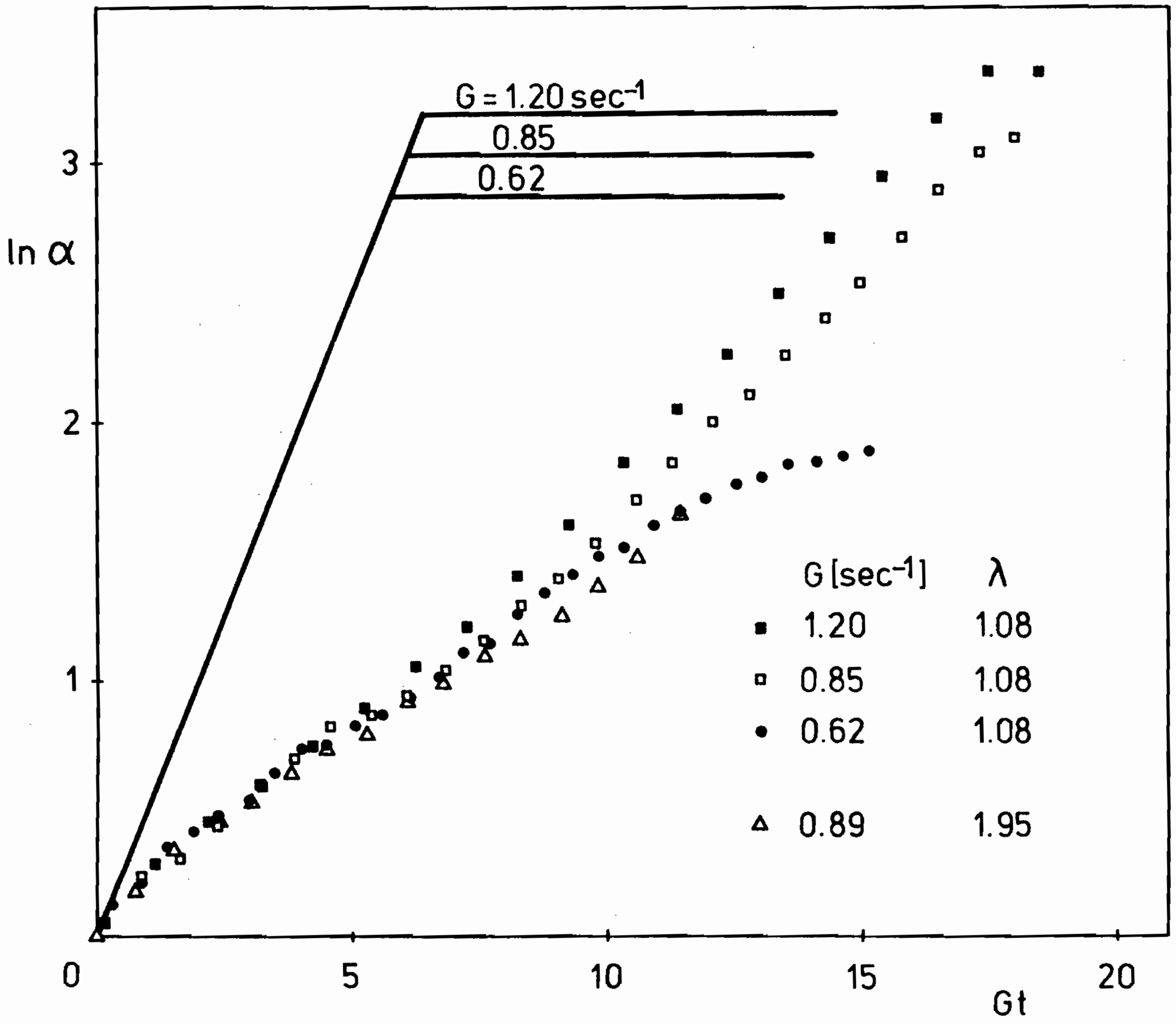

G = 1.20 sec⁻¹
0.85
0.62
3
2
1
ln α
G [sec⁻¹]
λ
■ 1.20 1.08
□ 0.85 1.08
● 0.62 1.08
△ 0.89 1.95
0
5
10
15
20
Gt

FIGURE 8

flow field; the reason for higher instability in this case is not understood. The deformation curve for this drop lies lower than that for $\lambda = 1.08$ at a similar shear rate. The difference in the viscosity seems to have only a small influence on the deformation behaviour in these cases. Experiments with drops having $\lambda = 7.44$ yielded coagulated drops only with small deformations indicating that the resistance to deformation is high due to the higher viscosity of the drop and skin formation. It may further be seen in Figures 7 and 8 that the theoretical curve seems to be tangential to the experimental data at $Gt = 0$. This suggests that the slope of the deformation curves at the origin is given by Taylor's theory[5]:

$$\frac{d \ln \alpha}{dGt} = \frac{5}{2(2\lambda + 3)} \quad . \tag{38}$$

Although the actual deformation behaviour of the drop is slower than predicted, the effect of the shear rate on the final fibre length is in agreement with the theoretical predictions (see Figures 4 and 5), i.e. the fibre length increases with the shear rate. This is also shown in Table 3, where the experimental and theoretical fibre lengths are tabulated as a function of the viscosity ratio and the shear rate. The influence of the initial droplet radius (c) on the fibre length is also shown in Table 3. In agreement with the predictions, the fibre length increases with c. At intermediate shear rates, the experimental results are in reasonable quantitative agreement with the theoretical predictions. At higher shear rates, however, the observed fibre length is considerably larger than that calculated. This deviation may originate in a stretching of the coagulated cellulose gel, which is close to the point of break-up. This inference derives from the observation that, at shear rates in excess of approximately 1.2 sec^{-1}, nearly all the fibres formed broke into two or more pieces. At small shear rates, the observed fibre length is

TABLE 3

Comparison of the fibre lengths obtained from the theory and the experiments. Gt^* is the dimensionless time elapsing until the deformation stops and G denotes the shear rate.

			Experiments		Theory	
λ	G	c	Gt^*	ℓ	Gt^*	ℓ
–	sec^{-1}	mm	–	mm	–	mm
0.377	0.45	1.1	10.0	17.5	5.07	28.00
"	"	1.3	12.0	30.4	5.34	38.71
"	0.65	1.1	11.0	30.3	5.50	33.26
"	"	1.3	13.0	42.8	5.73	46.64
"	"	1.4	12.0	49.4	5.93	54.51
"	0.89	1.3	13.0	72.0	6.09	55.13
"	"	1.0	12.0	51.8	5.50	32.28
"	"	1.1	13.0	58.1	5.72	39.22
"	1.21	1.1	12.5	64.2	6.07	46.00
"	"	1.1	13.0	78.4	6.07	46.00
1.08	0.62	1.4	14.0	39.9	5.87	53.35
"	"	1.3	15.0	16.7	5.69	45.70
"	0.85	1.3	16.5	61.1	6.05	53.77
"	"	1.4	18.0	65.3	6.16	62.12
"	"	1.4	14.0	44.7	6.16	62.12
"	1.20	1.1	19.0	74.9	6.06	45.81
"	"	1.0	20.0	67.0	5.85	38.13
"	"	1.3	19.0	74.9	6.33	63.38
1.95	0.89	1.2	–	–	6.68	46.26
"	"	1.1	–	–	6.49	38.73

smaller than the calculated, probably because the deformation ceased before all the cellulose solution was coagulated.

It is interesting to note that the time (Gt^*) required to form a fibre of a given length is 2 to 3 times longer than predicted by the theory, in spite of the fact that the observed and calculated fibre lengths are in reasonable agreement, at least at intermediate shear rates (see Table 3). In seeking to explain this anomalous behaviour, it seems pertinent to recall that it was assumed that λ remains constant with time. In fact, however, as will be shown subsequently, this assumption is not valid. Therefore the unexpected behaviour mentioned above may originate in the difference between the theoretically constant viscosity ratio, λ, and the apparent viscosity ratio, λ_{app}, which is obtained by experimental observation. Intuitively, the higher the viscosity of a drop, the lower the rate at which it can be deformed. Since λ_{app} is with time increasingly greater than λ, the deformation of the drop characterized by λ_{app} will be more and more retarded, giving therefore longer times, Gt^*, than for a drop characterized by λ.

Following the foregoing paragraph, it is of interest to use the deformation data to determine λ_{app}. For this purpose, the strain rate ratio 2k/G has to be determined (see eq. 26). This can be accomplished when the experimental deformation results are treated with the formulas for the droplet deformation developed earlier[3]. The differential equation for the deformation of the drop is

$$\frac{d\alpha}{dt} = k\alpha \ , \qquad 39$$

and can be written as

$$\frac{d \ln \alpha}{dGt} = \frac{k}{G} \ . \qquad 40$$

The strain rate ratio 2k/G may therefore be obtained at any time during the deformation by graphical differentiation of the deformation curves and by multiplying the result by two. When the strain rate inside the drop is known, the apparent viscosity ratio, λ_{app}, can finally be calculated when eq. 26 is rewritten as eq. 41.

$$\lambda_{app} = \frac{(\frac{G}{2k} - 1)\alpha^3\pi}{14(\ln\frac{4\alpha^2}{\alpha + 1} - \frac{3}{2})} + \frac{0.75}{1.75} \qquad 41$$

This equation describes for a given 2k/G at any λ the apparent viscosity of the drop. Due to the theoretical assumption of slender bodies[24,3], the expression is applicable for deformations higher than $\alpha = 3$. Typical results for the behaviour of 2k/G and λ_{app} are shown in Figure 9 and Appendix III. It can be seen that both 2k/G and λ_{app} fluctuate with time. Initially, it was thought that these apparent fluctuations might be due to small experimental errors magnified by the method of differentiation. However, a close inspection of the data revealed that the fluctuations must be genuine because in similar measurements, where no skin formation could occur[3], the differentiation of the experimental deformation curves would have given much smaller fluctuations in 2k/G, which could readily be associated with the experimental error. The fluctuations seem to be related to the formation and the break-up of coagulated layers of cellulose on the surface of the drop. Measurements over a range of shear rates (see Appendix III) indicate that the magnitude of the fluctuations appears to decline at higher shear rates (G). This might indicate that there is less influence of skin formation and skin rupture on the drop deformation at higher shear rates. 2k/G drops first sharply with time and then assumes during the main part of deformation values approximately between 0.3 and 0.7 under the present experimental conditions. At the end of the deformation process 2k/G drops to zero. The mean

Figure 9

The logarithm of the length ratio, $\ln\alpha$, of a coagulating drop is plotted as a function of the dimensionless time, Gt, for c = 0.11 cm, $\lambda = 0.377$, and $G = 0.45\ \mathrm{sec}^{-1}$. The strain rate ratio, 2k/G, can be obtained by graphical differentiation of the deformation curve (see eq. 40) and the apparent viscosity ratio, λ_{app}, can be calculated by eq. 41. The fluctuations in 2k/G and λ_{app} are probably due to skin formation and rupture.

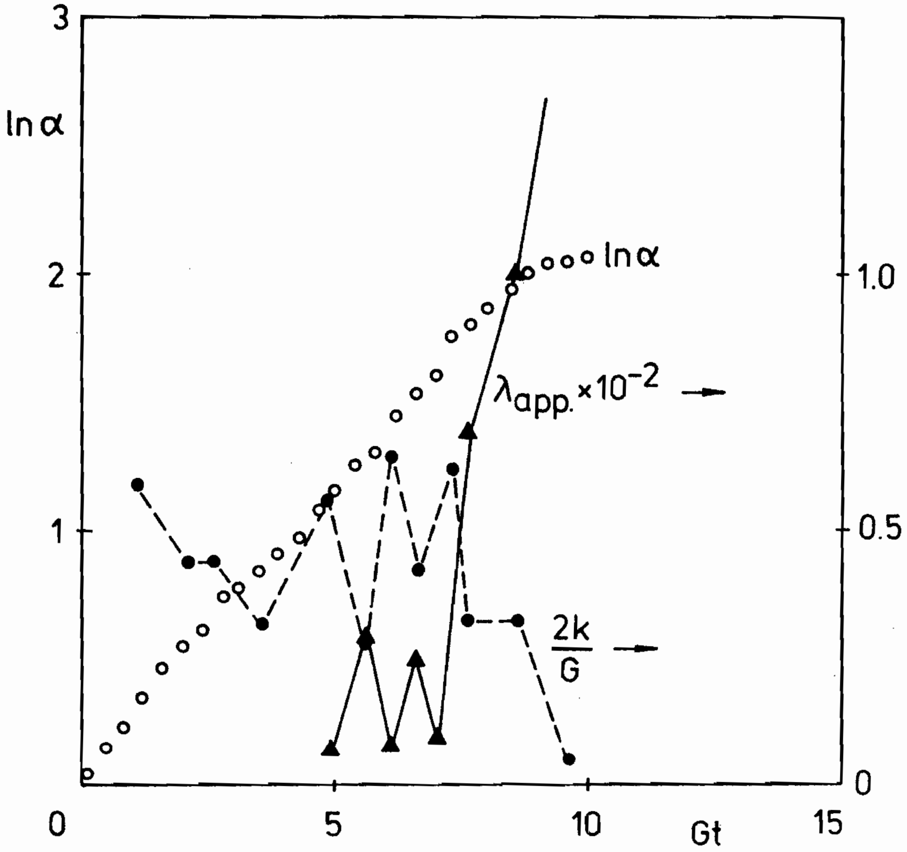

FIGURE 9

value of λ_{app} increases first slowly and rises after a certain time very fast. This time dependence of λ_{app} may now explain the observation that the coagulating drops in the experiments deform more slowly than those according to the theory.

The strain rate ratio described above is a measure of the strength of the extensional flow field inside the drop. It is well known that longitudinal velocity gradients (extensional flow) influence the molecular extensions[6-8]; i.e. higher gradients may increase the molecular extension and therefore the degree of orientation inside the fibres. Accordingly, a knowledge of the strain rate achieved inside the fibres is of interest for any further practical application of the fibre formation process.

The fact that no higher shear rates than 1.2 $\sec^{-1}$ could be employed without breaking the fibre can yield a further interesting result. Applying Cox's slender body theory[3,24], the force per unit length exerted on a fibre can be calculated. The relevant formula for the present conditions was derived earlier[3] and leads, after integration over the half of the length and substitution of $\ell = 2c\alpha$, to the force per unit cross-sectional area, F_α, given by eq. 42,

$$F_\alpha = \frac{\alpha^3 \mu (\frac{G}{2} - k)}{\ln \frac{4\alpha^2}{\alpha + 1} - \frac{3}{2}} \qquad 42$$

where μ is the viscosity of the coagulant. Eq. 42 is valid for slender bodies with an ellipsoidal cross-section. At the critical shear rate of about 1.2 $\sec^{-1}$ and, when the coagulation is completed, k becomes zero and the force corresponds to the strength of the gel-like fibre. An uncertainty in this calculation is, however, the magnitude of μ which depends on the concentration of DMSO in glycerol in the vicinity of the fibre. An estimate of μ = 20 centipoise (corresponding to roughly 50% DMSO) would yield for $\alpha = 20$ and $G = 1.2 \sec^{-1}$ a value of $F_\alpha = 33.9$ Pa. This resulting strength is very small, showing that stretching and break-up of the gel may easily occur. Of course, when faster coagulants are employed the resulting fibre may become crystalline giving therefore a much higher strength.

Finally, the observation that droplet break-up occurs when the shear rate employed is higher than a critical value, indicates the presence of two regimes of fibre formation:

1) Fibre formation without break-up.
2) Fibre formation followed by break-up of the fibre.

The first regime results in fibres described in the present work. The second is, however, expected to give shorter fibres probably having better orientation because of the stretching of the gel. This latter regime ought to be examined in any further theoretical and experimental studies.

CONCLUSION

Macroscopic cellulose fibres are formed when a viscous cellulose solution is introduced into a vigorously stirred coagulant. The viscous cellulose solution is dispersed as droplets in the coagulant and the droplets are deformed into thin threads which coagulate forming fibres. A detailed understanding of this process has been obtained by assuming an idealized model in which the droplet is homogeneous and deforms according to previously[3] derived expressions. The deformation stops and the fibre assumes its final length when a critical concentration of coagulant is reached at a certain position inside the drop. It has been shown that theoretical calculations based on this model can be used to make predictions of the fibre length as a function of various parameters. The fibre length e.g. increases with the applied shear rate, the original droplet diameter, and decreases with the diffusion coefficient of the coagulant in the cellulose solution. All results show qualitative agreement with the theoretical predictions and there is quantitative agreement at intermediate shear rates. Skin formation on the surface of the deforming droplets causes an increase in the apparent viscosity ratio of drop and coagulant; therefore the deformation of the drop is delayed with respect to the theoretical model process and accordingly the time needed in the experiment to form a fibre is longer than predicted. Refinement of the theoretical model by taking into account the change of the viscosity ratio with time would be expected to give a better quantitative agreement with the experimental results.

Experimentally observed fluctuations of the strain rate inside the drop and the apparent viscosity ratio can be explained in terms of skin formation and rupture during coagulation.

Although the present theory was tested with the specific system cellulose/DMSO/PF and glycerol, it is expected to be generally applicable to fibre formation processes involving other polymer/coagulant systems.

Finally, it may be noted that the present work chiefly leads to the prediction of fibre dimensions. However, another important property of the fibres is their tensile strength, which is closely related to the molecular orientation. It has been shown[2] that there is an apparent relation between fibre dimensions and molecular orientation. The detailed analysis of this problem remains for further investigation.

REFERENCES

1. Allen, S.L., Turvey, R.W., and Bolker, H.I., Appl. Polym. Symp. 28, 903 (1976).
2. Chapter II.
3. Chapter III.
4. Taylor, G.I., Proc. Roy. Soc. (London), A138, 41 (1932).
5. Taylor, G.I., Proc. Roy. Soc. (London), A146, 501 (1934).
6. Frank, F.C., Proc. Roy. Soc. (London), A319, 127 (1970).
7. Marrucci, G., Polym. Eng. Sci. 15, 229 (1975).
8. Peterlin, A., Polymer Preprints-ACS, 16, 315 (1975).
9. Hermans, J.J., J. Colloid Sci. 2, 387 (1947).
10. Vermaas, D., Textile Res. J. 32, 353 (1962).
11. Serkov, A.T., and Kotima, D.N., Faserforsch. Textiltech. 22, 434 (1971).
12. Parrish, E., McCartney, J.R., Morgan, P.W. (to du Pont), U.S. 2,988,782, June 20, 1961.
13. Parrish, E. (to du Pont), U.S. 3,114,747, Dec. 17, 1963.
14. Miller, I.K. (to du Pont), U.S. 3,338,884, Aug. 29, 1967.
15. Brundige, M.M., Hunger, G.K., Kohne, Jr., H.F., Kurrle, F.L. (to West Virginia Pulp and Paper Company), U.S. 3,342,921, Sept. 19, 1967.
16. Eckert, E.R.G., and Drake, Jr., R.M., "Heat and Mass Transfer", McGraw Hill, N.Y., 1959.
17. Crank, J., "The Mathematics of Diffusion", Clarendon Press, Oxford, 1956.
18. Swenson, H.A., Appl. Polym. Symp. 28, 945 (1976).
19. Johnson, D.C., Nicholson, M.D., and Haigh, F.C., Appl. Polym. Symp. 28, 941 (1976).
20. Pennings, A.J., van der Mark, J.M.A.A., and Booij, H.C., Kolloid Z.u.Z. Polymere 236, 99 (1970).
21. Pennings, A.J., J. Polym. Sci.: Polym. Symp. 59, 55 (1977).

22. Eliassaf, J., Silberberg, A., and Katchalsky, A., Nature 176, 1119 (1955).

23. Ono, K., and Murakami, K., J. Polym. Sci. B15, 507 (1977).

24. Cox, R.G., J. Fluid Mech. 44, 791 (1970).

CHAPTER VI

PROPOSAL FOR FIBRE SPINNING IN AN EXTENSIONAL FLOW FIELD

In spinning processes presently applied in the fibre industry[1], the polymer melt or solution is extruded through orifices with diameters of the order of micrometers. There are two disadvantages in the use of such orifices. First, they frequently become clogged by impurities, and secondly, the flow inside the capillaries is largely shear flow which is not capable of producing good molecular orientation and alignment, as required for the production of fibres of high strength. Shear flow is ineffective, because it contains both an extensional and a rotational flow component[2]. During rotation the molecule is periodically subjected to compression and extension, and any molecular extension that is produced is cancelled in the compressional phase. On the other hand, in pure extensional flow there is no rotational component and the molecules can be persistently extended. It follows from the above discussion that, due to the occurrence of shear flow in the capillaries, the extruded material is expected to have low molecular orientation. The filaments gelate or solidify by coagulation of the polymer solution in a coagulant bath, by cooling the melt, or by vaporization of the solvent from the polymer solution. After gelation or solidification of the polymer the necessary molecular orientation and strength of the fibres is achieved by means of a stretching process.

The intention of the present chapter is to propose a new principle of fibre spinning in which the above-mentioned disadvantages of conventional spinning processes are obviated. The new spinning process is based on the work on droplet deformations which was presented in earlier chapters[3-6] of this thesis. It was shown in these chapters that fibres can be formed by the introduction of droplets of cellulose solution into a flowing coagulant, where the coagulant usually has a lower viscosity than the polymer solution. The droplets deform by the action of extensional flow in the coagulant and the polymer precipitates when sufficient coagulant has diffused across the polymer-solution/

coagulant boundary. At this point the deformation ceases yielding a fibre of a certain length. As an important theoretical and experimental result, it was found that the strain rate of the extensional flow inside the deforming drop increases with deformation and reaches that of the flow field outside at high deformations, as may be seen for large values of α from the following expression[4]:

$$k = \frac{G/2}{\frac{8\lambda}{\pi}\frac{1}{\alpha^3}\left(\ln\frac{4\alpha^2}{\alpha+1} - \frac{3}{2}\right) + 1} \qquad 1$$

Here k and G/2 are the strain rates inside and outside the drop, α is the ratio of the length of the deforming drop and the original droplet diameter; λ denotes the viscosity ratio of polymer solution and coagulant. This expression was derived for low strain rates and high deformations, as well as under the assumption that no coagulation has occurred. Nevertheless, the equation describes at least qualitatively the development of the strain rate inside the drop when the coagulant is very weak. For deformations at high strain rates another theory derived earlier[5] may be applied. The strain rate is of significance for the extension and alignment of molecules[7,8] and therefore for the molecular orientation of the fibres. It is evident from the discussion above that, in order to achieve good molecular orientation in the fibres, the conditions during fibre formation must be chosen such that coagulation sets in when the strain rate inside the drop is sufficiently high and is applied for a long enough time interval.

On the basis of the above considerations, a spinning process may be proposed that involves the deformation of a drop by the application of extensional flow within the coagulant. Such a process is depicted schematically in Figure 1. The polymer is supplied through the opening on the top of the

<u>Figure 1</u>

Schematic diagram illustrating the proposed fibre spinning process.

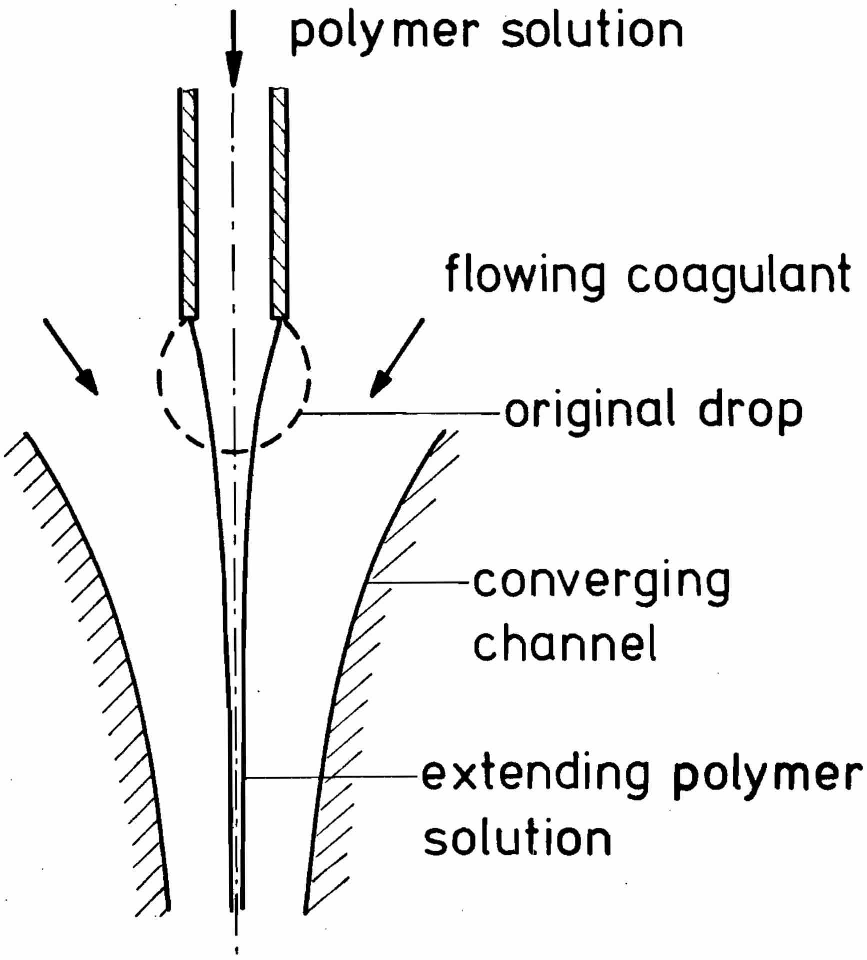
polymer solution
flowing coagulant
original drop
converging channel
extending polymer solution

FIGURE 1

apparatus illustrated. The diameter of the opening can be relatively large with respect to the diameter of the fibre produced, since it has no influence on the thickness of the fibre formed. When a polymer solution is injected, the initially nearly spherical drop is deformed by the action of the flowing coagulant in the convergent channel into a long liquid thread. Coagulation sets in when sufficient coagulant has diffused into the thread, somewhere in the lower part of the channel. An additional increase in the molecular orientation might be obtained due to stretching of the coagulating polymer solution. The flow of the coagulant can be achieved by pumping the coagulant through the convergent channel. Depending on the way the polymer solution is injected, whether intermittently or continuously, the product can be short fibres or an endless filament. The fibres can be collected by means of a screen or a take-up device.

Eq. 1 relates to the formation of short fibres. For the case of continuous fibre spinning no mathematical expressions have yet been derived. However, the two processes are closely related, since in the case of droplet deformation the strain rate inside the drop increases with time and is nearly constant within the drop while in the case of continuous filaments the strain rate increases with the distance from the orifice and is constant with time.

Attention should be paid to the fact that the flow field inside the extending thread is highly extensional in character especially when the thread is very thin[5]. The thinner the thread, the closer the strain rate within it approaches that outside, and the less shear flow is involved. Accordingly, the coagulant concentration and the length of the apparatus have to be chosen in such a way that the liquid thread solidifies when high molecular orientation is reached.

It is most important to note that such polymer/coagulant systems must be selected, for which the interfacial tension is small, since high interfacial tension may cause a break-up of the liquid thread into smaller drops[9]. Of course, when the viscosity of the polymer solution is high, the interfacial tension may become unimportant.

For completeness it should be mentioned that the proposed process may also be used in melt spinning processes, since instead of the coagulant, a flowing cooling medium (fluid or gas) that supercools the melt may be applied.

References

1. Mark, H.F., Atlas, S.M., and Cernia, E., "Man-Made Fibers", Interscience, N.Y., Vols. I and II, 1967 and 1968.
2. Frank, F.C., Proc. Roy. Soc. (London) A, 319, 127 (1970).
3. Chapter II.
4. Chapter III.
5. Chapter IV.
6. Chapter V.
7. Peterlin, A., Polymer Lett. 4, 287 (1966).
8. Marrucci, G., Polym. Eng. Sci. 15, 229 (1975).
9. Rumscheidt, F.D., and Mason, S.G., J. Colloid Sci. 16, 238 (1961).

APPENDIX I

THE FORCE PER UNIT LENGTH FOR A SLENDER BODY (SPHEROID) IN HYPERBOLIC FLOW

LIST OF SYMBOLS

a, b = major and minor axis of the prolate spheroid respectively

C = integration constant

$\underline{F}$ = force per unit length vector, dimensionless

F_1; $F(x)$ = force per unit length in the x-direction in dimensional and dimensionless form respectively

$G/2$ = strain rate of the undisturbed flow outside the body

$\underline{I}$ = Idem factor

k = strain rate of the flow on the surface of the body

$\underline{R}$ = $R(s)$, vector of the centre line of slender body

$\underline{\hat{R}}$, $\hat{s}$ = variables for the integration

R_i, R_j, R_k = components of the vector of the centre line of the body

s = x/a, dimensionless coordinate

$\underline{U}$, $\underline{U}^*$ = $\underline{U}(s)$, dimensionless velocity vector of the undisturbed external flow field and at the surface of the body respectively

U_k = components of the velocity vector, $k = 1, 2, 3$

$U_k(\hat{R})$, $U_k^*(\hat{s})$ = components of the velocity vector of the external flow and the surface of the body

δ_{ij} = Kronecker's delta

ε = arbitrary number, $\varepsilon \ll 1$

κ = b/a, for $a \gg b$

λ = $\lambda(s)$, dimensionless function of the body radius

The force per unit length acting on a long and slender body of circular cross-sections in a flow field was derived by Cox[1]. He gave a general expression for slender bodies which can have straight or curved centre lines and may be exposed to any mathematically describable viscous flow. The general expression is given by eq. 1,

$$\frac{\underline{F}}{2\pi} = \left[\frac{(\underline{U} - \underline{U}^*)}{\ln\kappa} + \frac{\underline{J} + (\underline{U} - \underline{U}^*)\ln(2\varepsilon/\lambda)}{(\ln\kappa)^2}\right]\left[\frac{d\underline{R}}{ds}\frac{d\underline{R}}{ds} - 2\underline{I}\right]$$

$$+ \frac{\frac{1}{2}(\underline{U} - \underline{U}^*)}{(\ln\kappa)^2}\left[3\frac{d\underline{R}}{ds}\frac{d\underline{R}}{ds} - 2\underline{I}\right] + \mathcal{O}\{\frac{1}{(\ln\kappa)^3}\} \qquad 1$$

where $\underline{J}$ is by definition a vector described by:

$$J_i = \frac{1}{2}\left[\int_{-1}^{s-\varepsilon} + \int_{s+\varepsilon}^{+1}\right]\left(\frac{\delta_{ij}}{|\underline{R} - \hat{\underline{R}}|} + \frac{(R_i - \hat{R}_i)(R_j - \hat{R}_j)}{|\underline{R} - \hat{\underline{R}}|^3}\right)$$

$$\times\left(\delta_{jk} - \frac{1}{2}\frac{\hat{R}_j}{d\hat{s}}\frac{d\hat{R}_k}{d\hat{s}}\right)\{U_k(\hat{\underline{R}}) - U_k^*(\hat{s})\}\, d\hat{s}\ . \qquad 2$$

For a spheroid with the semi-axes a, and b = c, the body centre line can be described by

$$\underline{R}(s) = \left|\begin{matrix} s \\ 0 \\ 0 \end{matrix}\right| , \qquad 3$$

with

$$-1 \leq s \leq +1\ . \qquad 4$$

$\underline{R}$ may further be written as:

$$R_i = \delta_{i1} s \, , \tag{5}$$

and the derivative has the form of eq. 6.

$$\frac{dR_i}{ds} = \delta_{i1} \tag{6}$$

For a hyperbolic flow field, the velocity field is given by

$$\underline{U} = \frac{2}{Ga} \begin{pmatrix} \frac{G}{2} x \\ -\frac{G}{2} y \\ 0 \end{pmatrix} = \begin{pmatrix} s \\ -\frac{y}{a} \\ 0 \end{pmatrix} , \tag{7}$$

and the velocity vector at the surface of the body may be described by eq. 8 (from chapter III):

$$\underline{U}^* = \frac{2}{Ga} \begin{pmatrix} \kappa x \\ -\kappa y \\ 0 \end{pmatrix} = \begin{pmatrix} \frac{2k}{G} s \\ -\frac{2k}{G} \frac{y}{a} \\ 0 \end{pmatrix} . \tag{8}$$

These expressions may now be substituted in eq. 2 and yield the following expressions for $\underline{J}$:

$$J_i = \frac{1}{2} \left[\int_{-1}^{s-\varepsilon} + \int_{s+\varepsilon}^{1} \right] \frac{1 + \delta_{i1}}{|s - \hat{s}|} \left\{ \frac{1}{2}\left(1 - \frac{2k}{G}\right) s - \left(1 - \frac{2k}{G}\right) \frac{\kappa y}{b} \right\} d\hat{s} \, . \tag{9}$$

Since $\kappa \ll 1$, the last term in the brackets may be omitted in the following. The integration may then be carried out and gives eqs. 10 and 11,

for $\hat{s} < s$

$$\int \frac{\hat{s} d\hat{s}}{|s - \hat{s}|} = -\hat{s} - s \ln(s - \hat{s}) + C \tag{10}$$

for $\hat{s} > s$

$$\int \frac{\hat{s}d\hat{s}}{|s - \hat{s}|} = \hat{s} + s\ln(\hat{s} - s) + C\ , \qquad 11$$

where C is the integration constant. If the limits of the integral are introduced,, J_i takes the following form:

$$J_i = \frac{1}{2}\left(1 + \delta_{i1}\right)\left(1 - 2k/G\right)\left(-s - s\ln\varepsilon + \frac{1}{2}s\ln(1 - s^2)\right)\ . \qquad 12$$

All expressions that are needed for the determination of $\underline{F}$ are now known and may be substituted in eq. 1:

$$\begin{aligned}
\frac{\underline{F}}{2\pi} = &\left[(1/\ln\kappa)(1 - 2k/G)\begin{vmatrix} s \\ -\frac{\kappa y}{b} \\ 0 \end{vmatrix} + (1/\ln\kappa)^2\left\{\frac{1}{2}(1 - 2k/G)\begin{vmatrix} 2 \\ 1 \\ 1 \end{vmatrix}\right.\right. \\
&\times\left(-s - s\ln\varepsilon + \frac{1}{2}s\ln(1 - s^2)\right) + (1 - 2k/G)\begin{vmatrix} s \\ -\frac{\kappa y}{b} \\ 0 \end{vmatrix} \\
&\left.\left.\times(\ln 2 + \ln\varepsilon - \ln\lambda)\right\}\right]\left[\begin{vmatrix} 1 & 0 & 0 \\ 0 & 0 & 0 \\ 0 & 0 & 0 \end{vmatrix} - \begin{vmatrix} 2 & 0 & 0 \\ 0 & 2 & 0 \\ 0 & 0 & 2 \end{vmatrix}\right] \\
&+ (1/\ln\kappa)^2\,\frac{1}{2}(1 - 2k/G)\begin{vmatrix} s \\ -\frac{\kappa y}{b} \\ 0 \end{vmatrix}\left[\begin{vmatrix} 3 & 0 & 0 \\ 0 & 0 & 0 \\ 0 & 0 & 0 \end{vmatrix} - \begin{vmatrix} 2 & 0 & 0 \\ 0 & 2 & 0 \\ 0 & 0 & 2 \end{vmatrix}\right] \\
&+ \mathcal{O}\left(\frac{1}{(\ln\kappa)^3}\right)\ . \qquad 13
\end{aligned}$$

Of interest in the present case is F_1, the force component in the x-direction. It can be shown that F_1 is expressed by:

$$\frac{F_1}{2\pi} = \left(1 - \frac{2k}{G}\right)\left(\frac{-s}{\ln\kappa} + \frac{(3/2 - \ln 2)s}{(\ln\kappa)^2}\right) + \mathcal{O}\left(\frac{1}{(\ln\kappa)^3}\right) . \qquad 14$$

Recalling that for $\alpha<<1$:

$$1 - \alpha \simeq \frac{1}{1+\alpha} , \qquad 15$$

eq. 14 may be written as:

$$\frac{F_1}{2\pi} = - \frac{(1-2k/G)s}{\ln\kappa\{1 + (3/2 - \ln 2)/\ln\kappa\}} + \mathcal{O}\left(\frac{1}{(\ln\kappa)^3}\right) . \qquad 16$$

The force per unit length of the slender body in the x-direction can finally be written in dimensional form and results in eq. 17.

$$F_{(x)} = \frac{2\pi\mu(\frac{G}{2} - k)x}{\ln\frac{2a}{b} - \frac{3}{2}} + \mathcal{O}\left(\frac{1}{(\ln\frac{b}{a})^2}\right) \qquad 17$$

Reference

1. Cox, R.G., J. Fluid Mech. 44, 791 (1970).

APPENDIX II

SOLUTION OF $\phi'' + \eta\phi' - 2\phi = 0$

For chapter IV, the solution of the differential equation:

$$\phi'' + \eta\phi' - 2\phi = 0 \ , \tag{1}$$

with the boundary condition, $\phi = 0$ for $\eta = \infty$, is required. The method follows usual procedures in solving differential equations[1]. One particular solution is given by

$$\phi_1 = \eta^2 + 1 \ , \tag{2}$$

and the general solution can be found by setting

$$\phi = \phi_1 \phi_2 \ . \tag{3}$$

This is substituted in the differential equation and yields:

$$5\eta\phi_2' + \eta^3\phi_2' + (\eta^2 + 1)\phi'' = 0 \ . \tag{4}$$

After integration, the solution for ϕ_2 can be expressed by eq. 5, where C_1 and C_2 are integration constants.

$$\phi_2 = C_2 \int \frac{1}{(\eta^2 + 1)^2} e^{-\eta^2/2} \, d\eta + C_1 \tag{5}$$

The general solution of the original differential equation may then be obtained by setting

$$\phi = (\eta^2 + 1)\phi_2 \ , \tag{6}$$

which yields:

$$\phi = C_1(\eta^2 + 1) + C_2(\eta^2 + 1) \int \frac{1}{(\eta^2 + 1)^2} e^{-\eta^2/2} \, d\eta \ . \tag{7}$$

In order to satisfy the boundary condition $\phi = 0$ for $\eta = \infty$, C_1 must be zero and also the second term has to converge to zero:

$$\lim_{\eta \to \infty} C_2(\eta^2 + 1) \int \frac{1}{(\eta^2 + 1)^2} e^{-\eta^2/2} d\eta = 0 . \qquad 8$$

That this is true can be proved in the following way[2]:

$$\lim_{\eta \to \infty} \frac{\frac{d}{d\eta}\left[\int \frac{1}{(\eta^2 + 1)^2} e^{-\eta^2/2} d\eta\right]}{\frac{d}{d\eta}\left[\frac{1}{C_2(\eta^2 + 1)}\right]}$$

$$= \lim_{\eta \to \infty} -\frac{C_2}{2\eta} e^{-\eta^2/2}$$

$$= 0 . \qquad 9$$

The required solution for the differential equation is therefore:

$$\phi = C_2(\eta^2 + 1) \int \frac{1}{(\eta^2 + 1)^2} e^{-\eta^2/2} d\eta . \qquad 10$$

References

1. Ayres Jr., F., "Theory and Problems of Differential Equations", Schaum Publishing Co., N.Y., 1952.

2. L'Hopital's rule (see e.g. Woods, F.S., "Advanced Calculus", Ginn and Company, Boston, 1934).

APPENDIX III

ANALYSIS OF ADDITIONAL EXPERIMENTAL DATA,

SUPPLEMENT TO CHAPTER V

Figure 1

The logarithm of the length ratio, $\ln\alpha$, of a coagulating drop is plotted as a function of the dimensionless time, Gt, for $c = 0.13$ cm, $\lambda = 0.377$, and $G = 0.45\ \text{sec}^{-1}$. The strain rate ratio, 2k/G, can be obtained by graphical differentiation of the deformation curve (see eq. 40, chapter V); the apparent viscosity ratio, λ_{app}, can be calculated by eq. 41 (chapter V).

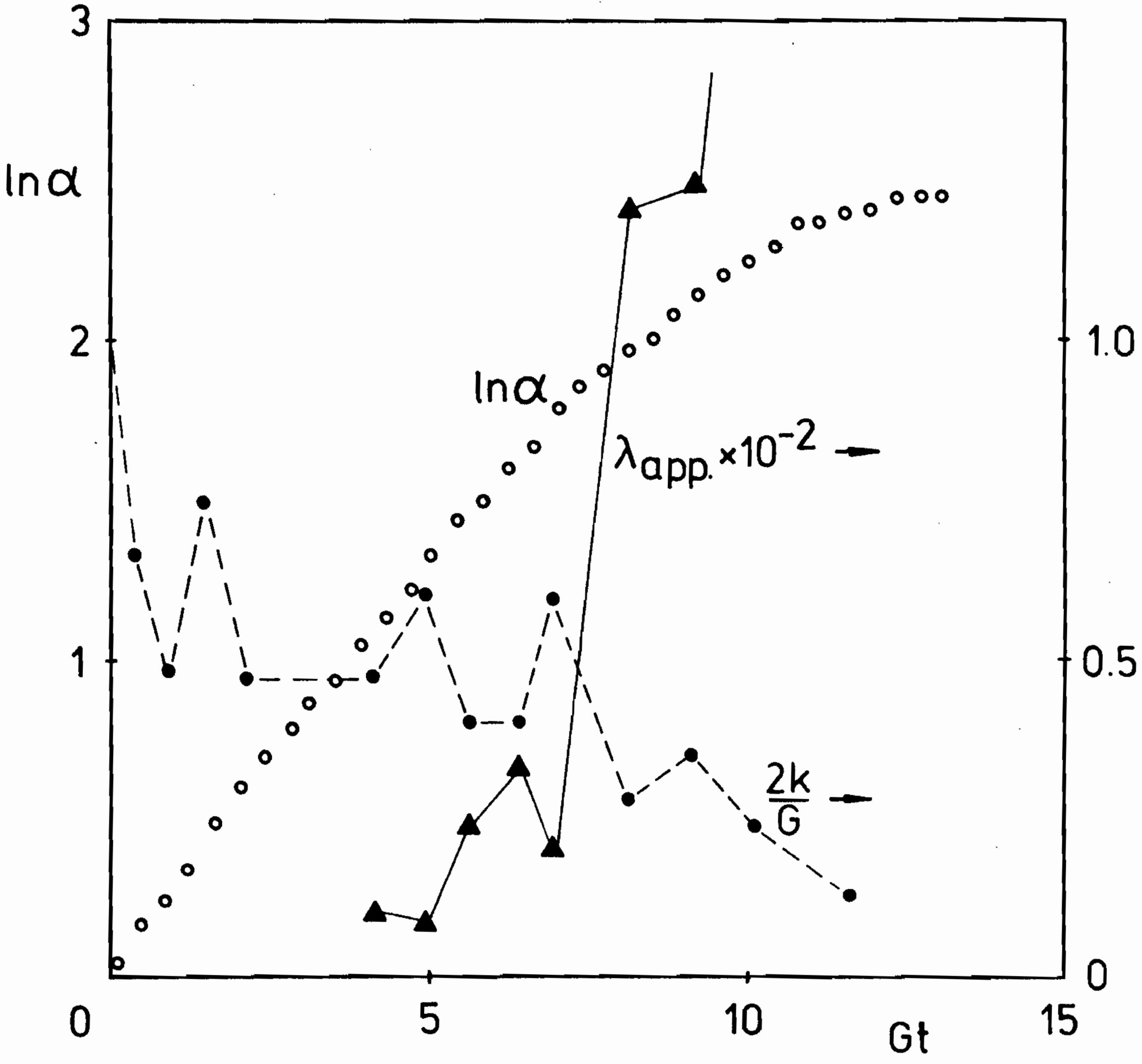

FIGURE 1

Figure 2

The logarithm of the length ratio, $\ln\alpha$, of a coagulating drop is plotted as a function of the dimensionless time, Gt, for $c = 0.14$ cm, $\lambda = 0.377$, and $G = 0.65$ sec^{-1}. The strain rate ratio, $2k/G$, can be obtained by graphical differentiation of the deformation curve (see eq. 40, chapter V); the apparent viscosity ratio, λ_{app}, can be calculated by eq. 41 (chapter V).

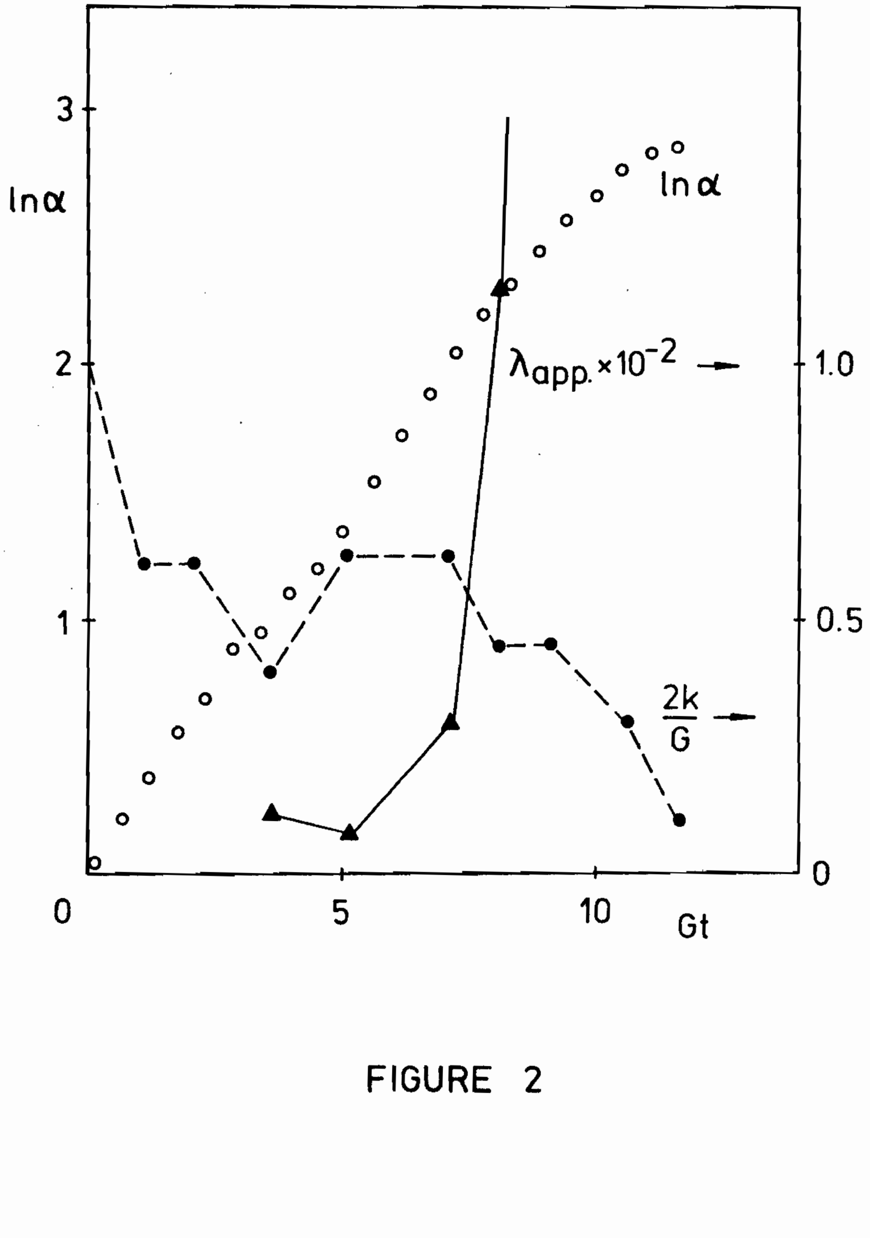

FIGURE 2

Figure 3

The logarithm of the length ratio, $\ln\alpha$, of a coagulating drop is plotted as a function of the dimensionless time, Gt, for $c = 0.13$ cm, $\lambda = 0.377$, and $G = 0.89$ sec^{-1}. The strain rate ratio, 2k/G, can be obtained by graphical differentiation of the deformation curve (see eq. 40, chapter V); the apparent viscosity ratio, λ_{app}, can be calculated by eq. 41 (chapter V).

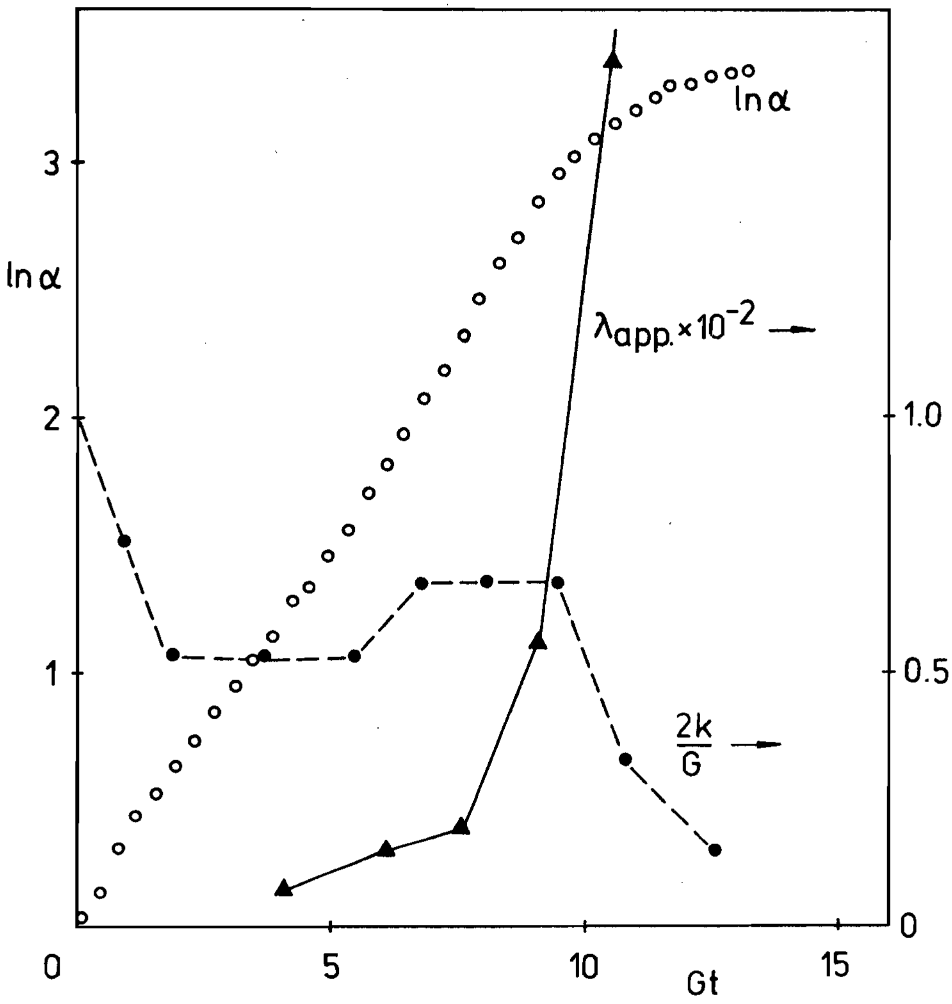

FIGURE 3

Figure 4

The logarithm of the length ratio, $\ln\alpha$, of a coagulating drop is plotted as a function of the dimensionless time, Gt, for $c = 0.11$ cm, $\lambda = 0.377$, and $G = 1.21\ \text{sec}^{-1}$. The strain rate ratio, $2k/G$, can be obtained by graphical differentiation of the deformation curve (see eq. 40, chapter V); the apparent viscosity ratio, λ_{app}, can be calculated by eq. 41 (chapter V).

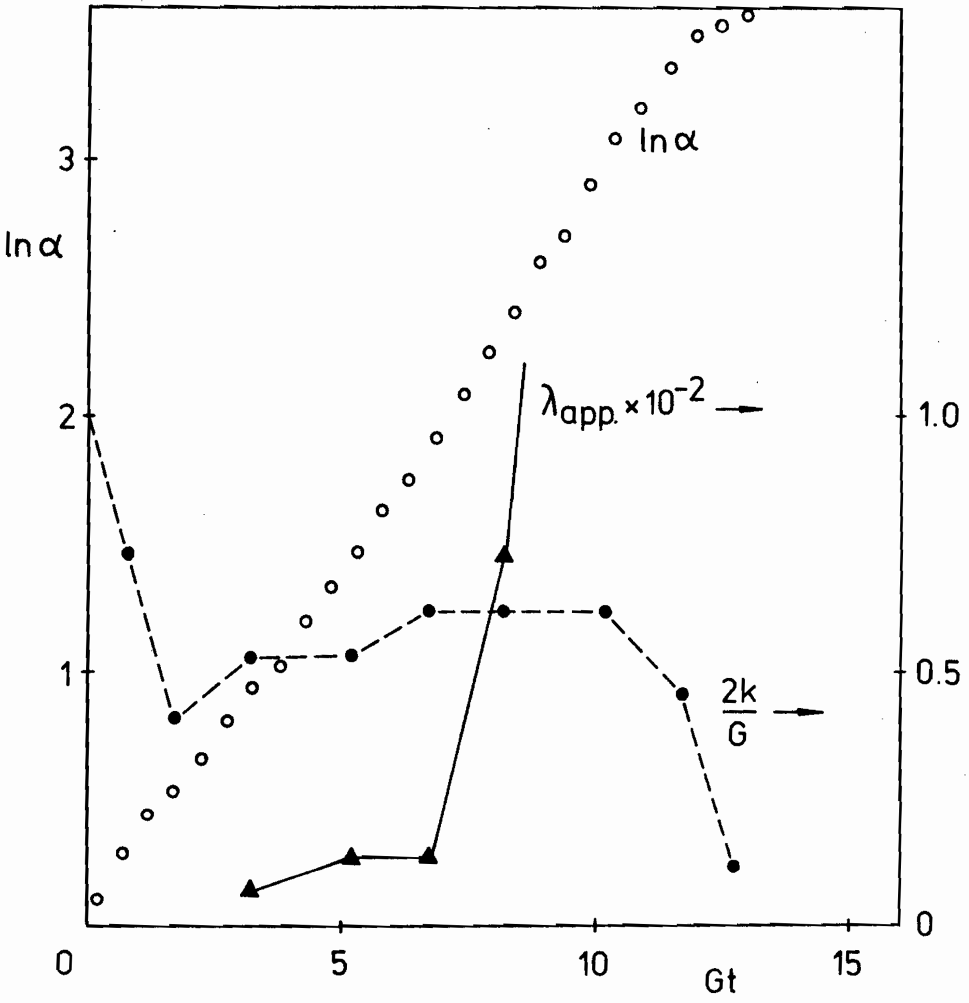

FIGURE 4

Figure 5

The logarithm of the length ratio, $\ln\alpha$, of a coagulating drop is plotted as a function of the dimensionless time, Gt, for $c = 0.14$ cm, $\lambda = 1.08$, and $G = 0.62\ \mathrm{sec}^{-1}$. The strain rate ratio, $2k/G$, can be obtained by graphical differentiation of the deformation curve (see eq. 40, chapter V); the apparent viscosity ratio, λ_{app}, can be calculated by eq. 41 (chapter V).

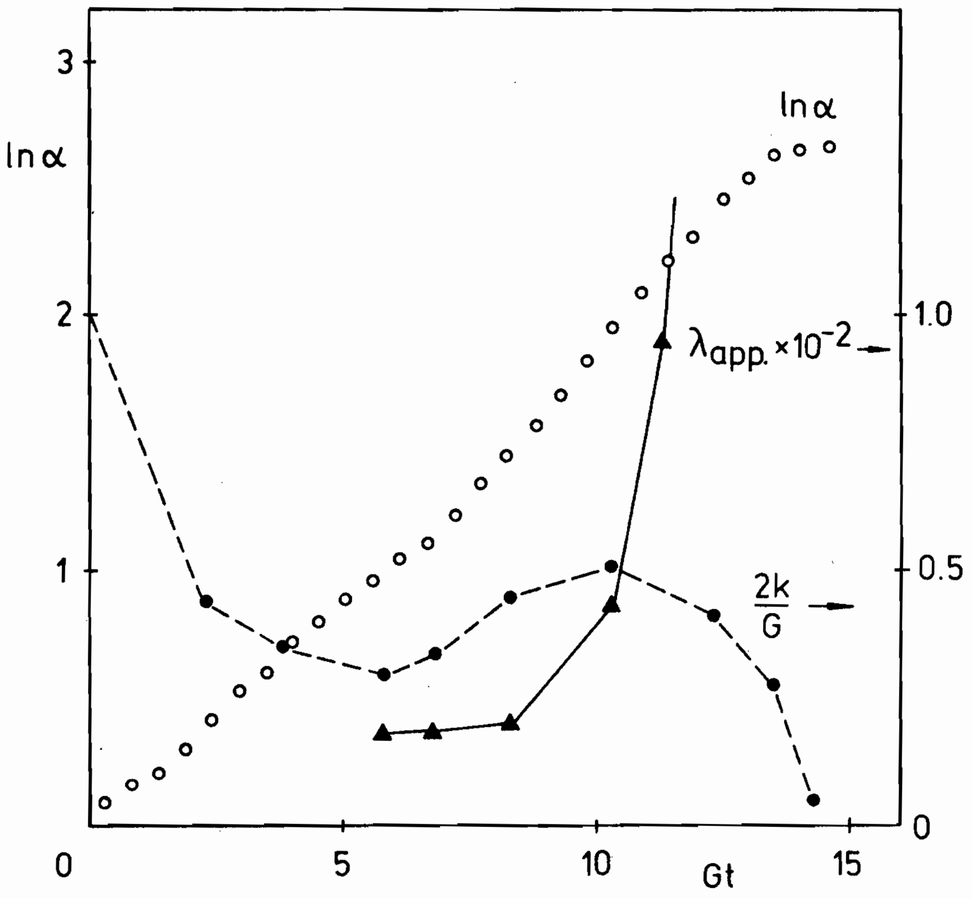

FIGURE 5

Figure 6

The logarithm of the length ratio, $\ln\alpha$, of a coagulating drop is plotted as a function of the dimensionless time, Gt, for $c = 0.14$ cm, $\lambda = 1.08$, and $G = 0.85\ \text{sec}^{-1}$. The strain rate ratio, $2k/G$, can be obtained by graphical differentiation of the deformation curve (see eq. 40, chapter V); the apparent viscosity ratio, λ_{app}, can be calculated by eq. 41 (chapter V).

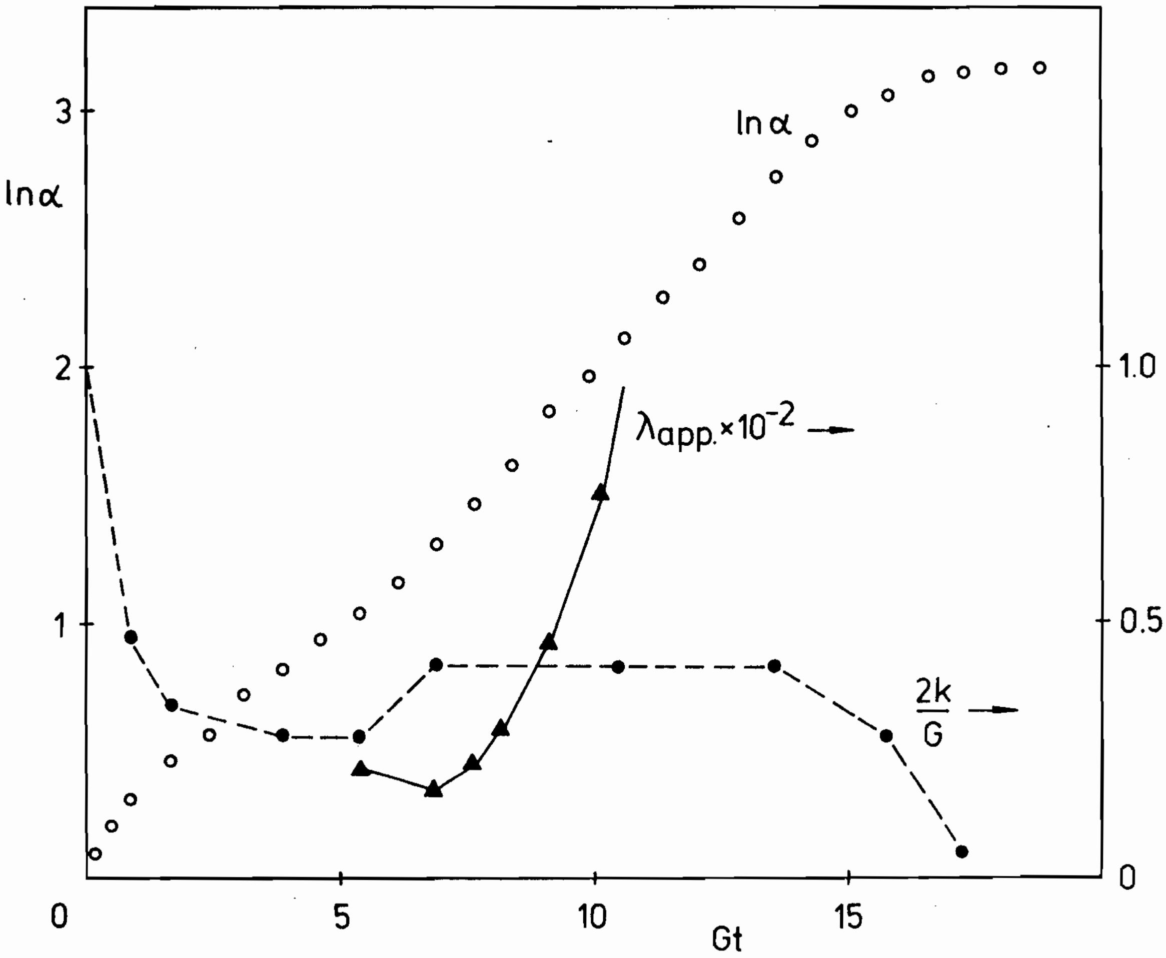

FIGURE 6

Figure 7

The logarithm of the length ratio, $\ln\alpha$, of a coagulating drop is plotted as a function of the dimensionless time, Gt, for $c = 0.13$cm, $\lambda = 1.08$, and $G = 1.2$ sec^{-1}. The strain rate ratio, $2k/G$, can be obtained by graphical differentiation of the deformation curve (see eq. 40, chapter V); the apparent viscosity ratio, λ_{app}, can be calculated by eq. 41 (chapter V).

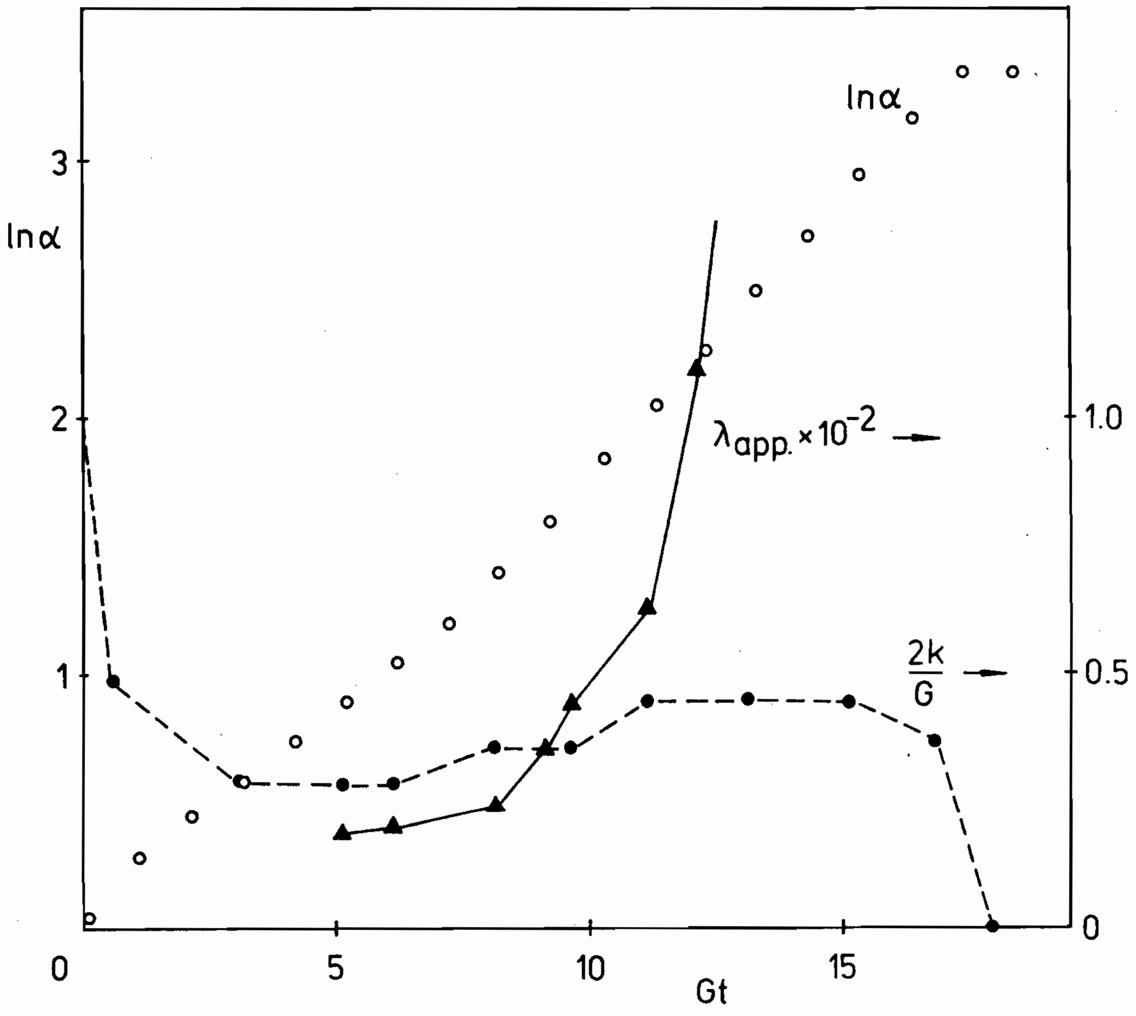

FIGURE 7

Figure 8

The logarithm of the length ratio, $\ln\alpha$, of a coagulating drop is plotted as a function of the dimensionless time, Gt, for $c = 0.12$ cm, $\lambda = 1.95$, and $G = 0.89$ sec^{-1}. The strain rate ratio, $2k/G$, can be obtained by graphical differentiation of the deformation curve (see eq. 40, chapter V); the apparent viscosity ratio, λ_{app}, can be calculated by eq. 41 (chapter V).

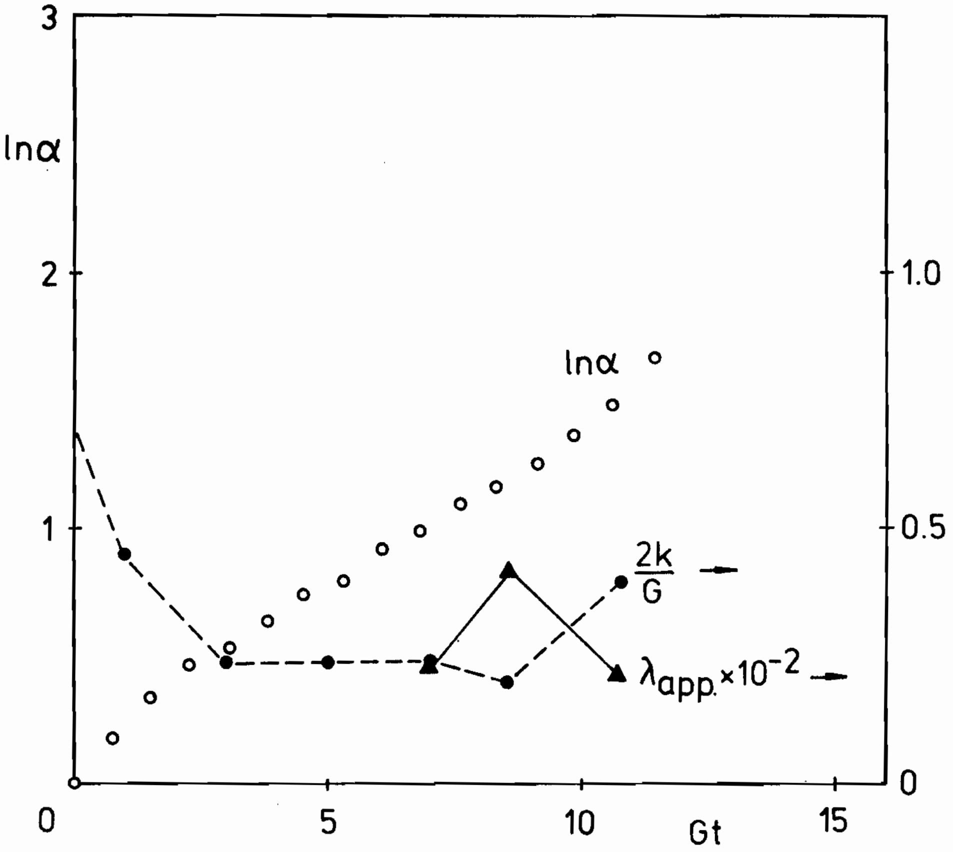

FIGURE 8

CLAIMS TO ORIGINAL RESEARCH

CHAPTER II

1. The precipitation of cellulose fibres from dimethyl sulfoxide/paraformaldehyde (DMSO/PF) by addition of coagulant to the stirred solution.
2. The study of the mechanism of fibre formation in the above-mentioned process which yields new information about the behaviour of cellulose molecules when precipitated from flowing solutions.
3. The process of coagulation of droplets of cellulose/DMSO/PF solutions in a stirred coagulant.
4. The discovery that the finer fibres produced by the method involving the deformation of droplets have the highest molecular orientation.
5. The precipitation of high molecular weight cellulose from dilute solutions in DMSO/PF by addition of water under quiescent conditions showing that 3.5 nm elementary fibrils are formed as the smallest morphological units.

CHAPTER III

6. The derivation of a theory for high droplet deformation in systems having negligible interfacial tension. On the basis of Cox's slender body theory, expressions have been developed for the variation of the length of a drop as a function of time in an extensional flow field. The theory applies for small strain rates.
7. The experiments on droplet deformation with miscible liquids in extensional flow at small strain rates. These are the first experiments for such a system that show the deformation behaviour for the whole range of small to large droplet deformations.

8. The derivation of semi-empirical expressions for the deformation of drops without interfacial tension. The expressions derived cover the whole range from small to very large deformations.
9. The recognition from the theoretical and experimental work that the strain rate inside an extending drop increases with time and eventually reaches that of the flow outside.

CHAPTER IV

10. The derivation of a theory for high droplet deformation at high strain rates in systems having negligible interfacial tension.
11. Solution of the boundary layer equations for extensional flow along a flat plate under deformation at a constant rate.
12. The recognition from the theoretical work that the strain rate inside the drop increases with the deformation at high strain rates.

CHAPTER V

13. The derivation of a theory for the coagulation of deforming drops under idealized conditions.
14. Solution of the one-dimensional diffusion equation for diffusion into a flat plate, where the plate thickness decreases with time.
15. Experiments on the coagulation of cellulose/DMSO/PF droplets in the four-roller-mill with glycerol as coagulant.

CHAPTER VI

16. Proposal for a fibre spinning process in which, during solidification of the fibre, extensional flow is applied.

SUGGESTIONS FOR FURTHER WORK

1. Experiments on the formation of fibres of viscose and synthetic polymers based on the droplet deformation mechanism in extensional flow. The coagulation experiments should be carried out at high strain rates. The resulting fibres might show high molecular orientation and strength.
2. The observations in chapter II indicate that cellulose fibres, precipitated from stirred solutions by addition of a coagulant, are formed by the lateral alignment and aggregation of elementary fibrils. The mechanism by which this occurs might be further investigated in model studies, that might be carried out with suspensions of flexible or rigid rods.
3. Refinement of the present coagulation theory, i.e. to include in the theory the increase of the apparent viscosity ratio with time. This might yield a better quantitative agreement of the theory with the experiments.
4. To derive a theory for the coagulation of drops at high strain rates, on the basis of assumptions similar to those (e.g. homogeneous drop) made in chapter V.
5. To perform fibre spinning experiments in converging channels, as suggested in chapter VI, in order to test the validity of the proposal.
6. To derive a theory for the formation and coagulation of a continuous liquid thread in another liquid with lower viscosity and which itself is undergoing extensional flow. Such a theory would be extremely useful in connection with fibre spinning experiments in converging channels.
7. Kinetic studies of the crystallization of cellulose from quiescent and flowing solutions to gain insight into the crystallization process of this particular polymer. Similar to chapter V, such studies might be carried out

with cellulose/DMSO/PF and glycerol or water as coagulants.

8. Investigation of the second regime of fibre formation, where the coagulated fibres rupture due to large hydrodynamical stresses. This regime is of interest, since the deformation of the gel up to its rupture may yield well oriented fibres.